UNIVERSITAT POLITÈCNICA DE CATALUNYA BARCELONATECH

Update urban basemap by using the LiDAR Mobile Mapping System. The case of Abu Dhabi municipal system

Omar Al Shaiba

Ph.D. Dissertation

Update urban basemap by using the LiDAR Mobile Mapping System. The case of Abu Dhabi municipal system

Omar Al Shaiba

UNIVERSITAT POLITÈCNICA DE CATALUNYA
BARCELONATECH
Departamento de Ingeniería Civil y Ambiental

PhD Program:
Geotechnical Engineering

Supervisors:
Dr. Mª Amparo Núñez Andrés
Dr. Nieves Lantada Zarzosa

March 2020

Acknowledgments

I am grateful to everyone who has helped me in my struggle to achieve the dream of becoming a PhD. I would first like to sincerely thank my PhD supervisors, Dr. Amparo Núñez-Andrés and Dr. Nieves Lantada for their expert guidance, valuable feedback and rapid responses. Their advice and comments helped me to make this thesis a success. They gave me all the support and tools I needed to complete the thesis.

In addition, I would like to thank the Universitat Politecnica de Catalunya (UPC) for hosting me while I prepared the PhD thesis.

I also acknowledge the contribution of the Department of Municipalities and Transportation and Al Ain Municipality for providing me with support and information that was vital to the thesis preparation. Thanks to the Mobile Lidar Unit that helped me to collect the Lidar data.

I would like to express my gratitude to my parents, my wife and family for playing a big role in encouraging me while I was working on the thesis, which helped me to reach this achievement. To my son Saif with my prayers and hope to see you well and in excellent health.

Special thanks to my brothers and friends for pushing me to complete the thesis. Thank you for this opportunity.

Abstract

Basemaps are the main resource used in urban planning and in building and infrastructure asset management. These maps are used by citizens and by private and public stakeholders. Therefore, accurate, up-to-date geoinformation of reference are needed to provide a good service.

In general, basemaps have been updated by aerial photogrammetry or field surveying, but these methods are not always possible and alternatives need to be sought. Current limitations and challenges that face traditional field surveys include areas with extreme weather, deserts or artic environments, and flight restrictions due to proximity with other countries if there is not an agreement. In such cases, alternatives for large-scale are required.

This Ph.D. thesis proposes the use of a mobile mapping system (MMS) to update urban basemaps. Most urban features can be extracted from an MMS point cloud using commercial software or even open libraries. However, there are some exceptions: manhole covers, or hidden elements even with captures from different perspective, the most common building corners. Therefore, the main objective of this study was to establish a methodology for extracting manholes automatically and for completing hidden corners of buildings, so that urban basemaps can be updated. The algorithm developed to extract manholes is based on time, intensity and shape detection parameters, whereas additional information from satellite images is used to complete buildings.

Each municipality knows the materials and dimensions of its manholes. Taking advantage of this knowledge, the point cloud is filtered to classify points according to the set of intensity values associated with the manhole material. From the classified points, the minimum bounding rectangles (MBR) are obtained and finally the shape is adjusted and drawn.

We use satellite imagery to automatically digitize the layout of building footprints with automated software tools. Then, the visible corners of buildings from the LiDAR point cloud are imported and a fitting process is performed by comparing them with the corners of the building from the satellite image. Two methods are evaluated to establish which is the most suitable for adjustment in these conditions. In the first method, the differences in X and Y directions are measured in the corners, where LiDAR and satellite data are available, and is often computed as the average of the offsets. In the second method, a Helmert 2D transformation is applied.

MMS involves Global Navigation Satellite Systems (GNSS) and Inertial Measurement Units (IMU) to georeference point clouds. Their accuracy depends on the acquisition environment. In this study, the influence of the urban pattern is analyzed in three zones with varied urban characteristics: different height buildings, open areas, and areas with a low and high level of urbanization.

To evaluate the efficiency of the proposed algorithms, three areas were chosen with varying urban patterns in the Abu Dhabi Emirate. In these areas, 3D urban elements (light poles, street

signs, trees and road curbs) were automatically extracted using commercial software. The proposed algorithms were applied to the manholes and buildings.

The completeness and correctness ratio, and geometric accuracy were calculated for all urban elements in the three areas. The best success rates (>70%) were for light poles, street signs and road curbs, regardless of the height of the buildings. The worst rate was obtained for the same features in peri-urban areas, due to high vegetation. In contrast, the best results for trees were found in peri-urban areas.

Our methodology demonstrates the great potential and efficiency of mobile LiDAR technology in updating basemaps; a process that is required to achieve standard accuracy in large scale maps.

The cost of the entire process and the time required for the proposed methodology was calculated and compared with the traditional survey method. It was found that mobile LiDAR could become a standard cost-efficient operating procedure for updating the basemap system frequently.

Resumen

La cartografía de referencia es la principal herramienta en planificación urbanística, y gestión de infraestructuras y edificios, al servicio de ciudadanos, empresas y administración. Por esta razón, debe estar actualizada y ser lo más precisa posible.

Tradicionalmente, la cartografía se actualiza mediante fotogrametría aérea o levantamientos terrestres, pero no siempre es posible emplear estas técnicas y deben buscarse alternativas. Las limitaciones y retos actuales que enfrentan la medición tradicional en algunas zonas del planeta, debido a la meteorología extrema (zonas árticas, desérticas, etc.) y con restricciones de vuelo debido a la proximidad de la frontera con otros países. En estas condiciones es necesario encontrar una opción válida para escalas grandes.

Esta tesis propone el uso del sistema Mobile Mapping System (MMS) para actualizar la cartografía urbana de referencia. La mayoría de los elementos pueden extraerse empleando software comercial o librerías abiertas disponibles, excepto para los registros de servicios. Los elementos ocultos son otro de los inconvenientes encontrados en el proceso de creación o actualización de la cartografía, incluso si se dispone de varias capturas desde diferentes puntos de vista. El caso más común es el de las esquinas de los edificios. El principal objetivo de este estudio es establecer una metodología de extracción automática de los registros y completar las esquinas ocultas de los edificios para actualizar la cartografía urbana.

El algoritmo desarrollado para extraer registros se base en parámetros como el tiempo, la intensidad y la forma de los registros, para detectarlos, mientras que para completar los edificios se emplea información adicional proveniente de imágenes de satélite.

En cada municipio, sus gestores, conocen el material y las dimensiones de los registros. Aprovechando el conocimiento de estos datos, el algoritmo propuesto filtra y clasifica los puntos de acuerdo a los valores de intensidad, de aquellos clasificados como registros se calcula el mínimo rectángulo que los contiene (Minimum Bounding Rectangle, MBR), finalmente se ajusta la forma y se dibuja.

Las imágenes de satélite son empleadas para obtener automáticamente la huella de los edificios. Posteriormente, se importan las esquinas visibles de los edificios obtenidas desde la nube de puntos, se realiza el ajuste comparándolas con las obtenidas desde satélite. Para llevar a cabo este ajuste se han evaluado dos métodos, el primero de ellos considera las diferencias entre las coordenadas X e Y, desplazándose el promedio. En el segundo método se aplica una transformación de Helmert 2D.

MMS emplea sistemas de navegación global por satélite (Global Navigation Satellite Systems, GNSS) e inerciales (Inertial Measurement Unit, IMU) para georreferenciar la nube de puntos. La precisión de estos sistemas de posicionamiento depende del entorno de adquisición. Por ello, en este estudio se han seleccionado tres áreas de estudio con distintas características urbanas (altura de edificios, nivel de urbanización y áreas abiertas) con el fin de analizar su influencia tanto en la captura como en la extracción de los elementos.

Para evaluar la eficiencia de los algoritmos propuestos, se han seleccionado tres zonas con diferentes patrones urbanísticos en el Emirato de Abu Dhabi. En estas áreas de captura, la extracción automática de elementos urbanos 3D (farolas, señales viales, árboles y aceras) se ha realizado mediante software comercial. Y para los registros y edificios se han aplicado los algoritmos propuestos.

Las ratios de corrección y completitud, y la precisión geométrica se han calculado en las diferentes áreas urbanas. Los mejores resultados (>70%) se han conseguido para las farolas, señales y bordillos, independientemente de la altura de los edificios. La peor ratio fue obtenida se obtuvo para los mismos elementos en áreas peri-urbanas, debido a la vegetación. Resultados opuestos se han conseguido en el caso de los árboles

La metodología propuesta demuestra el gran potencial y eficiencia de la tecnología LiDAR móvil para la actualización de la cartografía de referencia, cumpliendo los requisitos de precisión para las escalas grandes.

El coste del proceso completo y el tiempo consumido empleando la metodología propuesta resulta inferior al de los métodos de levantamiento tradicionales. Lo cual prueba que el sistema MMS y el tratamiento automático de las nubes de puntos es un procedimiento eficiente para la actualización frecuente de la cartografía de referencia.

Table of Contents

Table of Figures

Table of Tables

1. Introduction

The world has witnessed continuous change and growth in infrastructure and construction projects in recent years. Therefore, there is a constant need for accurate, efficient, cost effective, automated updating methods for existing maps. The availability of updated maps and 3D spatial data is very important for applications such as environmental monitoring, transportation, town planning, oil and gas exploration, mining and road designs to support land use decision-making.

Information about facts and objects with spatial references, i.e. geospatial information, is a key element of global and local networks in the information society. It is calculated that around 80% of our everyday decisions depend on geospatial information (Okeke & Karnieli, 2006). Thus, Geographic Information Systems (GIS) that permit the attainment, storage, management, examination, visualization and broadcasting of geospatial information are increasingly important to the public. GIS applications require large amounts of up-to-date information. Therefore, geospatial information must be updated continuously. A database's prevalence is considered a vital part of the quality factor of the spatial data set (Sonnen, 2007).

Database update is defined as the job of evaluating two or more data sets (one showing a database's present status, the other(s) depicting more recently obtained data) to identify and make changes, and to introduce these changes into the database, while maintaining the latest data in accordance with the current data (Kalantari et al., 2009). To modernize a GIS database, it is essential to utilize several sources of data. According to Heipke (2004) and from the perspective of photogrammetry, updating directly from images is the best practice for various reasons.

Traditional surveys can be used to update maps. However, they can be costly and may not achieve the high level of accuracy required for town planning purposes. They also require a lot of manual work that may result in human errors and put surveyors in danger.

The main source for updating maps has been remote sensing imagery, which includes satellite imagery and aerial photography. Types of remote sensing techniques include: Airborne Laser Scanning (ALS), static Terrestrial Laser Scanning (TLS) and the Mobile Mapping System (MMS), which is also called the Mobile Mapping Laser Scanner (MMLS) or the Mobile Laser System (MLS). These systems have recently been established as leading technologies for the acquisition of high-density 3D spatial data and are used for mapping and other surveying applications. Each of these systems typically consists of one (or multiple) laser scanners, with an Inertial Navigation System (INS) and Global Navigation Satellite System (GNSS).

The laser scanner's function is to obtain 3D coordinates of the distance and angle measurement for each point in its direction of view. The GNSS and INS component function is to provide the position and orientation of the platform. Thus, the location of the points along the mapped surface (trajectory) can easily be determined.

There are few studies on how photogrammetric data is updated in basemaps with a scale of 1:1000 using advanced technology i.e. mobile Light Detection and Ranging (LiDAR) instead of traditional means of aerial photography. In this study, the upcoming technology is examined

to analyze how it could improve on aerial imagery. In this study the buildings, roads, trees, urban furniture and manholes are recognized as objects. The reason for choosing buildings, roads and compound walls is that they are frequently changed and are significant for map updating.

1.1 Research motivation

Town planning services must have up-to-date 3D spatial data before they make decisions. The need to update maps is increasing daily. Traditional surveying methods can be used to update maps, especially in places that need frequent surveys. However, these methods are labor intensive, time-consuming, costly (field operation costs), sometimes dangerous and highly disruptive to traffic. In harsh environments (with high temperatures and high humidity, and in desert areas and border areas) traditional survey methods may put surveyors' lives in real danger. In these environments, collecting data for large areas may take days or even months, because surveyors can only work at certain times when the temperature is acceptable.

This research was undertaken due to a need to overcome the problems and challenges of traditional surveying methods for updating spatial data. The reduction of human involvement in updating data must be the main priority in any project of this kind. Consequently, improving and automating the data updating process through mobile LiDAR and daily transactions is central to this study. Many studies have been conducted on effective means of categorizing multispectral photography and mapping the outcome (Jensen, 2005).

The final aim of this study is to establish a methodology to support the updating of spatial data through mobile LiDAR methods. The aim is also to approve the methodology of updating basemaps in real time using daily transactions and mobile LiDAR so that this becomes a trusted and cost-efficient operating procedure for updating the basemap system. Over time, Mobile LiDAR technology could be adopted to supplement existing daily operations and processes.

1.2 Research objectives

Currently, traditional methods of aerial photography are used to update basemaps. However, there are a lot of inefficiencies in the updating of spatial data:

- Cartographers face several challenges when they use traditional aerial photography to update basemaps.
- Resources such as plane aerial photography and a specialized workforce may be required to complete the update process (outside of the country). For numerous reasons, the cost of these resources can be too high. Furthermore, it is difficult to get permission to fly near country borders.
- Capturing and digitizing the information requires a lot of time. Using aerial photography to update basemaps takes a minimum of eight months in some areas.
- All activities require permission in the form of infrastructure and building permits from customer services, especially projects related to updating basemaps.

- Detecting small objects such as manholes using traditional methods is very challenging due to variance in shape, color and dimensions. In addition, manholes may be covered or hidden by other objects when aerial images are captured.
- Frequently, building changes are not available in information gathered by traditional methods, as the update process take place every few years. Therefore, another solution is needed, especially in highly developed cities. Moreover, it is hard to capture points of the façade in aerial surveys if an oblique camera is not available.

In this thesis we will show how Mobile Laser Scanner (MLS) technology is the most efficient method to update basemaps of urban areas when it is not possible to use traditional survey methods. This cartography helps municipalities to serve their citizens better by updating spatial data so that it can be used in daily transactions.

Daily transactions are any services or transactions in municipal customer service related to building permits, roads, infrastructure, utility lines and assets. In daily transactions, clients (such as consultants, developers and contractors) are required by municipalities to obtain permission to construct a building or add assets to the ground. This should be reflected in basemaps.

This thesis will show how we can use client services and activities to update our basemap daily. Consequently, if there are any new roads or projects, the basemap will be updated and ready to use.

The main purpose of this study is to develop and design a framework to update spatial data semi-automatically in areas where using the traditional survey methods is limited. This main objective could be divided into the following specific objectives:

a) To evaluate the efficiency and usefulness of mobile LiDAR for basemap updating in municipal activity.

b) To integrate mobile LiDAR effectively to facilitate the updating of spatial data and reduce the use of traditional methods for updating spatial data.

c) To improve automatic urban feature and building extraction process.

d) To integrate mobile LIDAR data in municipal daily transactions relating to basemap features such as roads and buildings, so that the benefits of the transaction can be used to update the basemap.

- The integration of mobile LiDAR to facilitate the updating of spatial data operations will be analyzed and assessed.
- The suitability of the methodology will be addressed through its application to an urban zone of Al-Ain in the Abu Dhabi Emirate (UAE). This pilot area was selected because it has three urban patterns.
- A set of tests will be established that evaluate the effectiveness and performance of the method. Also to utilize and use the mobile LiDAR to support the municipal daily transactions.
- The costs and benefits of their involvement will be quantified to identify advantages and disadvantages.

1.3 Thesis structure

This first chapter introduces the subject with a brief description of the research motivation and background. It also explains the research objectives and thesis structure.

Chapter two presents a literature review that covers the basic and updated principles of geomatic techniques to update cartography: photogrammetry and LiDAR as well as the integration of this information in Geographic Information Systems (GIS).

Chapter three contains information about the proposed methodology for basemap updating using data gathered by LiDAR system.

Chapter four explains the methodology for updating Spatial Data Services Transaction and provides an example of the daily transaction process.

Chapter five describes how the basemap was updated in Abu Dhabi municipalities using the proposed methodology: from project planning phase to quality control and basemap update phase.

Chapter six presents the research conclusion and recommendations for future studies. Finally, Appendix A includes the quality control charts for positioning the MMS and the script of MATLAB used in the thesis.

2. Literature review

This section provides an overview of types of spatial information and the geomatic techniques used to capture and update cartography. To explain the importance of this research in the technologically advanced world of cartography, photogrammetry, mobile mapping and LiDAR and Geographic Information System (GIS) techniques are discussed in detail.

2.1 Photogrammetry

Photogrammetry is an art, a technical science and a modern technology for gaining valid information from sensor systems and non-contact imaging of the Earth, its environment and other physical objects. The procedure involves collecting information through measurement, recording, analyzing and representation (Craig, 2000).

The scientific process of photogrammetry involves planning the project and image capture, processing the image, data control for image orientation, compilation of data and presentation of the end product (Sonnentag et al., 2012). This final stage of the photogrammetric process can incorporate either the values of single points, a resolved image of the ground's surface as a graphical representation or orthophotos.

Various types of photogrammetry are utilized depending on the object's features which must be modelled. A primary categorization is based on whether the images are captured from the ground or from the air. In aerial photogrammetry, images are captured from an airplane to represent the terrain surface. In terrestrial photogrammetry, pictures are taken from a point close to the ground, and normally represent artificial or minor details rather than terrain. Aerial photogrammetry can only be utilized for enormous objects and when greater amounts of hardware equipment are available. In this case, Global Navigation Satellite System (GNSS) must be used to establish the coordinated reference system.

The main advantages of the use of this technique are:

- Photogrammetry provides a stable photographic record of situations that occurred at the time the midair photographs were taken. The result is a pictorial and an exact measurable record.
- It is not essential to undertake the field work again when the information needs to be re-accessed or resurveyed. The same images can be used in further evaluations and new data can be found for the new demand. Thus, lost data, such as inappropriate offsets for cross segments, can be improved definitively (Craig, 2000).
- It can deliver a vast mapped area. Therefore, line studies can be replaced with a similar source of information. Moreover, it can be applied economically and smartly, unlike other conventional methods.
- It detects cultural and topographical features as it delivers a large view of projected surface.

- Photogrammetry is helpful in those locations that are insecure, problematic or inaccessible. It is a perfect method for surveying in hazardous areas in which a field crew would face difficult circumstances.
- A big challenge of photogrammetry is to undertake road surveys without closing lanes, which exposes field crews to hazards and could cause traffic problems. Once an image of a road has been recorded, the rest of the work, including advancement of road data and measurement of road structures and features, can be done in an office rather than in the field (Lato & Diederichs, 2014).
- Inter-visibility regarding points and unnecessary surveys to spread the control to a distant area of a project are not essential. No more expenses are required to incorporate each point into the mapping area.
- Photogrammetry images are used to share data or information with the public, the government, federal agencies and related institutions (Barazzetti et al., 2013).

2.1.1 Aerial photogrammetry

Aerial photogrammetry is the art of capturing photographs of any landscapes, attributes or phenomenon on the Earth's surface to build maps, using cameras that can be placed on an aerial platform (Gilvear & Bryant, 2005). In 1858, Persian balloonist and photographer Felix Nadar captured the first aerial photograph from an air balloon. It was a view of a French village taken from a tethered hot-air balloon, 80 meters above the ground. This historical mapping is about 9 x 9 inches.

Now, the usual technique for creating and updating regional cartography is aerial photogrammetry. The main government agencies, such as Infrastructure Divisions, Spatial Data Divisions and the Department of Transportation, use aerial photogrammetry surveys frequently to update their basemaps (ASPRS, 2004). This process takes place every few years, depending on the economic feasibility of this technique in each country.

Recently, integrated navigation systems have been increasingly adopted. They are less costly, more accurate, safer, more effective and use fewer Ground Control Points (GCP) than conventional methods (Cramer & Stallmann, 2001). Digital cameras can provide high resolution images. This technique perfectly captures buildings' roofs but has difficulties in capturing points of the façade (Yang et al., 2012) that may be offset from the roof line. The development of oblique cameras partially corrects this problem (Ostrowski, 2016), but it is still an immature technique (Qiu et al., 2016).

The following are the advantages of aerial photogrammetry:

- Aerial photographs are useful in providing a true picture of the ground surface. The benefit of utilizing an image is that it permits identification of elements on the surface by photointerpretation.
- Aerial photography provides an enhanced vantage point.
- It has better geometric fidelity and spatial resolution than several ground-based sensing methods.

- Aerial photography offers eternal memorializing of recent views of the surface of the earth and its data.

However, aerial photogrammetry also has some weaknesses, which are given below:

- The main disadvantage of an aerial photograph is that it is distorted. It requires spherical rectification to be converted into map or ground coordinates.
- Because of deficient contrasting tone and colours, it is difficult to utilize photographs in dim light.
- Snowfall, and other seasonal situations, will provide false impressions since it covers and may destroy the target area, therefore affecting aerial photographs. Consequently, in many areas only a limited period (from November to March) is ideal for aerial photography. However, a well-organized construction site, or a main road that is not blocked by trees is less affected by this limitation. These kinds of projects are favourable for photography most of the year (Craig, 2000).
- The correctness of the cross sections and mapping lines are associated with the exactness of the field survey and flight height (Barazzetti et al., 2013).

Therefore, the main drawbacks of aerial photogrammetry include the fact that it uses expensive equipment that is dependent on weather conditions. The process of updating only takes place every few years, and it does not capture hidden ground or the buildings' facades. This problem could be solved with an Unmanned Airborne Vehicles (UAV), but in some areas, mainly near borders between countries, any kind of aerial photogrammetry is unsuitable as permission to fly is not always obtained.

Regardless of these disadvantages, aerial photography is considered essential for making maps, even today (Campbell, 2002). An example of aerial photography for Abu Dhabi is shown in Figure 2-1.

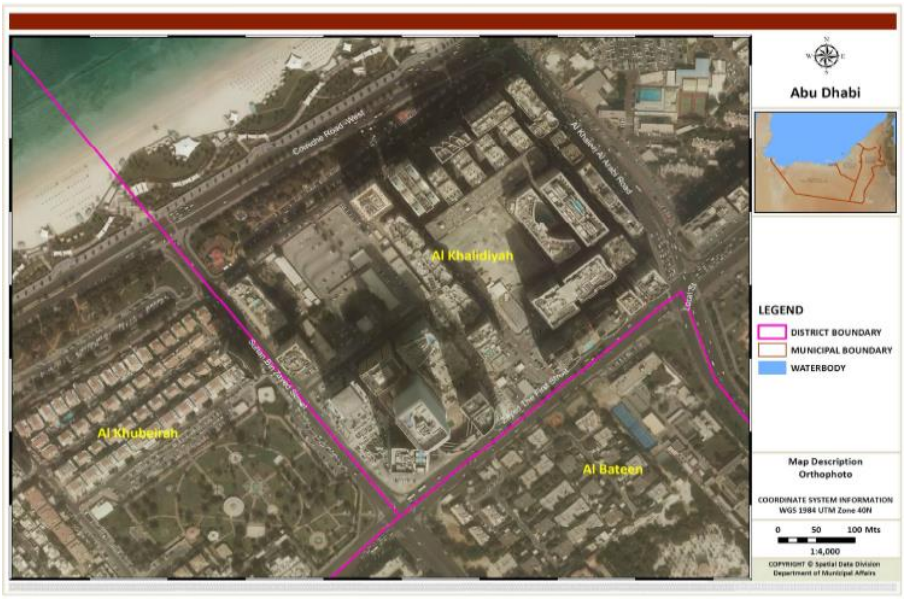

Figure 2-1: Example of aerial orthophoto, Abu Dhabi (Courtesy of the MSSI application, Department of Municipal Affairs, 2016)

2.1.2 Unmanned Airborne Vehicles (UAV)

Unmanned Airborne Vehicles (UAV) have a long history in military applications. The use of these technologies in civil domains that require "less skilled" pilots is very recent. The mapping field is no exception. Drones have been frequently used for such purposes in military operations over the last decades (Vallet et al., 2011).

Since the mid-2000s, research has focused on the use of such vehicles to acquire low cost mapping datasets, mainly based on imagery and georeferencing sensors (Wendel et al., 2006). They represent a low-cost alternative to airplane platforms (Nex & Remondino, 2014).

In recent decades, UAVs have been used with increasing frequency. The acquisition system is based on a very lightweight UAV (weighing less than 500 g). The use of ultra-light UAV combined with a compact digital camera provides mapping products such as the Digital Elevation Model (for terrain or surface) and orthoimages. The quality of the mapping products generated by this system seems to depend on the processing tools that are used. The use of standard photogrammetric software provides an elevation model with an accuracy of ~30 cm within the GCP area (Vallet et al., 2011).

These systems acquire images that can have a Ground Sampling Distance (GSD) of 1 cm, since they can fly nearer the surface than airplanes. Moreover, they can obtain images from facades. The main problem with these systems is image registration, since the photos may have varying resolution, geometry and radiometry characteristics (Xu et al., 2016). However, this problem can be resolved with algorithms such as Sift (Lowe, 2004) or A-Sift (Morel & Yu, 2009).

These new aerial platforms have the same flight restrictions in border areas as traditional planes. Moreover, restrictions in each country vary depending on regulations (Dolan & Li, 2013; Nex & Remondino, 2014; Stöcker et al., 2017). This restriction led to the need to find another method for performing frequent basemap updates in conflictive areas.

2.2 LiDAR surveying

Light detection and Ranging (LiDAR) is a distant or remote sensing method. In the LiDAR method, light works in the form of pulse lasers to measure a range of distances to the Earth (Cracknell & Hayes, 2007). The light pulses are recorded by either an airborne (air platform) or terrestrial (land vehicle) system and then incorporated with other data to produce very brief, three-dimensional data about the Earth's characteristics and shape.

Airborne Laser Scanning systems (ALS) have four major hardware components: a laser scanner, differential Global Navigation Systems (GNSS) or Global Position Systems (GPS) in aircraft and ground units, a highly sensitive inertial measurement unit (IMU) attached to the scanning unit, and an on-board computer to control the system and store data from the first three components. The position and attitude of the scanner, at the time each pulse is emitted, are determined from data collected by the GPS and IMU units. LiDAR systems used for topographic mapping applications usually operate in the infrared range of the spectrum (700-1200 nm) (Grant, 1995; Kim, 2007).

In recent decades, Terrestrial Laser Scanners (TLS) have been developed with similar components to the aerial one. Therefore, they are very useful in urban surveys.

2.3 Mobile mapping

Mobile mapping is the method of gathering geospatial data from a mobile vehicle. The Mobile LiDAR System (MLS) have a combined collection of time-harmonized navigation sensors and imaging sensors attached to a mobile platform: LiDAR, photographic or other sensing systems, GPS receivers and IMU (Tao & Li, 2007), as shown in Figure 2-2. Such systems provide basic outputs after processing that include: digital maps, videos and images of georeferenced and GIS data (Gao, 2008).

Figure 2-2: Abu Dhabi Mobile Lidar (LYNX) (Courtesy of Al Ain City Municipality)

The MLS has been developed over the last 20 years and new applications and trends have been introduced. They have already reached the industrialization phase. Data provided by these systems can be characterized by the following technical parameters: a) point density in the range of 100-1000 points per m2 at 10 m distance, b) distance measurement accuracy of 2–5 cm, and c) operational scanning range from 1 to 100 m (Kaartinen et al., 2012a). We will focus on the most commonly used application of mobile LiDAR mapping systems.

Prior to MLS, other Mobile Mapping Systems were used that were based on photogrammetric methods. One example is GPS Van, which was created in the early 1990s by the Center for Mapping at Ohio State University. This system involved GPS, two digital CCD cameras, two video cameras, two gyros and one odometer. Its relative accuracy was 10 cm and absolute accuracy 1–3 m (Novak, 1991).

After years of development of the MMS, the MLS was introduced. Most MLS incorporated direct georeferencing components, such as GNSS and an IMU. The GNSS/IMU systems work together to continuously calculate the most likely Position and Orientation (POS) of the vehicle. When satellite visibility is poor, the IMU manages the position determination. When

satellite visibility is good, the IMU's positional information is continually improved by a feedback signal from the GNSS (Barber et al., 2008).

Additionally, the IMU must continually fill gaps between GNSS observations. Since most GNSS receivers can be configured for observation with a sampling rate of 1–10 Hz through the duration of a second, the platform will experience movement and vibration, especially when it is driven at relatively high speed. The IMU provides measurements at higher rates, typically from around 100 to 2000 Hz (Shan & Toth, 2009; Yousif et al., 2010).

GNSS/IMU data quality is one of the primary factors that affect the final point cloud accuracy (Ussyshkin & Boba, 2008). Detailed mission planning and precise satellite orbits and almanac checks can certainly improve positional accuracy (Barber et al., 2008).

The instrument called DMI (Distance Measurement Instrument) is a precise odometer that calculates the distance travelled to improve GPS/IMU processing. It is mounted on one of the vehicle's wheels in some MLS systems (Kingston et al., 2007).

Inaccuracies in the relative orientation of MMS instruments lead to systematic errors when several scanners are used. The accuracy of the relative orientation between mapping instruments needs more attention. For example, if an object occurs twice in the point cloud due to imperfect boresight calibration between two scanners, this will make automatic modelling of the object much more challenging (Kaartinen et al., 2012a). The accuracy of the resulting georeferenced point cloud is highly dependent on GNSS visibility during data acquisition. In addition, the season can affect satellite visibility, for example, when tall trees and buildings are too close to the trajectory.

MMS integrates navigation sensors and algorithms together with sensors that can be used to determine the positions of points remotely (Ellum & El-Sheimy, 2002). To calculate an accurate object ground coordinate from a mobile laser scan, the value of 14 parameters must be found for the single LiDAR scanner system. These parameters are the X, Y and Z coordinates of the GNSS antenna and the orientation angles (roll, pitch and yaw) of the platform, and the three boresight angles from each individual scanner to the IMU body frame, the X, Y and Z lever arm offsets to the IMU origin from each scanner, the scanner mirror angle and the range measurement (Glennie, 2007).

Another feasibility study was performed to determine the object point coordinates by MMS sequenced images using multiple image matching. The coordinates of points of interest can be determined by space intersection of the images, whose interior and exterior orientation parameters are determined from navigation and calibration data. This is much more efficient than manual measurement. However, the factors of scale variations, different fields of view, and occlusion may result in incorrect matching points. An example of incorrect matching problems were shown by (Wang et al., 2011) (Figure 2-3). These problems in matching are scale variation, different fields of view and occlusion. After overcoming image space matching problems, the coordinates obtained by this method have about 10 cm precision and 50 cm accuracy. Accuracy can be improved if the positioning and orientation system of the MMS are improved (Wang et al., 2011).

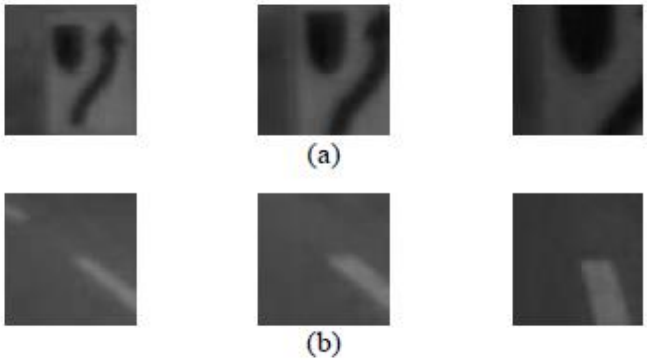

Figure 2-3: Problems in matching. (a) Scale variation, (b) different fields of view (Wang et al., 2010)

A Mobile Mapping System can then be used to generate synthetic facade structures for unobserved building parts. Despite the high geometric accuracy that is feasible for terrestrial point clouds, this data frequently suffers from unavailability of measurements for hidden building parts.

The calibration method used to calculate the lever arm vector collects multiple LiDAR strips over the same road. The lever arm offsets are propagated through the data and can be reduced by analyzing differences between the separate strips (Barber et al., 2008). The boresight angles error can be calculated by carrying out multiple strips over a region and resolving the discrepancy between the orientation of each strip in comparison to the others. These boresight angles can be determined using a least squares adjustment (Glennie, 2009).

MLS point cloud data will be converted to CAD models to update the basemap ground information. This area is still under study and development. However, automated and semi-automated algorithms are continually advancing and being improved. There are many examples of how basemap data can be used for further construction development. They include, but are not limited to, the slope and profile of the road, improvement projects, pavement monitoring, volume calculation and pre-accident condition data (Jacobs, 2005).

Asset Management is considered an important application for MLS, which is also known as inventory mapping (Duffell & Rudrum, 2005). It may involve any street features such as pavements, signage, fire hydrants, traffic signals and light poles. These features can be extracted from the point cloud manually or automatically (Kingston et al., 2007).

The MLS can be used to model building facades. One application of these models is to select the facades with the highest solar potential. This would allow individuals to easily see where solar panels should be placed on their building (Jochem et al., 2011).

2.3.1 Accuracy of mobile LiDAR

In terms of the accuracy and quality control of LiDAR data, many methods have been invented to verify the accuracy of the final point cloud. The accuracy of MLS surveys is very high in open areas. VISATTM, which the University of Calgary in Canada developed, can provide absolute positioning accuracy of 0.3 m and relative accuracy of 0.1 m for object points within

a 30 m corridor, at vehicle speeds of 50–60 km/h (El–Sheimy, 1996; Li et al., 1994; Schwarz et al., 1993; Tao, 1999).

Another method is ground control points adjustment, which uses a system of six base stations and ground control points every 50–80 m distributed over the scanning area to accomplish 1–2 cm accuracy (Ussyshkin & Boba, 2008). Another alternative is a well-georeferenced Terrestrial Laser Scanner (TLS) point cloud to verify the accuracy of the MLS using poles and other features for accuracy validation. The RMSE values were 3.5 cm vertically and 2.5 cm horizontally (Yu et al., 2006).

Haala et al. (2008) demonstrated that the Streetmapper system could produce dense 3D measurements at accuracy of 30 mm in good GNSS conditions. They also reported that, under degraded GNSS conditions, a georeferencing error up to 1 m for the horizontal position could occur.

A permanent test field works well for verifying and comparing the performance of mobile laser scanning systems. (Kaartinen et al., 2012a, 2012b) tested the performance of various LMMS equipped with mobile laser scanners on established urban test fields under good coverage of GNSS. Several commercial (e.g. Riegl, Optech and others) and some research mobile laser scanning systems surveyed the test field using predefined driving speed and directions. The acquired georeferenced point clouds were delivered for analysis. The geometric accuracy of the point clouds was determined using the reference targets that could be identified and measured from the point cloud. The results showed that in good GNSS conditions most systems can reach an accuracy of 2 cm in plane and elevation. The accuracy of a low-cost system, the price of which is less than a tenth of other systems, seems to be within a few centimetres at least in ground elevation determination. This high accuracy of LMMS has led to its application in many surveying and mapping areas. This test result and the detailed comparison between various LMMS will be explained in the section on the evaluation of the LMS system.

Another way to verify the performance of mobile laser scanning systems is by comparing the accuracy of the static RTK-GPS/Total-Station measurement and the MMS mobile on the same road feature. The proposed road feature localization method can be considered valid and effective, as the position error is within 0.3 m (Ishikawa et al., 2006).

Recent studies on MLS systems and their accuracy, as well as environmental modelling completed with MLS, can be found in (Graham, 2010; Kaartinen et al., 2012a; Lehtomäki et al., 2010; Lin & Hyyppa, 2011; Lin et al., 2010; Petrie, 2010) among others.

Schloderer et al. (2010) discussed the accuracy of RTK technique and presented that it was capable of achieving a level of accuracy sufficient to develop a reliable topographic map at a scale of 1:1,750. At this scale, RTK technique achieved a horizontal accuracy of 2 cm and a vertical accuracy of 28 cm.

Kang et al. (2008). discussed the accuracy of mapping using aerial digital camera imagery technique and presented that it presented RMSE of around 18.91 cm in X direction, 18.25 cm in Y direction. As the authors proved, these results are in allowable accuracy and it would be possible to apply digital imagery on a scale 1 to 1,000 in digital mapping.

2.3.2 System calibration

As in any surveying technique, calibration is a vital parameter that is needed for each of the MMS instruments to determine error. Calibration can be defined as “the process of estimating the parameters that need to be applied to correct actual measurements to their true values” (Schofield & Breach, 2007). To achieve the potential accuracy of MMS systems and assurance the accurate multi-sensor combination a careful system calibration must be consider.The system calibration include sensor calibration and related system elements(e.g., the GPS, IMU, and the imaging sensors) (Rau et al., 2011). Therefore, we mean calibrating each component of the MMS such as the laser scanner and the digital camera. Usually, the system provider delivers a recent calibration report that includes the calibration parameter for each instrument. In addition, the displacement and orientation of system components should be calibrated.

Under these good conditions, the remaining differences between the point clouds from scanners can be traced back to imperfect boresight calibration of the upward looking scanner, which can be corrected during post-processing. An example of horizontal data accuracy after post-processing is shown in Figure 2-4 where green represents the areas with the best accuracy, above 0.43 m, while red represents the areas with the worst accuracy.

Figure 2-4: Estimated horizontal accuracy of the trajectory after GNSS/IMU post-processing (Haala et al., 2008)

2.3.3 Data Acquisition and georeferencing

A mobile LiDAR system will often record two channels of data: the 3D measurements from the scene relative to the vehicle (often referred to as intrinsic data) and the vehicle trajectory and orientation (extrinsic data).

Georeferencing (also called registration) is the method of merging intrinsic and extrinsic data to produce a single point cloud that is tied to a given coordinate system. A mapping sensor is

georeferenced when its position and orientation relative to a mapping coordinate frame is known. The integration of MMS data requires a unified model for georeferencing such data. In this context, unification means that the model can be applied to most, if not all, sensor data without the need to account for a different set of parameters for each sensor (El-Sheimy, 2005).

To improve georeferencing process accuracy, a post-processing step is required after all the data and information have been collected. When data processing is carried out to improve position and orientation data, it includes all the calculations needed to create georeferenced points and a point cloud so that the points can be used in different products.

2.3.4 Integration and data fusion

Data fusion generally means that data from various sources and types are merged to provide a versatile resource for mapping applications. Model integration and data fusion are comprised of all the steps required to extract the desired result from the georeferenced images. If the objective is to extract 3-D coordinates of objects in the images, then the application of geometric constraints, the handling of redundant images of the same object and the fusion of data of different types and quality are important considerations. An example of a mobile mapping system is shown in Figure 2-5, which uses digital images and laser profile data for the imaging component and GPS, INS and ABS (Anti-lock Braking System, odometer type device) data for georeferencing the two other data types (El-Sheimy, 2005).

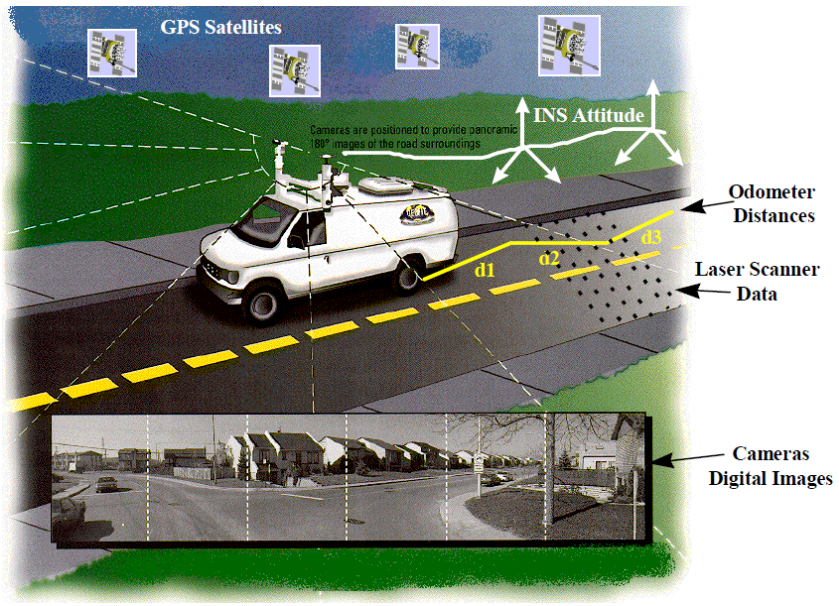

Figure 2-5: An Example of data fusion in close-range applications (El-Sheimy, 2005)

2.3.5 Data quality control

Quality control usually has a real-time component and a post-mission component. GPS/IMU data quality is typically the main factor to obtain the highest accuracy for a LiDAR point cloud

(Ussyshkin & Boba, 2008; Yoo et al., 2010) demonstrate how a wrong scanner orientation on the mobile platform can have drastic effects on the quality of data captured.

Many methods have been employed to verify the accuracy of the final point cloud. For example, ground control points, or already georeferenced points are used to verify and evaluate the accuracy of MLS data. Additionally, (Graham 2010) recommends that final quality control is performed by someone other than those involved in registering the dataset.

2.3.6 Automated extraction of basemap features from a Mobile LiDAR Point Cloud

The Mobile LiDAR System provides good, accurate coverage of 3D points in urban areas, which is useful for many mapping applications. As an example, the data can be used to extract geometric features like windows or doors on the captured building facades (Haala et al., 2008). Also to extract the building features by using Mobile LiDAR to define the design of doors and window. Also to use the photogrammetric to have more detail about frame of this features (Becker & Haala, 2007).

Usually, feature extraction is the first step for basemap update, 3D city modelling and street-scene modelling. It took place after capturing spatial data in urban areas at the street level. Therefore, many algorithms are being developed for automatic and semi-automatic feature extraction from a point cloud. Most are semi-automatic and require significant user interaction to validate the results. Several structures were introduced for features, including how they can be automatically detected and converted to shapes for use in GIS platforms (McQuat, 2011).

Feature extraction usually starts by separating the point cloud points to ground (road and curb) and non-ground points such as pole and signs. Non-ground points are separated based on their height threshold. Once the separation done, the road elements can be extracted from the non-ground points as explained in the next paragraphs. Zhang, (2010) proposed a robust and real-time road and road-edge detection technique using LIDAR to identify road regions and road-edges. In this study, the road segment and road-edge points are identified, then the identified 3D road-edge points are further projected and validated on the 2D ground plane.

Hu et al. (2004) proposed a road-marking extraction algorithm of “stand for what” data. It consists of curb-based extraction of road surfaces, generation of georeferenced intensity images with a histogram equalization-like strategy and the extraction of road markings using point-density-dependent, multi-threshold segmentation and a morphological closing operation.

The separated points are further segmented to remove non-road points based on their height threshold. The outlines of road markings are extracted from the segmented points using semantic knowledge of road markings. The results presented in (Yang et al., 2012) demonstrate that the method was very promising for automatic extraction of road markings from LiDAR point clouds collected by a land-based mobile LiDAR system. This is a method for extracting road markings in large volumes of MLS datasets that has been effective since the time of the study.

A complete survey was carried out in Xiamen Island, China, Guan et al. (2014). The Figure 2-6 shows examples of road markings extracted from the datasets, along with the extracted road markings overlaid on the GRF image.

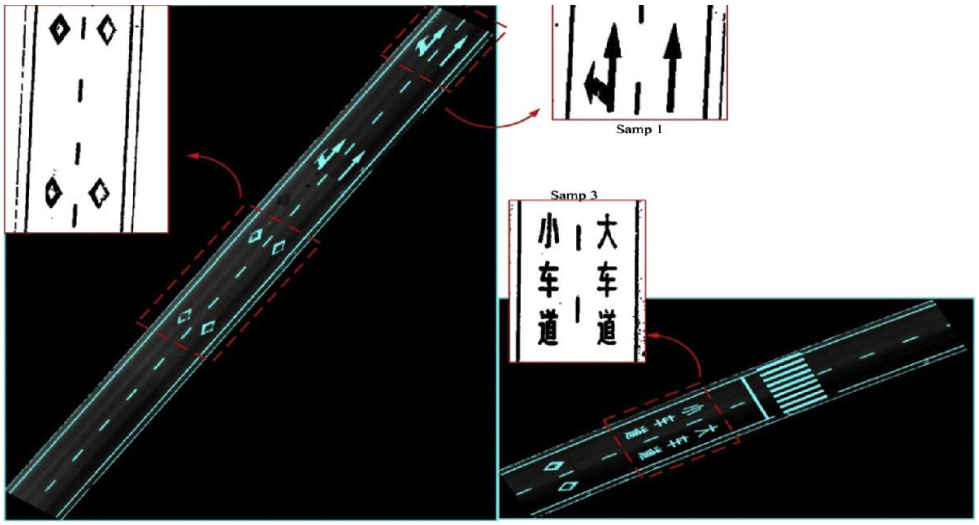

Figure 2-6: The final results of road markings overlaid on the georeferenced intensity images: (left) Huandao Road, Xiamen Island, China and (right) ICEC International Conference and Exhibition Center datasets (Guan et al., 2104)

Che et al. (2019) recently review and summarize the state of the art for MLS data processing approaches, including feature extraction, segmentation, object recognition, and classification. The review includes MMS data processing with relevant generalized algorithms for feature extraction and segmentation. As per their review, the approaches that widely used for object recognition and classification, are including; 1) Hough Transform (originally developed for detecting lines in 2D imagery), 2) Random Sample Consensus (RANSAC, applied to detect pre-defined geometric primitives), 3) Principal Component Analysis (PCA, is a data analysis technique that has been widely used for feature extraction from point cloud data), 4) Fast Point Feature Histograms (FPFH, widely used in classification and registration), 5) Region Growing, Connected Components, and Supervoxelization (approaches used to segment the LiDAR data).

Toa et al. (2001) used Model-based feature extraction to extract the road centerline, lane markers, and street light poles. Also by using the several images for matching can be help to achieve more reliable accuracy which to improve the geometry of the photogrammetric beam connection. In additional in this research used "shape from image sequences" to automatic re-define of road centerlines.

Once the roads have been extracted, there are several methods for extracting the main urban elements. (Yokoyama et al., 2013) used Principal Component Analysis (PCA)-based methods to detected pole-line objects from irregular point clouds. The extraction of pole-like objects and tree trunks from irregular point clouds were the focus of other studies (Brenner et al., 2008; Chen, 2007; Guan et al., 2015; Jaakkola et al., 2010; Lehtomäki et al., 2010; Yokoyama et al., 2013).

Many studies worked on extracting different features and objects from the mobile laser scanned point clouds. Pu et al. (2011) and Yu et al. (2015) discussed methodologies to detect light poles from LiDAR point cloud. Both methodologies classified the generated point cloud into categories, then removed the ground points to reduce the data size for easy use and processing. (Pu et al., 2011) used the Connected Components approach, one of the object recognition and classification approaches. Their study classified the generated point cloud into three larger categories: ground surface, objects on ground, and objects off ground point cloud.

Based on characteristic such as size, shape (man-made objects often have regular and common shapes), orientation and topological relationships these objects (on ground) are assigned to more detailed classes. Traffic signs, light pole, trees, building walls and barriers are examples of these detailed classes.

The poles are recognized using two methods:

1. The regular method which analyses the size (2D radius and height), position and orientation. Trees and small traffic poles in the middle of the road are not recognized by this regular method because it is shorter than the height constraint (1 m).
2. Second method is, percentile based pole recognition algorithm which proposed in their study. This method has the advantage to exclude disturbing structures, which might occur on the bottom or top of the object (e.g. tree crowns or lamps or concrete base) while detection.

The methodology of Yu et al. (2015) proposes a semi - automatic algorithm for extracting street light poles from the generated point cloud. As shown in Figure 2.7 presents an algorithm flowchart to extract street poles from point cloud data. A series of road profiles is generated along the vehicle's trajectory. Then an algorithm rapidly detects and extract curblines (curbs that are usually located at a height of 10–20 cm above the road surface) and used to segment the point-clouds into road and nonroad surface points using a voxel-based elevation filter. These filtered points are clustered into groups based on a Euclidean distance clustering method (Euclidean distance clustering approach used to organize the discrete points into clusters that represent individual objects). Using the knowledge that light poles always have some geometric constraints, such as height, low-height clusters are eliminated to reduce computational complexity. The remaining clusters that contain more than one object are further segmented using a normalized cut segmentation method (NCut segmentation in Figure 2-7) to segment these clusters in order to obtain separated objects. Finally, light pole extraction algorithm is used to identify whether this object is a light pole based on the pairwise 3-D shape or not.

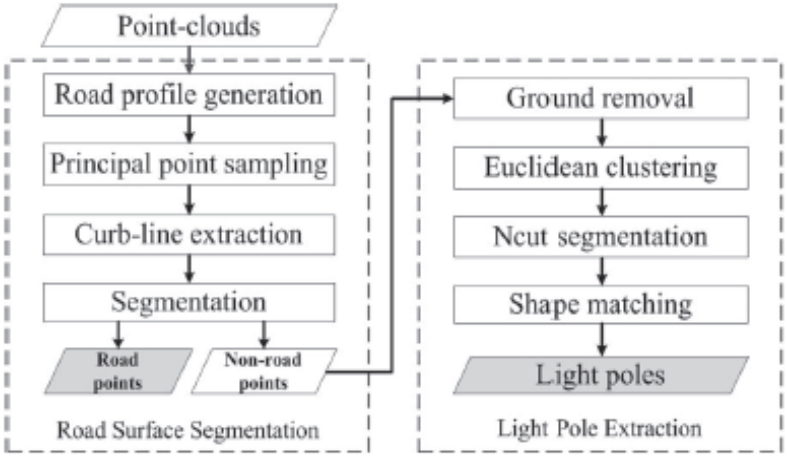

Figure 2-7: Algorithm flowchart to extract street poles from point cloud data (Yu et al., 2015)

Most 3D urban furniture features can be extracted automatically with a high success rate, except manhole covers. Manholes and sewer wells in urban areas are used to conduct rainwater, drainage, power and telecommunication cables, among other elements. They are usually protected with a metal cover to keep things from dropping into the wells. However, if the cover is removed or broken for any reason, manholes become hazardous to moving cars and pedestrians. Therefore, efficient, cost-effective means and methods for monitoring potential road disasters are needed urgently. In addition, the automatic identification of manholes can be affected by occlusion (due to traffic, vegetation, parked vehicles, etc.), and differences in light exposure due to rust and dirt (Yu et al., 2014a).

Manhole cover localization is a challenging problem in the feature extraction process. Moreover, other structures such as drainage covers (Hu et al., 2011) may confuse the system. The number of false detection and missed manhole errors must be very low for automated methods to be useful at all (Yu et al., 2015). This is the main reason why human operators currently carry out most of this work. A previous study of (Timofte & Van Gool, 2011) described for the first time a system based on vision that was used successfully for the task of manhole mapping. The study focused on the automated extraction of manholes and curbs from images obtained from the point cloud

Yu et al. (2014a), Yu et al. (2014b), and Yu et al. (2015), instead of processing road surface point clouds in 3-D space, proposes rasterize the road surface points into a 2-D georeferenced intensity image through inverse distance weighted interpolation (IDW). However, Yu et al. (2014b) improved the IDW method and developed a new strategy to generate the georeferenced intensity image. Figure 2-8 present the segmented road surface and the generated georeferenced intensity image for (Yu et al., 2014b; Yu et al., 2015) respectively.

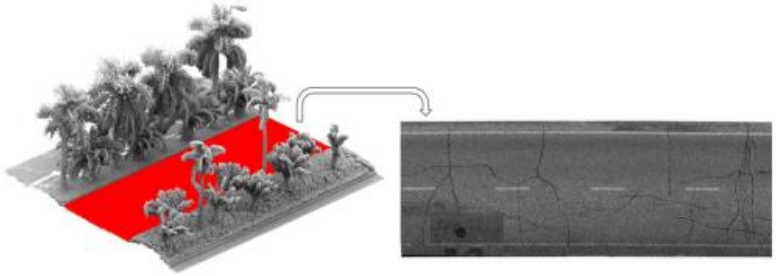

Figure 2-8:Mobile LiDAR point cloud with segmented road surface in red(left). Generated georeferenced intensity image of the road surface point cloud (right) (Yu et al., 2014b)

After the generation of the2-D georeferenced intensity image (Yu et al., 2014b) applied the proposed marked point process based detection algorithm to them to detect road manhole and sewer well covers using the reversible jump Markov chain Monte Carlo (Fan & Sisson, 2011) (RJMCMC) algorithm (Green & Hastie, 2009). The majority of the manhole and sewer well covers were detected. The problems appear with dark spots in the image (false positive) or regions are too bright (undetected manholes).

The study carried out by Tatoglu and Pochiraju (2012) showed the different response to the absorbance of the laser beam, and in consequence to the intensity, of the materials aluminum (Al), copper (Cu), foam (grey and white), steel and wood. Therefore, intensity is a relevant piece of information to segment the point cloud and classify features.

Intensity is used to classify materials in many applications. One example in cultural heritage can be found in (Núñez et al., 2008). In this case, the intensity is used to highlight spaces among stones in a wall, which are difficult to detect through images.

Balaguer-Puig et al. (2017) sought to determine the mathematical relationship between TLS intensity values and colorimetric data in the point cloud through the use of a color chart. The main objective was to use the color characteristic to better define feature details. It was found that the relationship between intensity values and luminance (the Y color value in the CIE color space) contributes to correcting the intensity values. This correction increases contrast and allows better definition of the details compared to the initial intensity values.

In Yu et al. (2015) based on the generated orthoimages a supervised deep learning model is developed to construct a multilayer feature generation model describing the high-order feature representation of a local image patch. Next, a random forest model is trained to learn mappings from high-order patch features to the probabilities of the existence of road manhole covers centered at specific locations. Finally, road manhole covers are detected based on the combination of these models with better results in correctly detecting different types of road manhole, relatively less false positives and taking less time than (Yu et al., 2014b).

Previous studies by Yu et al. (2014a, 2014b) and Yu et al. (2015) detected both circular and rectangular manholes from mobile LiDAR data. The detection task was achieved by rasterizing the road surface segments into a group of georeferenced intensity images in both cases. Then the process differed. In Yu et al. (2014b), the marked point process of disks was simulated and optimized by rasterizing road surface points into a 2D georeferenced intensity image based on

the intensity information of the laser points. In Yu et al. (2015) it was completed by generating a multilayer feature model and random forest model.

Another study combines camera images collected from the MMS with the point cloud data to detect manholes. Wei et al. (2019) used high-density laser-scanned point clouds and ultra-high-resolution ground images that collected by the MMS to automatically detect manholes covers. Fist, the conversion of 3D laser-scanned point cloud data into intensity-based images was applied and ground orthophotos were generated. Second, the manholes covers were extracted from both the intensity images and ground orthophotos. Finally, acquisition of manhole maintenance and ownership information was identified

Commandre et al. (2017) presents a method for automatic detection and localization of manhole using very high-resolution aerial images by deep convolutional neural network. They concluded that manhole cover localization is a challenging due to the variance of object colours, non-uniform background, shadows and being small objects to be detected from aerial images.

Generally, in manhole detection, most researcher uses point cloud data or images data captured by the cameras that mounted above the MMS vehicle. Wei et al. (2019) presents a research that detects manholes by combining both point cloud and ground images.

Regarding buildings' extraction, a study completed by San and Turker (2010) proved that high resolution satellite images have become quite valuable data sources for geographic information extraction. An approach was developed for automatic extraction of rectangular and circular buildings from high-resolution satellite imagery using the Hough transform. The results indicate that high-resolution satellite imagery has great potential in building extraction. In the case study, delineation of the building boundaries was carried out from a panchromatic building patch image, which is generated by masking classified building areas. Therefore, the success of the developed building extraction approach is dependent on the success of detecting building patches. If building patches are not detected accurately due to the characteristics of the land use classes, the buildings may not be delineated correctly. This is because of two reasons; some of the buildings are quite small or the buildings, which are close to each other but not adjoined, were delineated erroneously as a joint building.

By confining the search area over the candidate building patches, the building delineation process becomes easier as unnecessary edges are not included in the process. Therefore, the processing operations are carried out over the building areas only. The algorithm developed in this study was tested in residential and industrial urban areas that contain different shapes and dwelling types. In Figure 2-9, the extracted building boundaries are illustrated for urban blocks that contain (a) rectangular industrial buildings, (b) rectangular residential buildings and (c) circular residential buildings.

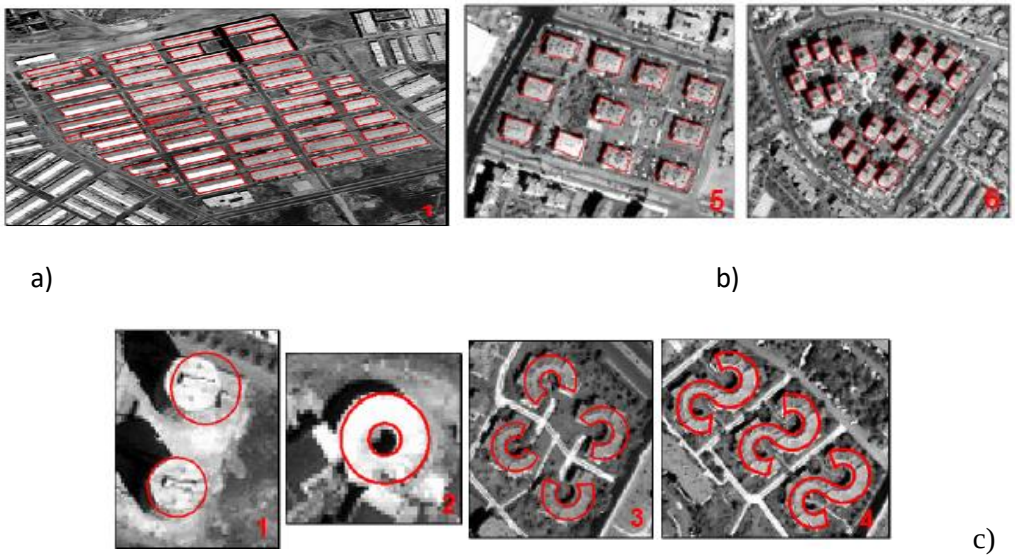

Figure 2-9 : The delineated building boundaries for urban blocks that contain (a) rectangular industrial buildings, (b) rectangular residential buildings, and (c) circular residential buildings (San & Turker, 2010)

For rectangular residential buildings, the average Building Detection Percentage (BDP) and Quality Percentage (QP) values were 95.34% and 79.05%, respectively. For circular residential buildings, the average BDP and QP values were 78.74% and 66.81%, respectively. The results prove that if the mutual lines of the buildings are parallel and the angles between the adjacent lines are perpendicular, or if the buildings are circular or curved, the Hough transform is an efficient technique.

For the industrial buildings, the study obtained quite satisfactory results with average (BDP) (completeness) and (QP) (Correctness) values of 93.45% and 79.51%, respectively.

Alshehhi et al. (2017) discusses a single patch-based Convolutional Neural Network (CNN) architecture for extraction of roads and buildings generally. The study extracts roads and buildings from high-resolution satellite imagery. The method does not require any pre-processing stage. Low-level shape features for building regions for example, (compactness and density) are integrated with CNN features to and complete irregular boundaries of building regions. Although the experiments prove that the proposed method achieves good performance in the extraction process, it required additional processing to outline boundaries more accurately. Same as the previous study, some adjacent small buildings appear as one connected region, which are difficult to separate from each other. However, this study achieved correctness percentage higher than those from the previous study (94.6%) of San and Turker (2010). Maltezos et al. (2018) proposed a methodology to extract urban building using airborne LiDAR data by applying deep Convolutional Neural Networks (CNN) architecture for classifying building structures from LiDAR data. However, these techniques are not allowed

in all the areas and countries since sometime there are flight restrictions due to proximity to military zones, border between countries, etc.

2.3.7 Application of Mobile Laser Scanner (MLS)

Today, a considerable amount of research is being conducted on using MLS (as shown in Figure 2-10) to construct geographical information databases, with the introduction of the mobile laser scanner and the development of many software applications for MLS. For example, Ishikawa et al. (2006) have studied the automatic production of road data by linking data from the mobile laser scanner and digital camera of the MLS.

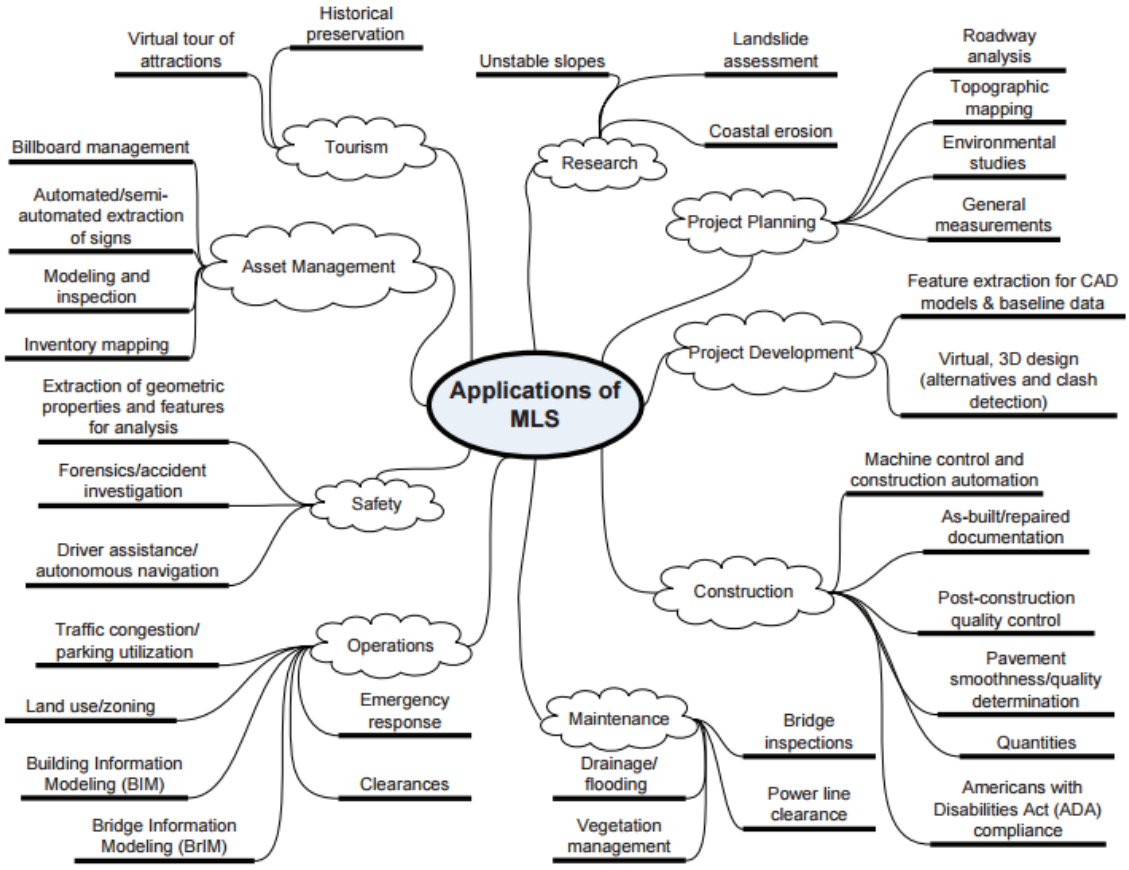

Figure 2-10: Transportation applications of mobile LiDAR (current and emerging) (Olsen et al., 2013)

Results of experiments on a point cloud with almost a billion points suggest that the system is scalable and provides fairly accurate results for cases in urban environments. The use of the method to collect data from other cities and countries, as well as the possibility of extending it to rural environments, is an interesting direction for future research (Golovinskiy et al., 2009).

As-built surveys are also an important application for MLS, as the infrastructure life cycle passes through various stages including planning, design, construction and maintenance. As-built data that is delivered to the audit authority should match the planning drawings. As-built scanned records introduced by mobile LiDAR can provide considerably more details and higher resolution than traditional methods (Singh, 2008).

2.3.8 Evaluation of a LiDAR Land-Based Mobile Mapping System

The task of evaluating and comparing mobile laser scanning systems is challenging (as mentioned earlier) as the accuracy of the georeferenced point cloud is highly dependent on GNSS visibility during data acquisition and satellite geometry is constantly changing.

Infrastructural mapping and monitoring has become an integral part of academic, commercial and government needs. Mobile Mapping Systems (MMS) play an important role in monitoring changes in the environment. Recent research studied and evaluated the LMS for these purposes.

Bitenc et al. (2011) is one recent study monitored sandy coasts for defense against flooding of the hinterland. As the most dramatic changes to the beach and the first line of dunes happen during storms, it is important to assess the state of the coast immediately after a storm. This is costly and difficult to consolidate with Airborne Laser Scanning (ALS). So, the performance of a Land-Based Mobile Mapping System (LMMS) in mapping a 6-km stretch of sandy Dutch coast near the municipality of Egmond was evaluated. Figure 2-11 presents an overview of the steps to evaluate the quality of the LMMS data and products. The acquisition took place on 27 November 2008 at low tide. Within two hours, a 6-km stretch of beach 180 m wide had been covered. The point cloud consisted of about 56 million laser points. A smaller representative test area of 213 × 101 m was chosen. The data set consisted of 1,220,825 laser points. Each record of a laser point had 15 attributes: nine original attributes written in the *.las file of laser points and six additional attributes. The attributes were: 3D laser point position X,Y and Z, intensity I, class number C, scan angle Θ, time of point acquisition T, drive-line number DL and scanner number SC, range R, incidence angle α, footprint diameter Dfp, range error due to the scanning geometry δR, measuring precision σZm and geometrical precision σZ, δR. In addition to the 3D laser point data, the data of trajectories given in (*.trj) file format was used. The methodology chosen for this research consisted of several steps.

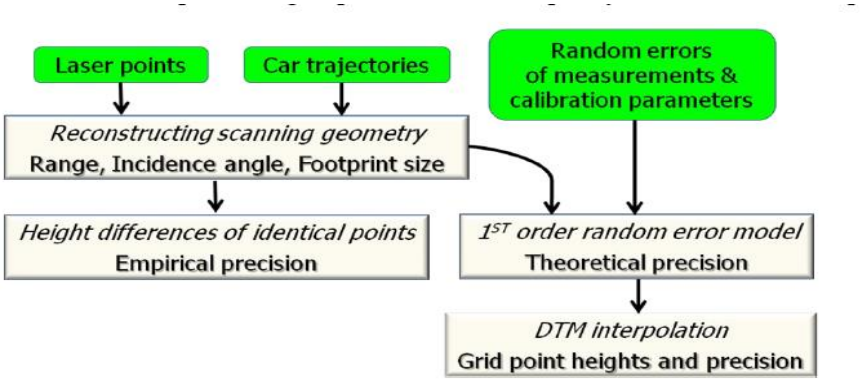

Figure 2-11: Overview of steps to evaluate the quality of LMMS data and products (Bitenc et al., 2011)

The median a priori measuring precision was 2.88 cm, which was dominated by the GPS error. The QC results showed very small numbers: the average precision of the height differences between identical points lying on the horizontal plane was 3 mm.

A comparison of the theoretical and empirical precision of height differences revealed large differences. This is because the theoretical precision also includes the GPS/INS positioning error and is therefore considered absolute precision. In contrast, the empirical precision accounts for the relative precision between two laser points. Thus, choosing the nearest neighbors might already minimize the empirical error.

Another study focused on evaluating the geometrical properties of laser point clouds collected by various commercial and research-based MLS systems in good GNSS conditions, on an established urban test field (Kaartinen et al., 2012a). The test field was implemented in Espoonlahti, about 16 km west of Helsinki. The test field was one block around the Lippulaiva shopping mall covering 1700 m of road environment.

Planimetric accuracy was evaluated by measuring the reference targets in the received MLS point clouds and then computing the differences in easting and northing. The planimetric accuracy of the tested MLS systems in two driving directions is shown in Figure 2-12. The left column stands for counter-clockwise, CCW, and the right column for clockwise, CW. The maximum standard deviation value is 3.9 cm in the Roamer system. The minimum value was 1.2 cm and was found with the Riegl system. The evaluation accuracy for the Optech Lynx system was around 2.6 and 2.7 in the two driving directions. Our study on the basemap update requires an accuracy from 2–5 cm, which means that the Optech Lynx system can provide the required accuracy.

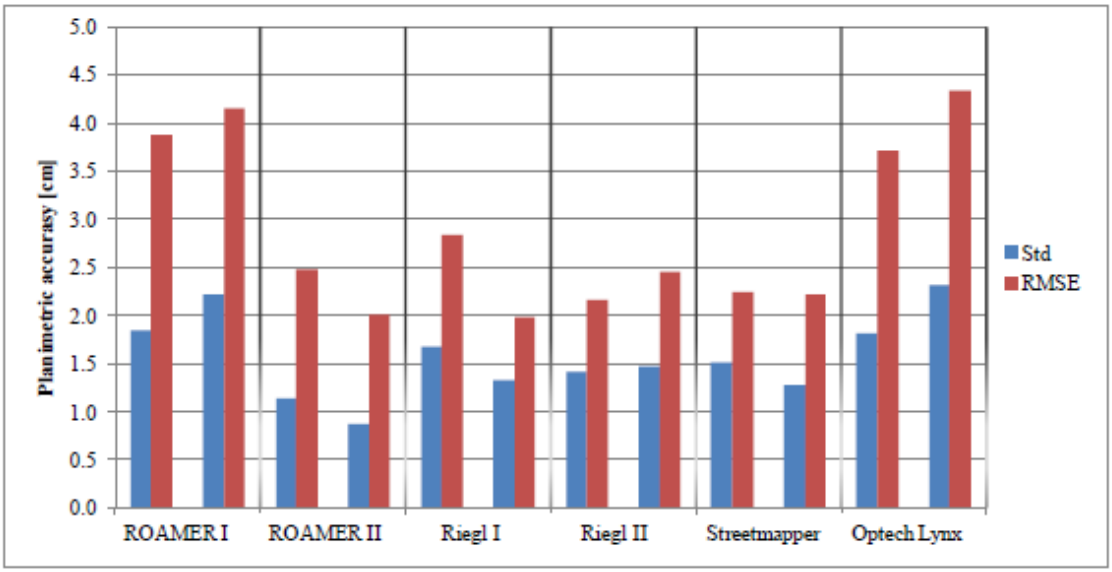

Figure 2-12: Planimetric accuracy of the tested MLS systems in two driving directions (Kaartinen et al., 2012b)

For the planimetric accuracy, the maximum standard deviation value was 2.3 cm in the Optech Lynx system, while the minimum value was 0.9 cm and was found with the Roamer system. The maximum root mean square (RMS) value was 4.3 cm in the Optech Lynx system, while the minimum value was 2.0 cm and was found with the Riegl system. The planimetric accuracy (standard deviation) for the Optech Lynx system was around 1.8 and 2.3 in the two driving directions. As mentioned before, our study on the basemap update requires an accuracy from 2–5 cm, which means that the Optech Lynx system can provide the required accuracy.

3. Basemap updating

The municipal system generally plays a central role in the Spatial Data Infrastructure program of all cities, especially as basemap datasets are critical to the work of most, if not all, communities. From this, one key requirement emerges: a smooth two-way flow of data from municipalities to the rest of the community and back from the community to the municipalities.

Spatial data should be updated in a timely manner to reflect continuous changes, since this information is needed for all government institutions and communities to improve the quality of decision making about urban management, infrastructure and construction projects. In addition, up-to-date spatial data is needed for comprehensive maintenance and management systems for road infrastructure purposes. The update process could be significantly reduced by introducing algorithms that allow automatic steps.

In recent decades, basemaps were mainly updated using aerial photography. Expert, qualified staff members were required to perform this task, as well as staff who were properly trained in the updating of basemap datasets or the importance of keeping datasets current.

The need to find an automated, more efficient, faster method for frequent updating is due to the difficulty and cost of updating basemaps using aerial photography. A new methodology is also needed to avoid the difficulty in sending surveyors or aircraft to borders or dangerous areas.

The cartography used for urban management should include a high level of detail, so a suitable scale is 1:500. At this level of detail, all buildings and urban features are represented in the map, including signs, poles and manholes. Therefore, it is essential to extract these elements automatically. Under normal circumstances, 1:500, 1:1000 and 1:2000 are the three scale products that are used in urban infrastructure mapping. These maps are produced and updated by country mapping departments (Zhu et al,. 2013). Therefore, obtaining the required dataset involves new terrestrial methodologies to cover the entire territory and capture all the urban elements in the field with fewer staff. Hwang J et al. (2013) used mobile LiDAR system to update and enhance the accuracy of national basemap in South of Korea. He also to analyzed the maximum range cover of mobile LiDAR system which help to align with standards of National Base Map production for map scale 1:1000 with define the feature can be update by this technology.

As mentioned before, basemaps are regularly constructed and updated using aerial photogrammetry. This process updates large areas and takes place every few years, depending on the economic feasibility of aerial photogrammetry in each country, the seasonal conditions and the weather conditions. High resolution satellite imagery is also a source of images that is available to civilian public users, and many proposals have been made concerning map updating. A single satellite image covers a large area and has a reduced visit time compared to aerial photogrammetry. Unmanned airborne vehicles (UAV) also have a long history in military applications. The use of ultra-light UAV combined with compact digital cameras generates mapping products such as Digital Elevation Models (terrain or surface) and orthoimages.

However, aircrafts cannot be used in all localizations, especially in border areas when there is a conflict between countries. Therefore, another method is needed to update basemaps, especially in fast-growing cities to meet the demand for geographic information and applications that are based on location activities. A good option is the Mobile Mapping System (MMS). This system can be used to frequently update topographic details and urban furniture in the basemap in these areas. Furthermore, it improves the updating of the basemap. The process consists of complete planning of the project, which involves selecting and studying the required area, mission planning and base station selection. The result of the data collection is a point cloud that needs to be managed to extract road and building features and update the basemap. A quality control process is applied to the output to ensure the accuracy of the results.

3.1 Mobile Mapping System

The common workflow for some municipalities to update their basemaps starts with paperwork. For example, when a landowner or company requires digital data exchange permission from the municipality, they need to provide their working plans (Figure 3-1, left). These plans need approval from the municipality. Before approving the plans, the municipality sends surveyors for field data acquisition and data verification purposes. Data field acquisition consists of two steps: the surveyor collects objects and measures their characteristic points (e.g. buildings, road signs, power lines and manhole covers) and qualifies them by typing in a code or comment. Back in the office, data is imported into the software that updates the basemap.

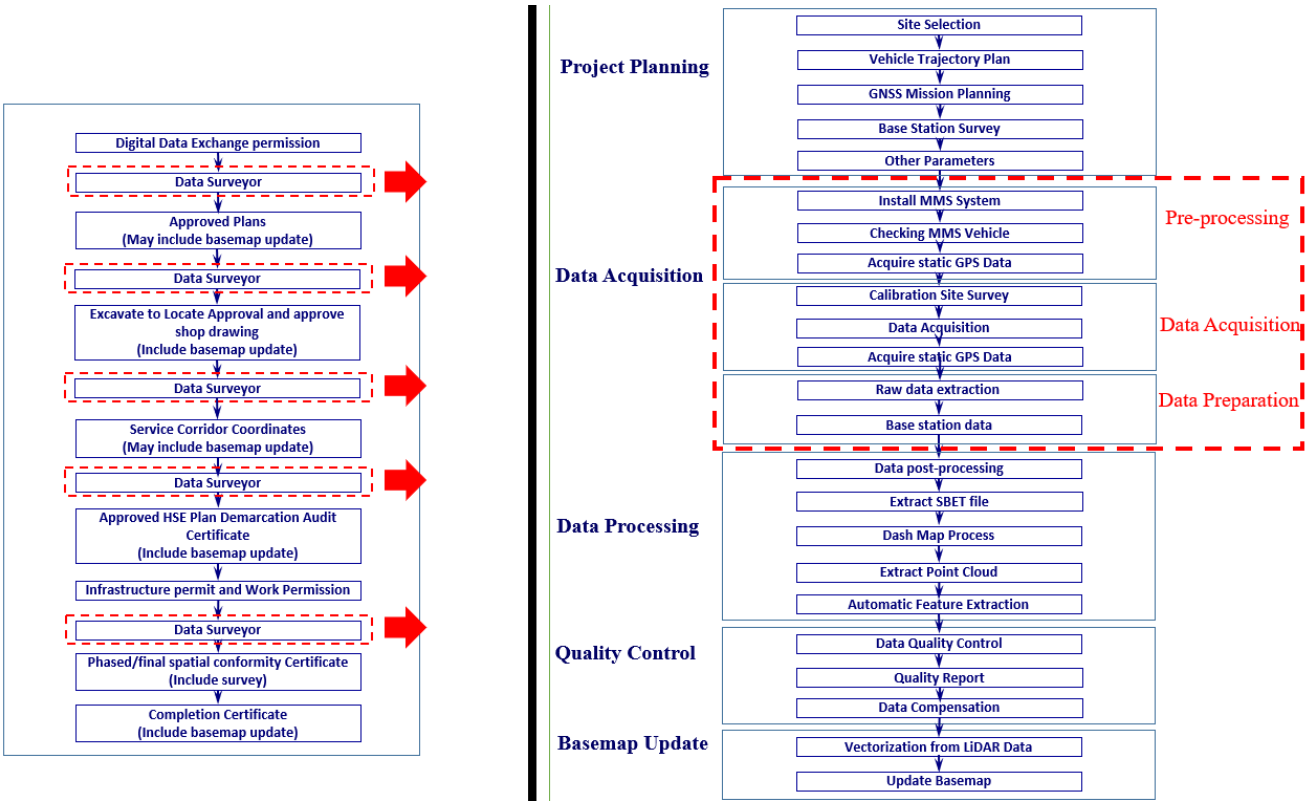

Figure 3-1: Current workflow of basemap updating (left) and proposed workflow with MMS (right)

The proposed methodology (the workflow on the right of Figure 3-1) introduces the use of MMS and automates some processes of the current workflow of updating basemaps (see the red boxes in Figure 3-1, left). The process covers complete planning for the project including selecting and studying the required area, mission planning and base station selection. Then, data is acquired using the LiDAR Mobile Mapping System (MMS). The data is collected and processed using software to extract a point cloud file. Subsequently, the quality control process is applied to the output to ensure the accuracy of the results. This point cloud file is used to extract road and building features, in order to update the basemap. The methodology uses the current daily transaction service in the municipality. The existing service can be taken as an example and the use of LiDAR in this service can be compared with the traditional survey method.

A more detailed general workflow for the MMS (Figure 3-2) starts with the planning process. The purpose of this step is to plan the required strips to cover the survey area. Normally, this phase is supported by applications such as Google Earth to design the strips using the application's drawing capabilities. Additionally, GNSS observation plans are used to make sure that the number of satellites, dilution of precision (DOP), cut-off angles of the GNSS antennas, and ionosphere activity are within acceptable ranges before the start of the data acquisition mission.

The second step is data acquisition. During this step, the system is used to plan and control the survey and display the route plan and system status information. Internal software is used to display useful positioning and GNSS information during the survey, and it applies lever arm measurements to the positioning and GNSS data. Another software program used during the survey is a real-time point cloud viewer, to control the capture process. After the data acquisition, the following information is available: point cloud, range, image data, positioning and the GNSS data collected. Positioning and GNSS data are processed to create a final trajectory and then used to geo-reference the point cloud. After that, a 3D point cloud with LAS file format (the *ASPRS* LIDAR data exchange format standard) is created.

Specific software is used to extract raw camera images collected during the survey. To calibrate the boresight, special software is used to boresight the sensors by aligning two sets of control points and LAS files to calculate the calibration corrections. Once the camera images have been processed, the RGB values for each pixel are used to give color to the point cloud. In the current system, the final step in the processing is importing the point to a drawing tool to start the digitizing process, with CAD or GIS software.

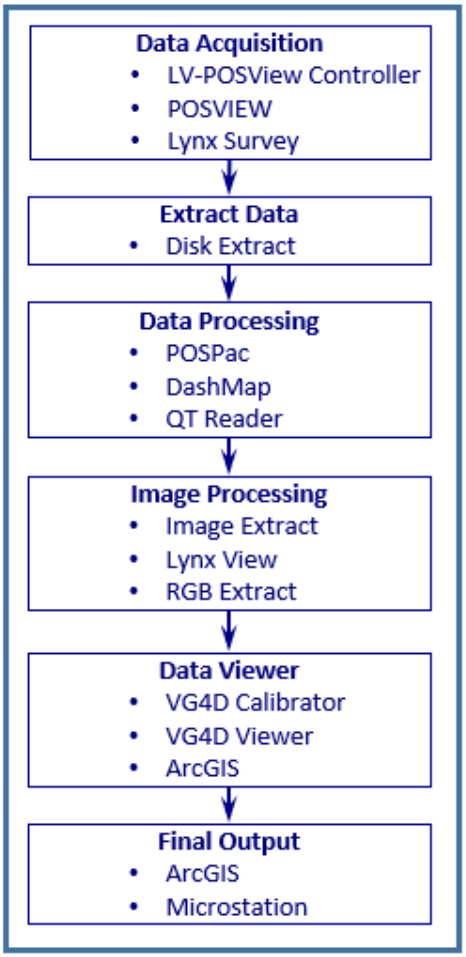

Figure 3-2: Workflow of the Mobile Mapping System with examples of software for each step.

Proposed methodology for basemap updating

3.1.1 Mobile LiDAR Mission Planning

The mission planning must establish the trajectory to be driven. There are several phases in the process of achieving this, the most important being GNSS mission planning. This generally includes checking the satellite almanac to guarantee good geometry for the collected data. This step studies the expected satellite positions and numbers that will cover the selected area during the data collection process time. During the data collection, there will be a minimum of five satellites in view for the GPS Control Stations. Additionally, the maximum PDOP value during acquisition will be less than five (<5). If the PDOP is expected to be very high, at five or six, the data collection time should be changed. In addition, the ionosphere and tropospheric parameters can be considered. Accordingly, it will be easier to choose the proper time for the data acquisition.

A site reconnaissance should be completed before the data acquisition to fine-tune the mission plan, in case of any obstacles on the site such as high-rise buildings or dense vegetation. Thus, it can be confirmed that the area meets all requirements.

The selected site should not include obstructions to the satellites, so it is preferable to avoid areas with high buildings and trees. Once the project area has been selected, an application such as Google Earth can be used to determine the road drive path, the planned trajectory to help the survey team identify the start point, the planned trajectory and the end point. The vehicle speed should be identified during the planning phase to determine the maximum speed in order to obtain the required density.

During the survey, the data is stored on the hard drive. Therefore, before beginning the survey, it is necessary to ensure that there is enough storage on the hard drive. The manufacturer should provide a way to calculate the storage area on the hard drive according to the required data acquisition. The weather forecast should be checked before the survey to ensure good atmospheric and driving conditions for the survey time and location.

3.1.2 Data Acquisition

The process of data acquisition includes the MMS system calibration. This step should be completed after every installation (including the first installation) or after modifying the position of instruments relative to each other.

Some parameters that need to be measured in the installation process are the distance between the distance measuring instruments (DMI) center with respect to the inertial measurement unit (IMU) center (Lever arm measurement 1), the distance between the primary GNSS antenna and the IMU center, as well as the distance between the two GNSS antennas and the DMI scale factor.

The lever arm (which is the measurement between the physical 3D offset between the navigation center and the laser center) and the boresight angles (which are the angular offsets between the laser[s] and the IMU) are the main source of errors in the MMS. Accurate IMU data can be provided by driving the survey vehicle in a figure of eight. Therefore, the provider should be asked for a full calibration report for the system to estimate accuracy, as well as a detailed calibration procedure.

Some parameters need to be checked in the MMS vehicle before starting the survey. The batteries should be fully charged, the gas tank full, all the vehicle lights must be functioning properly, the tires should be inflated to an acceptable pressure, the fans underneath the LiDAR sensors must be clear and able to rotate without obstruction and the cables must be securely connected.

During the data acquisition, a certain procedure should be followed to make the data processing phase easier and to protect the data from error propagation. The in-mission procedure includes, but is not limited to:

1. Monitoring the GNSS solution to keep it in a fixed state throughout the mission time.
2. Collecting static data for five minutes before and after the data acquisition, which would help in post-processing to fix ambiguity and lock the satellite.
3. Monitoring the system sensors to keep the temperature within the operating temperature stated in the system manual.

4. Monitoring the storage of the system to avoid data loss by monitoring the storage consumption in the system.
5. Ensuring that the planned strips are carried out properly and cover the required area with no data gaps by comparing the mission plan strips with the actual collected strips.
6. Keeping the IMU in the adjusted mode i.e. getting accurate measurements by doing the eight-figure calibration when possible.
7. Handling GNSS signal absence by collecting static data for five minutes when the GNSS signals go down.

Five minutes of static GNSS observation are necessary to calculate the distance between the antennas in the system to allow the GAMS (Azimuth Measurement Subsystem) solution to work effectively. GNSS GAMS is a unique feature of POS MV software that allows the system to achieve exceptional accuracy in the measurement of heading. The GNSS sampling rate is 1 Hz, which means the antenna will log one GNSS signal every second. The signal is logged once in the internal flash drive in the system and once in the acquisition computer. These parameters guarantee sufficient accuracy in positioning to update the basemap. The camera frequency is adjusted to 1 Hz to ensure that one photo is taken each second.

Another study was taken as a reference to set the vehicle speed during the survey as follows. The vehicle-driving speed through populated urban areas was between 24 and 32 Km/h, while the collection speed through outlying rural areas was 40 to 50 Km/h (Leslar et al., 2010).

When the vehicle moves slowly (at a velocity of 5 km/h to 40 km/h) or if the object is near the vehicle, the 3D point cloud is dense. However, the density of a 3D point cloud decreases as the vehicle speed increases or as the vehicle and the object move farther apart (Ishikawa et al., 2006). The system allows scanning at a speed of up to 100 km/h and obtains accuracy better than 5 cm with up to 7 mm resolution (Conforti & Zampa, 2011).

3.2 Data Processing

LiDAR data processing algorithms have become increasingly popular in the geospatial arena and each vendor in the industry is trying to provide the best state-of-the-art classification and feature extraction techniques to enable manipulation of point cloud data and to make use of this data in everyday spatial work.

Figure 3-3 shows the suggested workflow for feature extraction. This workflow started with the LAS file that had been extracted from previous trajectory data processing. Since point cloud data is a huge dataset with intensive points, an algorithm is essential to handle the data. This workflow should be started by dividing the data into smaller groups called tiles. A tile is a small manageable part of the dataset obtained by dividing datasets into small portions to enable the computer to manage the data easily and more efficiently. The second step is the data thinning process. This process uniformly reduces the number of points in the point cloud, which helps to manage the size of the huge dataset. The third step is data classification. Object-based classification methods have two main steps: segmentation and recognition. In the Segmentation process, raw LIDAR points are separated into two groups: ground points and no ground points.

In the recognition process, features are extracted from the point cloud. The fourth step is data cleaning to remove unnecessary points after applying certain filters in the feature extraction process. Finally, vectors are drawn to update the basemap.

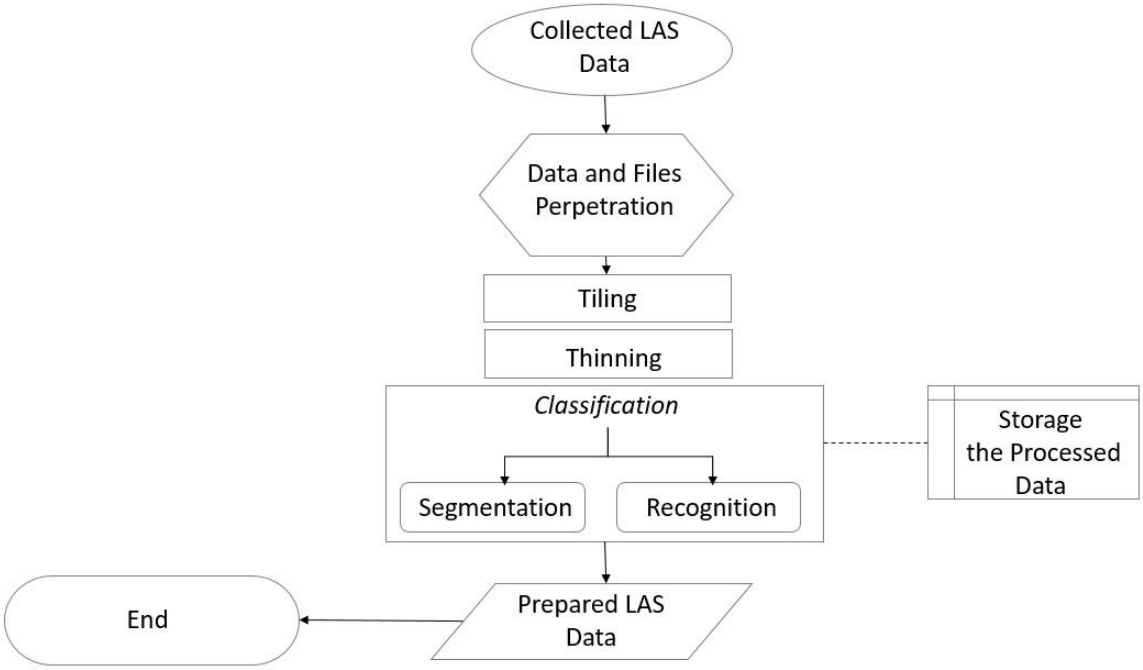

Figure 3-3: Automated workflow to prepare the data prior to feature extraction

3.2.1 Algorithms to manage the point cloud

Manual digitization takes an enormous amount of time and requires numerous team members, even for small patches of data. In contrast, automatic feature extraction saves time and resources to map all street furniture, assets and roads with a high accuracy and success rate. In the following figure, the proposed workflow is applied automatically to the mission point cloud with no human interactions. However, a Quality Control (QC) procedure should be conducted to ensure proper extraction of the features.

The smartness of the algorithm that is used inside the automatic extraction tools is generally associated with the combination of point cloud data attributes and trajectory data. In other words, the algorithm makes use of the adjusted trajectory data to estimate the configuration parameters of the filters at each observation point on the trajectory. This is the key idea in automating feature extraction: recalculation of the configuration parameters for each tile of the data. This improves the success rate of the algorithm since there is variation in the ground height in each tile. Additionally, the smaller the tile size, the better the results will be from the configuration parameters.

The following section explains the automated workflow of the feature extraction, step by step (the workflow in Figure 3-3), in the proposed method.

Data Tiling Algorithm

The purpose of this step is to uniformly divide the LiDAR point cloud into small manageable components (tiles) so that standard computer cannot load, view and manipulate the data without experiencing low performance but computers can dividing the mission area into a uniform grid i.e. tiles. Each tile includes all the points captured from the mission strips and located inside the tile's borders or area.

Input: all the point cloud strips

Output: uniform tiles with the same extension

- *The algorithm parameters:*

Tile size: represents the required cell size in meters

Buffer: represents the overlapped area required between tiles. The main a reason to have tiling overlap is to reduce the edge effects of LiDAR point data

Data Thinning

Terrestrial mobile LiDAR data is dense, which means that it has a big file size. Hence the thinning step is required to reduce the number of point clouds per tile to a reasonable number, while maintaining a high level of detail and resolution.

In the study, the data thinning step is handled in a simple way by dividing each tile again into uniform grids with a smaller tile size i.e. 2 cm. Then the algorithm will keep the lowest height, highest height or pick a random point in each small tile and remove all the other points in this cell.

One example in our study of the data thinning on actual Las file from the research dataset, the point cloud file was reduced from 238 MB to 153 MB, from 8,557,891 points to 5,538,735 points. It is noteworthy to mention that the thinning reduction depends on the area of the tile, the density of the features, and the feature dimension variations.

- *The algorithm parameters*

Tile size: represents the required cell size to control the point density in meters

Thinning flag: lowest, highest or random point

Example: If the cell size is 5 cm, the algorithm will keep the lowest point in each 5 cm.

Segmentation

Segmentation is defined as the process that segments points in the point cloud based on their characteristics. Several approaches are used for the segmentation process. They differ in the method or criteria that are used to measure the similarity between a group of points, and then use this measure to group points. An example of a segmentation approach could be the separation of points based on their intensity

values. In this case, points are segmented into low, medium and high intensity (Fernandez et al., 2007; Rabbani et al., 2006). The approach is used in this study in a first step to detect road features in the point cloud based on their intensity. After in the different sets is used to detect other elements as manholes".

3.3 Feature Extraction

It is widely known that LiDAR data processing and feature extraction rely on the usability of multi-stage filters with different configuration parameters. Each point in the LiDAR cloud data consists of a lot of useful information, such as the point spatial location (XYZ), intensity, scanning angles and return number. In the following section, the algorithm makes use of multiple filters with certain parameters to extract some features from the point cloud data such as manhole covers, road features including edges (curbs), buildings, light poles, street signs and trees.

3.3.1 Urban Elements

The thesis is focused on updating the basemap from MMS data. Today, some software and tools allow the automatic extraction of urban elements such as street lights, street signs, poles and trees (see Figure 3-4) and elements to define the street such as the road centre line, curb stone and road edge. Other elements such as manholes are more difficult to extract. In the next section, we focus on manholes. However, it is also necessary to analyse how the commercial software works and which parameters are needed in the identification of the complementary data required to update the basemap.

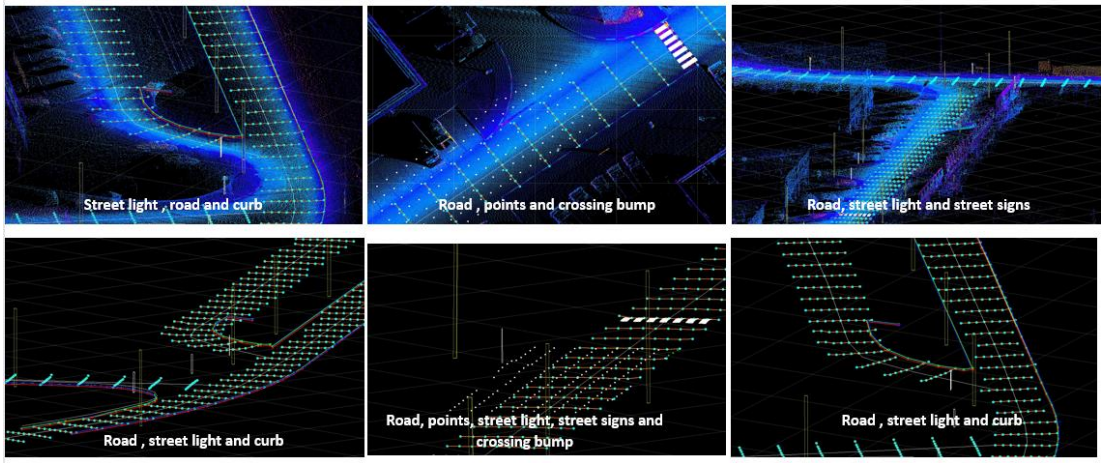

Figure 3-4: Sample of features in the point cloud for the study area

In this phase, we checked some of the available tools that detect road features. Several well-known commercial software programs are on the market for point cloud feature extraction, including Topodot, Lastools and Orbit.

There are two phases: data classification and cleaning. In the first phase to extract the feature, we can consider several parameters:

- Define the approximate height of the feature (so that the tools can easily define the feature)
- Define the cell (this involves drawing the shape of the feature)
- The intensity range

Some items must be extracted manually due to their complexity. These include driveways, car parks or footpaths. Automatic detection includes the following steps:

Data Classification

A first classification between ground and non-ground points is made according to the height of the points determined from the point cloud. The purpose of splitting the ground and over-ground data is to make the task easier for the filters. For example, to extract light poles, the light poles filter will only be applied to the over-ground data, but to extract the road edges, the filter will be applied to the ground data.

In this step, the points that determine the data acquisition trajectory are useful since they are located on the road. Then, we will run a triangulation process from this point and reject points over a certain slope threshold. By extracting the low slope points "points on the paved road only" when the road edge is reached, the algorithm will stop and state that we have reached the road edge.

This algorithm works following an iterative process. The algorithm calculates the difference in slope between each adjacent point and if the slope is smaller than the threshold, the point is on the road. When the slope is above the threshold, the algorithm assumes that we have reached the road edge (pavement).

One road point from the adjusted trajectory will be the starting point for triangulation, as shown in Figure 3-5. The following algorithm will reject any triangles outside the gray borders, which have a higher slope than the threshold of the road edges.

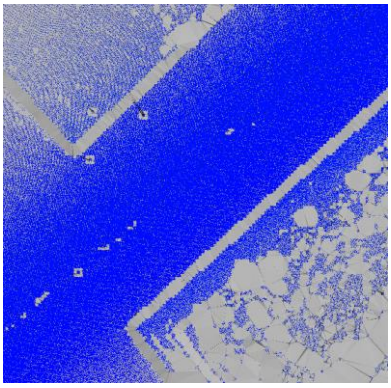

Figure 3-5: The output of the triangulation process and triangles are colored according to the slope

All the fixed-height street features will be extracted according to the threshold parameters that we set in the algorithm input.

Subsequently, many of the other elements can be extracted since they have a standard height in cities. For example, light poles are almost 14 meters high, so a filter will be applied on the point's height from the ground, which will be known from the seed point of the trajectory to the ground height plus 14 meters.

Data Cleaning

For each classification, a cleaning process should be carried out to exclude improper features and noise.

The purpose of data cleaning is to clean up the unnecessary point cloud data after applying certain filters to extract specific features. For example, if a height filter is used to extract the advertisement sign on the road, all the features that have the same height range will appear with the advertisement signs. To remove unnecessary points, a cleaning process should be applied, such as removing certain point densities from the data or removing points far from the road edges, since most road furniture is located very close to the edge.

After considering the characteristics of software programs, we decided to use Topodot as it is stronger than Orbit in feature extraction and easier to use than Orbit and Lastool.

The main reason for selecting Topodot instead of other tools is its power and technical capabilities to detect features like signs and light poles of road assets. If we determine parameters such as height and intensity, the software can perform better at detecting these features. Users can try different values of these parameters drawn from asset standards and specifications to define the detail and determine the detection percentage. That is why Topodot was chosen in this study, to be able to examine several values until the best detection percentage (completeness) was achieved.

Finally, there are some limitations of commercial software in terms of the ability to extract features using software tools. These can be summarized as follows.

- Lidar data is large and must be divided by a suitable size to be able to open files.
- Automated feature detection does not accurately detect features with highly accurate positioning. To achieve this, manual detection is required to enhance the positioning and height of features such as streetlights, street signs and trees.
- Building layout and manholes require manual extraction or an improvement in the new methodologies.

3.3.2 Manholes

Some urban features can be extracted using suitable parameters in the commercial software. This is not the case of manhole covers. Therefore, an algorithm was designed to extract these elements.

The algorithm was designed to detect the different materials of the manholes based on the returned reflection value (intensity). Since manholes are usually made of steel and iron, this is a characteristic that can help in their detection, and based on as previous studies that have demonstrated the effectiveness of using this parameter from the point cloud information (Tatoglu and Pochiraju 2012; Núñez et al., 2008; Balaguer-Puig et al. 2017).

Color is not usually a representative parameter in the properties of manholes. Therefore, the algorithm designed in this thesis to detect manholes is based on the geometry (circular or rectangular) (Figure 3-6) and intensity, i.e. the algorithm will check the shape for matched intensity objects and skip objects that are not the required shape. It starts by defining the variables that will be used, such as the coordinates (X, Y, Z), time (t) and intensity (i), then uploads the LiDAR data in LAS format.

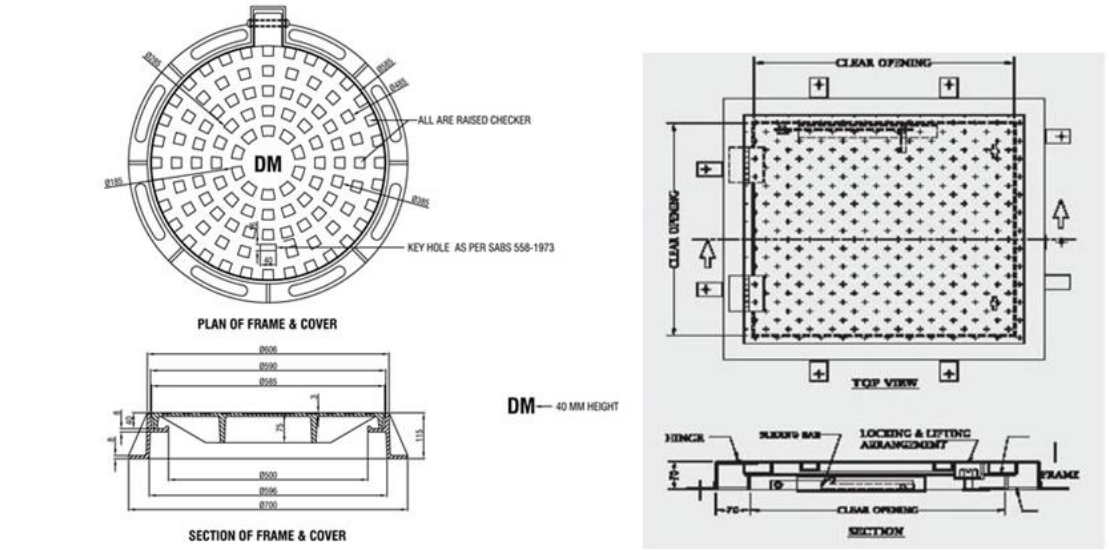

Figure 3-6: Sample of circular manhole with a diameter of 59.6 cm (left) and a rectangular manhole (right) provided by the manufacturer (http://www.nibf.co.za/product/circular-manhole-cover-and-frame-type-2a-and-2b/)

Figure 3-7 shows the flowchart of the procedure in every step of the method for manhole detection. The entire algorithm has been implemented in Matlab script, so that it can be used by any operator automatically.

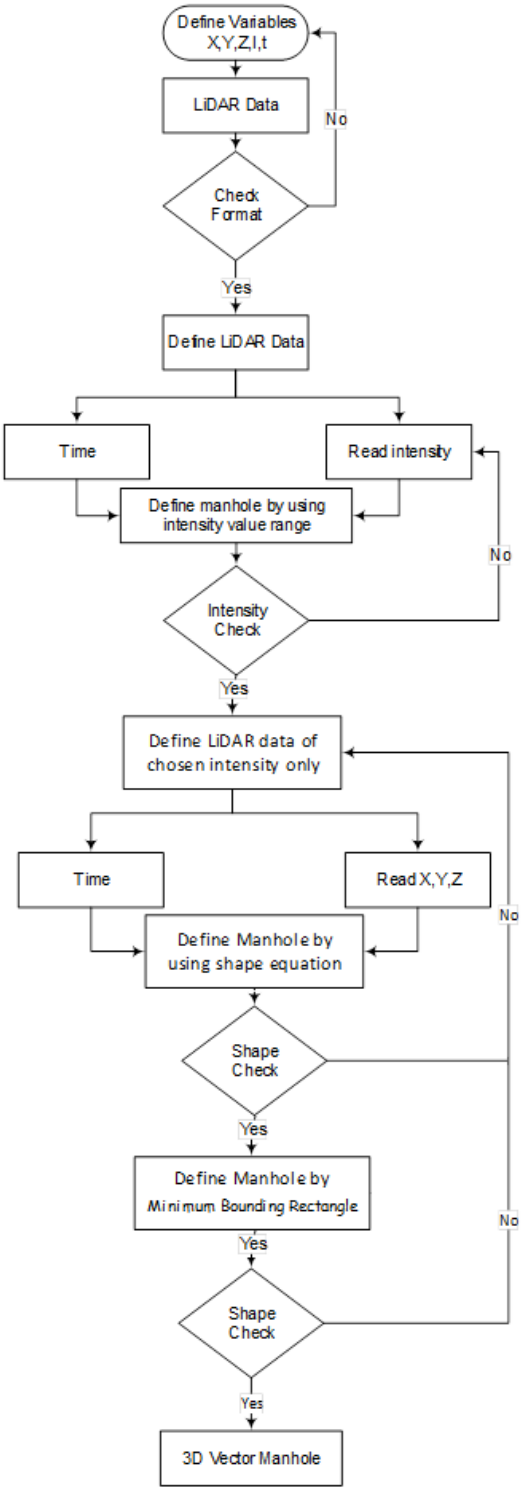

Figure 3-7: Detecting manholes workflow

The first step after checking the data is related to the intensity. This variable is used to segment the point cloud regarding the manhole material. The time variable is used to link with other variables, as the LiDAR data is recorded by time. Eventually, coordinates are used to detect the shape of the manhole.

Manholes have a different intensity due to their material than the points around them that belong to the pavement. These values were determined based on the manhole material, which was identified after contacting the manufacturer, and the wavelength of the laser beam that was used.

The proposed algorithm first defines the intensity for the input data objects, then if the object intensity I_{point} is different from the required value $(I_{min} - I_{max})$, it skips this feature and searches for the next one. The intensity value should lie between the minimum and maximum intensity values set previously in the algorithm by the operator who knows the values range. Objects with the required intensity will be run through the next step, which is the shape check.

In the second step shown in Figure 3.3. the point cloud is checked to detect the manhole covers based on their shapes. The parameters given by the operator are the sides for rectangular manholes or the radius for circular ones. For rectangular manholes, the shape can be calculated from a plane (Equation 1).

$$S = \frac{|ax + by + cz + d|}{\sqrt{a^2 + b^2 + c^2}} \qquad (1)$$

Where 'a' is dimension in the x direction, 'b' is dimension in the y direction, 'c' is dimension in the z direction and 'd' is the distance from the origin to the required plane. Since all detected manholes are at pavement level, the coefficient "d" will be the same as the pavement height, in this case the "c" value will be zero.

For circular manholes, the shape can be calculated from a plane (2).

$$x^2 + z^2 - r^2 = o \qquad (2)$$

Where 'x' is dimension in the x direction, 'y' is dimension in the y direction, and r is the radius.

The manhole shape and dimensions in the selected area are usually known by the municipality from the current basemap. The manhole features that match this known shape and dimensions will then be detected and extracted in the output. These identified cluster objects are irregular, so a last step is required to refine the shape of each identified manhole to a perfect plane with four straight sides and four right angles with equal or unequal adjacent sides, as per the manhole shape. To identify the perfect plane boundaries, the Minimum Bounding Rectangle (MBR) from the convex hull is computed to obtain the envelope of each cluster object (Kwak et al., 2012).

Considering that the target manhole shape in the study area is composed of sets of rectangles, it can be refined as several rectangles that represent the manhole boundaries.

Some steps must be considered to implement the MBR:

- Define the convex hull (Polygon) from all the points. The MBR-derived rectangle is represented by the minimum and maximum coordinate values for the boundary points in 2D. It is determined by choosing the minimum area rectangle among the rectangles

with an arbitrary orientation that contains the vertices of boundaries (Figure 3-8: 1,2 and 3).

- For each edge/segment of the convex hull polygon:
    - Find and calculate the edge orientation
    - Find each segment by rotating the convex hull using the previous orientation, in order to easily compute the bounding rectangle area with min/max of x/y of the rotated convex hull (Figure 3-8: 4).
    - Return the rectangle corresponding to the minimum area found

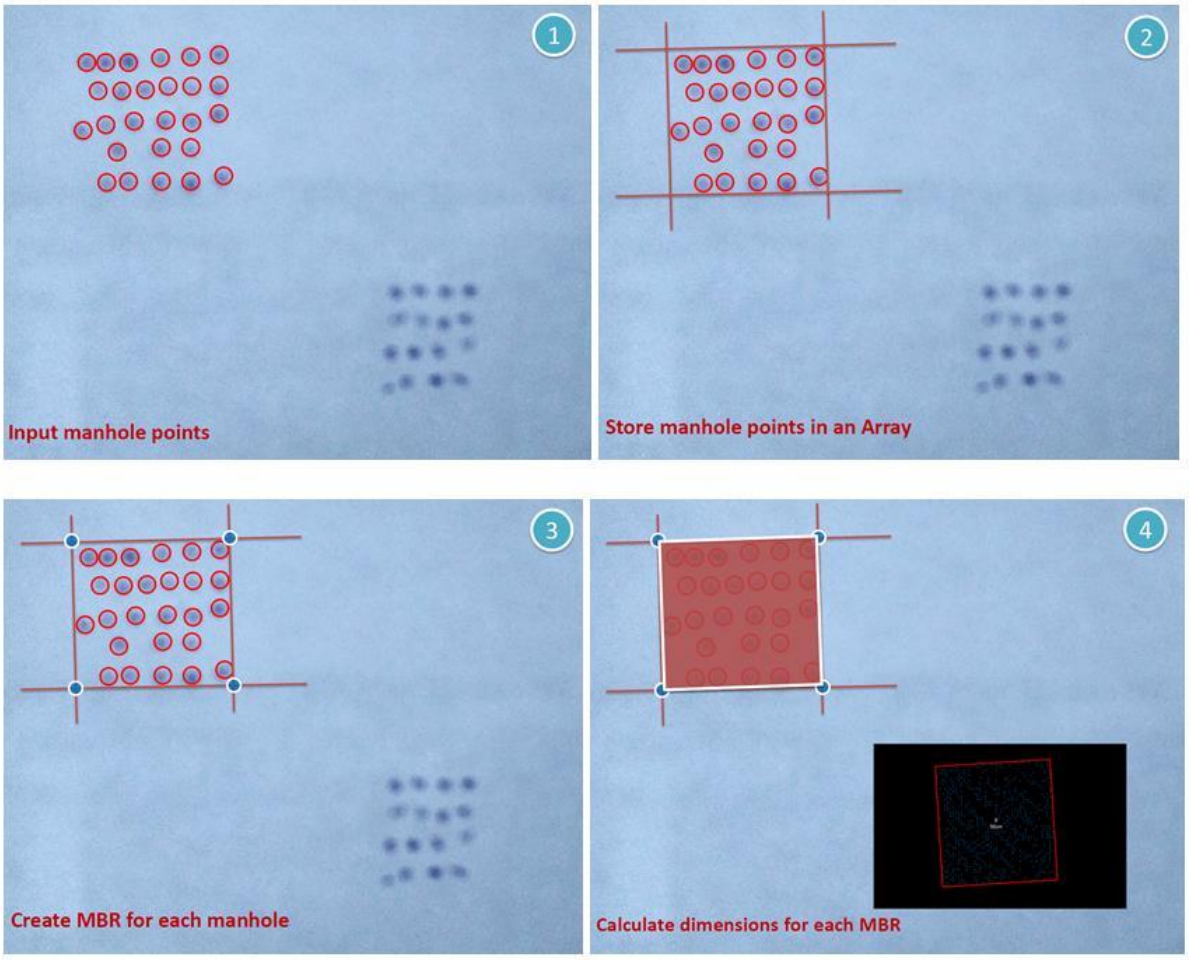

Figure 3-8: Manhole detection steps: 1) Result of the filter by intensity, 2) Identification of the points in each cluster, 3) Obtaining the MBR of each cluster, 4) Final shape adjustment based on the known dimensions.

The process is repeated with all known dimensions until all valid manholes with the required criteria (shape and intensity) are detected. Figure 3-9 shows the minimal bounding rectangle around the LiDAR points for a rectangular manhole.

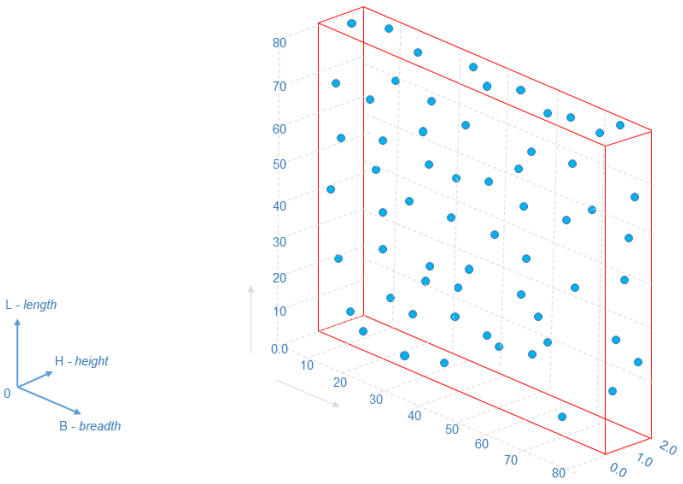

Figure 3-9: Minimal bounding box for a square manhole around 3D MLS point cloud manhole points (units in cm)

In our methodology, unlike other previous studies that use intensity-based images or ground orthophotos (Yu et al. 2014a, 2014b; Yu et al. 2015; Wei et al. 2019), we integrate intensity with collection time to filter the point cloud that is defined as high intensity in the same time period. We add the MBR method that adjusts the final shape of the manhole using the benefit of previously known dimensions in the selected area.

3.3.3 Building's Roof

LiDAR sensors in the mobile mapping system do not cover all building facades and corners (Figure 3-10). Therefore, it is difficult to capture a complete building layout from MMS. To cover the missing information, we needed to find a solution using satellite imagery and available LiDAR data. Figure 3-10 shows on the left a sample of building corners covered by LiDAR data, while the right shows building corners that are not covered. The colors reflect the height levels.

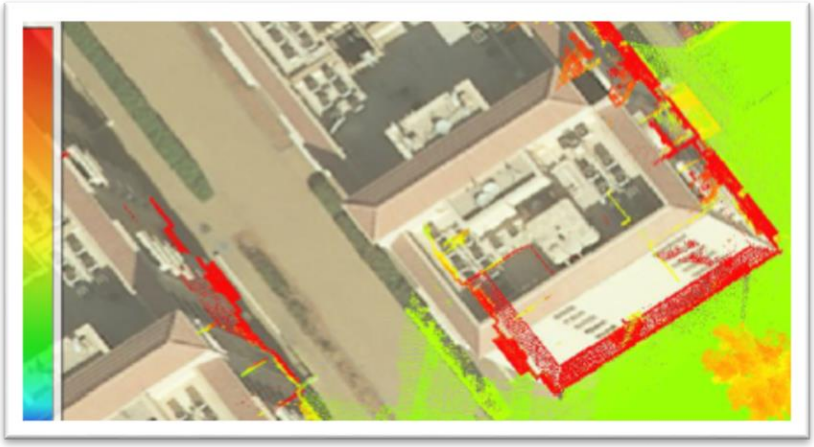

Figure 3-10: Building corners covered by MMS (left) and not covered by MMS (right). Red color presents the LiDAR points while the green color presents the ground level

A study by San and Turker (2010) proved that high resolution satellite images have become quite valuable data sources for building extraction, using an edge detection algorithm to detect building edges. Several studies such as San and Turker (2010) and Alshehhi et al., (2017) extracted building outline boundaries from high-resolution satellite imagery. In contrast, our study, which initially digitized all building footprints from the satellite image, benefits from the combined use of the satellite image with the LiDAR point cloud, from which the visible corners of buildings are imported.

Edge detection in the satellite image is carried out semi-automatically. However, the satellite image includes a lot of hidden areas as it is only a top-down view due to the orientation of the satellite. Therefore, points that lie beneath other points, and objects in very narrow streets, will be hidden. Aerial Lidar Scanners (ALS) are not recommended in this case as they have the same hidden area problem. Another problem appears due to the height required for the acquisition process, since the data are typically at low resolution. These problems can be resolved using ground LiDAR.

To carry out the proposed method, some satellites provide images with a resolution better than 65 cm, such as the Quickbird satellite (panchromatic resolution 65 cm, multispectral resolution 2.62 m), the WorldView-2 satellite (panchromatic resolution 46 cm, multispectral resolution 1.84 m) and GeoEye-1 (panchromatic resolution 41 cm, multispectral resolution 1.65 m).

In the application of this methodology to Abu Dhabi, we used QuickBird images. In most of the applications, ortophotographs are used since they have metric properties. However, one problem with the available images is that they are not true ortophotos, so the high elements have more displacement on the top. The accuracy of the point cloud collected by the MMS system is higher than the satellite image coordinates. Therefore, first we used satellite imagery to digitize the entire building layout in the study area with automated software tools. Software was used to automatically detect the building layout by drawing polygons linking the four building corners. Then the LiDAR data was imported and a fitting process was performed by

comparing the visible corners of the building from the LiDAR point cloud with corners of the building from the satellite image, to measure the differences in X and Y directions.

To detect hidden buildings by fitting the LiDAR point cloud over the satellite image, two different processes, both are quite simple in order not to require much computational cost, will be carried out in this phase to establish the most suitable one for the adjustment in these conditions (Figure 3-11). Some additional probes were made with more complex transformation but due to the area extension and the coherence between the pair of coordinates to transform the results did not have an improvement and the cost of computation was increased.

In the first process, the average value for all corner differences in the X and Y direction, Eq. (3) and Eq. (4) respectively, were applied to all buildings in each area extracted from LiDAR data. In the second process, a Helmert 2D transformation was used to improve the accuracy of the adjustment. First we computed the transformation parameters: the translation in X and Y, the scale factor and one rotation for different areas. Then these parameters were used to compute the new coordinates, X_L and Y_L (Equations 5 and 6).

$$\boldsymbol{Fitting\ Difference\ X} = |\boldsymbol{Difference\ X}| - \boldsymbol{Average\ Difference\ X} \quad (3)$$

$$\boldsymbol{Fitting\ Difference\ Y} = |\boldsymbol{Difference\ Y}| - \boldsymbol{Average\ Difference\ Y} \quad (4)$$

The resulting layout, with a corrected LiDAR data building layout, was used to extract the missing corners that were away from the LiDAR sensor to complete the building features, Figure 3-11.

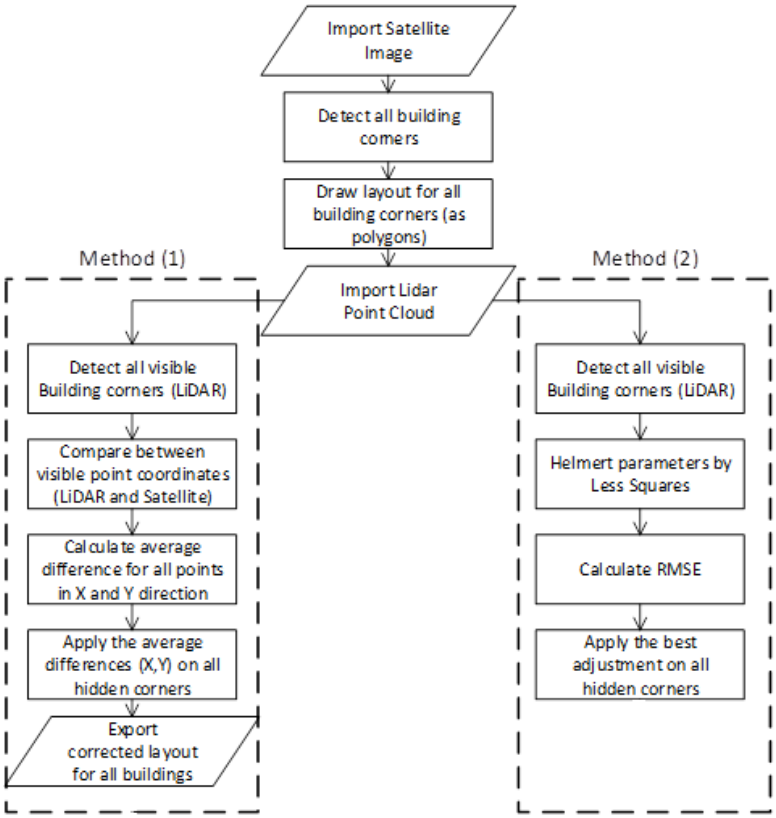

Figure 3-11: Detecting hidden building corners workflow (Method 1 average on the left and Method 2 Helmert on the right)

The satellite image used was georeferenced with available control points. First, we used satellite imagery to digitize the entire building layout in the study area with automated software tools. Then, we evaluated the accuracy of the extracted building corners from the satellite image by comparing the corners of the building from the LiDAR point cloud, to measure the difference in X and Y directions (left workflow in Figure 3-11).

Since the difference between the LiDAR data and satellite image could be in meters, we tried to improve the accuracy by using a Helmert 2D transformation (right workflow in Figure 3-11).

We computed the parameters of the Helmert transformation, translation in X (Tx) and Y (Ty), scale factor λ, and rotation between systems α for different areas, and then these parameters Figure 3-12 could be used to compute the new coordinates (5 and 6).

$$\boldsymbol{X_L = T_X + a_1 X_S - a_2 Y_S} \quad (5)$$

$$\boldsymbol{Y_L = T_Y + a_2 Y_S + a_1 X_S} \quad (6)$$

Where $a_2 = \lambda \sin \alpha$ and $\alpha_1 = \lambda \cos \alpha$,

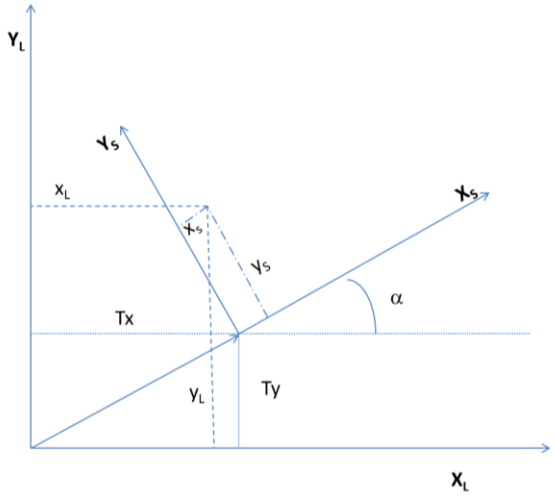

Figure 3-12: Helmert transformation from system X_L and Y_L to system X_S and Y_S

In this process, to obtain the 2D Helmert transformation parameters, a shift to the centroid of each set of buildings should be performed on the coordinates, because the transformation is very sensitive to any change in the value of the rotation. A total of at least six control points have been selected in each area, with low and high buildings, to solve a set of twelve equations with four parameters.

4. Use of daily transaction information to complement MMS data for updating basemaps

Each municipality provides many services for the local community. One of these is the issue of building permits in the case of a new building, a building extension or the construction of a building after demolition. Another service is the issuing of a license for development and infrastructure projects, such as a processing site verification.

Municipalities have numerous clients (developers, consultants and contractors) for these transactions who seek permission for their work and activities, which may change the basemap. Therefore, such works and changes need to be reflected in the basemap directly.

In summary, the fact that transactional data is not updated across entities contributes to the issue of data currency. Today, the focus is on updating spatial data through day-to-day business transactions in municipal departments and sections, including those responsible for road and building permits. Daily transactions include any services or transactions carried out by municipal customer services and related to building permits, roads, infrastructure, utilities and assets.

While they undertake these daily transactions, surveyors could update topographic details and urban furniture such as road networks, lamp posts, telephone booths, bus stops and road signs, which can also be updated by an automated and integrated solutions between transaction and spatial data. Hence, daily municipal transactions can be used to support to update basemaps.

Updating basemaps using these daily business processes provides wide geographical coverage, accurate spatial data and continual updating of data. Most daily municipal services that are associated with land updates should be reflected in the basemap, according to standard basemap updating process.

An example of these services is the issue of licenses for building roads in the public domain. This service is called on when road construction or maintenance is required. The consultant and contractor visit the municipal customer services to submit an application for an official license to construct or maintain roads.

Daily transactions are essential processes in any city in the world for development purposes. Some examples of these transactions are listed below:

- Request and obtain proof of land ownership with the property dimensions.
- Request and obtain approval for construction (a building permit) from the municipality.
- Request and obtain project clearance from different departments.
- Request and obtain connections to utility services.
- Request and obtain water and sewage installation on a specific site.
- Receive an on-site technical inspection of a finished building or project by a supervisory body and prepare the final inspection report.

The data collected from each transaction is used to update the basemap. The transaction process usually starts when the municipality receives a request from the contractor. The municipality then assigns the field survey mission to a surveyor, who collects feature and attribute data (see Section 4.2). The surveyor can use instruments such as total station, laser scanners or GNSS with an assigned computer (controller) to survey points over the existing utilities lines, cadastral plots or road features. The data collected from field measurements is then downloaded and different software programs are used to read the collected data and manually audit it if required. Once the survey professionals have validated the accuracy of the measurements, the data is used to update the basemap. The contractor then obtains the updated geoinformation to use in their work.

4.1 Updating basemaps using daily services transactions

Developers, business unit consultants, contractors and government utility authorities usually request land plots and reserved utility corridor services. These services require field surveys taken by means of traditional surveyors who collect field data. This data can then be used to update current basemaps. Examples of the surveying services for a municipality are plot demarcation, providing site reports, as-built utility checks and no objection certification (NOC) checks.

Each of the above services requires a surveying team to visit the site and take highly accurate measurements using GPS/GNSS, laser scanner or total station equipment. The operating costs for these teams are relatively high compared to the service fees. The proposed idea is to make use of measurements that are already carried out in the field to update the basemap. In turn, this will achieve a return on investments in the equipment and operating costs of the team.

All this data can be supported by using a mobile mapping system and integrated into the basemap, as explained in Chapter 3. First, the system is installed in a moving vehicle (instead of the field surveyor) to collect IMU, GNSS and DMI data. Secondly, the data is downloaded in the office and processed using software that joins the previous data with the base station data and results in survey trajectories. Then the resulting files are used with the laser measurements to create a georeferenced point cloud. This point cloud could be used to extract road edges and centerlines, urban features and building corners. All of the files can be imported into the existing basemap for updating purposes.

Later in this section, an example of a service process map shows the possibility of using accurate data collected by MMS to update basemap data in the organization database.

4.2 Daily functional service in Abu Dhabi Municipalities

A list of the current functional services that are provided across the municipal sections and their status in the Abu Dhabi municipalities is shown in Table 4-1. The table also includes the level of importance (High, Medium, Low and Not Available) to integrate each process with CAD/GIS to update the basemap. This example is concerned with one of the highly important services that need to be integrated into a basemap update.

SECTIONS	Functional services	Current spatially enabled	Level of importance
Infrastructure and municipal asset	License infrastructure service lines		High
	Issue a license to build roads in the public domain	X	High
	License infrastructure lines in territorial waters		High
	Removal request for paved road (asphalt)		High
Spatial information	Basemap update	X	High
	Survey a piece of land	X	High
	Audit on an existing fence		Medium
	Checking approved paths of service lines	X	Medium
Building permit	Request a building permit ● Request to reveal a structural site/location ● Request for a certificate of completion for a building	X	High
	License issued for the demolition of a building		High

Table 4-1:List of related transactions to update maps in the Abu Dhabi Municipality

In the Abu Dhabi municipalities, there are general customer service counters throughout the entire region of the emirate that provide all the building and infrastructure services directly related to the basemap update. Any building or infrastructure license has multi-level approval from the building permit department and the urban planning required to have a integration with spatial data divisions to update a geographic information and basemap.

The current business process uses traditional survey work or aerial photography to update the basemap. In this study, we focus on assessing the current situation and examining scenarios that might fit the current business process of "Issue a license to build roads in the public domain", under infrastructure permits. Infrastructure permits must have no objection certification (NOC). NOC requires clearance certificates from all utilities and asset owners including, but not limited to, the Water and Electricity Authority and Telecommunications Companies within the project area. Another daily transaction service is provided by the municipality, called the "as built" service. Both these services will be explained in detail in the next two subsections.

4.2.1 "Issue a license to build roads in the public domain" service

The "Issue a license to build roads in the public domain" service is explained phase by phase in the following paragraphs. Figure 4-1 presents the service workflow and the task planned for each step. Some of these steps are outside the scope of this study as they include paperwork and other tasks that are not of interest here. The steps that we believe will benefit from using and integrating MMS are marked in green.

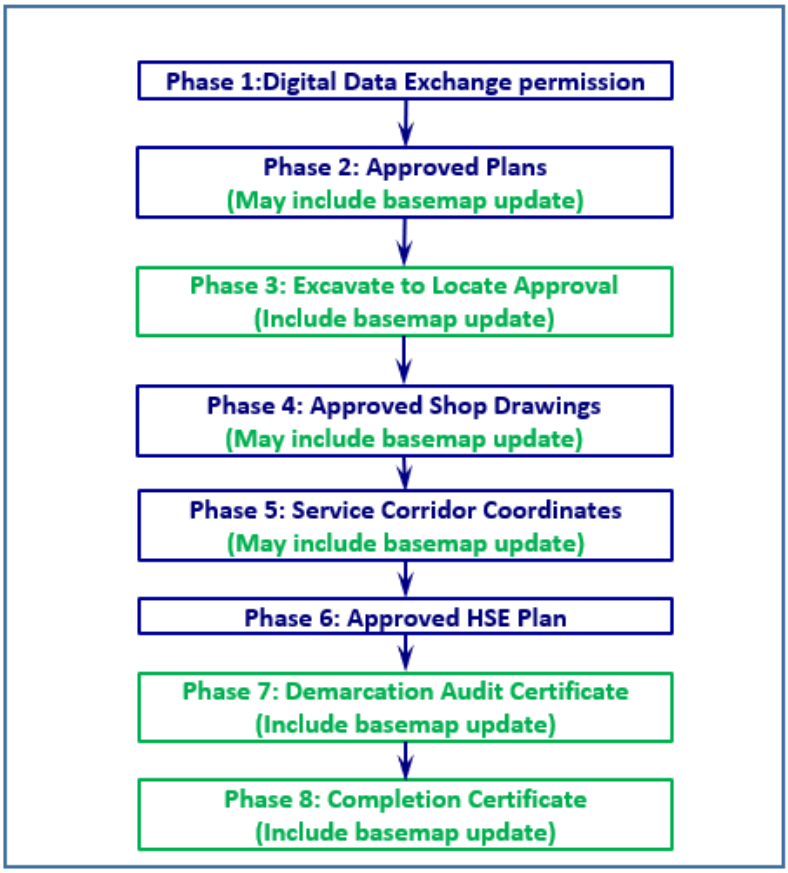

Figure 4-1:The current "Issue a license to build roads in the public domain" service workflow. Boxes and text in green could benefit from using and integrating MMS

Phase 1: Digital data exchange permission

Consultants and contractors must come to customer services in municipalities to submit applications for official licenses to construct and maintain roads from the Infrastructure Coordination Division. They must request Spatial Digital Data Exchange Permission. This is done to provide the client with a Digital Data Exchange License, in order to obtain precise, complete current spatial data (CAD or GIS data) during the approval phase, at the time of submitting documents or on completion of the project. This data is generally used for design and study purposes for the company that will construct the project (a road in this case).

When this permission has been given, the contractor will be asked to deliver an as-built drawing during and after the construction process. This permission will be presented along with the no objection certificates (NOCs) at planning approval phase.

Phase 2: Approved plans

After receiving the current spatial data, the contractor/consultant should submit the initial planning drawings of the infrastructure project along with the required format to the Town Planning department. The infrastructure project should be thoroughly investigated at this stage

to confirm the presence or absence of underground utilities. The utilities section reviews the drawings and approves or rejects them according to the planning and infrastructure guidelines.

Phase 3: Excavate-to-locate approval (update in the geo-database)

During the planning approval phase, the contractor/consultant will submit a request to obtain "Excavate-to-locate" permission via a formal letter along with the plans approved by the relevant authorities (the Town Planning and Survey Sector, the owner and the consultant) for the requested area, which show the location of the work.

After Town Planning has approved this permission, it will send surveyors for field verification and inspection purposes to check the existence or non-existence of utilities in the intended roads. The contractor/consultant will need NOCs from the existing utilities in the intended road, according to the inspection process. The planning drawings may need to be modified as a result of the field verification and inspection process. Furthermore, the as-built drawings may need to be altered, which will result in spatial data updating. The basemap will be updated in two parts in this phase.

Part one: In the field, surveyors identify existing utilities lines and road features, usually by means of GPS. It is common in the municipal system to collect sampling points on linear features, which should be distributed every few meters (approximately 10 m). This is estimated by municipality standards in the urban area. This data describes and indicates what the point is, that is, whether it a road centerline, a road corner, a point on a roundabout or a tree, etc. The municipality subsequently uses a feature code to make it easy to identify every feature automatically. Therefore, there are unique codes for a tree, others for edges and corners, and so on.

Part two: when the surveyor gets back to the office he should:

1. Download the point's coordinates (and data) from the GPS receiver to an office PC. Every point will have an easting and northing (UTM coordinates and WGS84 datum), ellipsoidal height and feature code.
2. Then, the surveyor will connect to the CAD or GIS software and it will read the data, draw it and identify each feature code automatically and add its symbol to the drawing.
3. The surveyor will audit the drawing that was drawn automatically by CAD/GIS and manually correct any errors (for example if a single point was not aligned with the others).
4. Then, he will send the final data to the person responsible for the basemap update. This person has a script to merge and update the CAD/GIS file with the system (the existing basemap).
5. The last step in the current methodology is the digitization process, in which vectors are drawn on the LAS files for the road centerline, features, etc. These drawings will be used as the final drawings to update the existing maps.

This is the methodology that is used currently, but our proposal is to change it using MMS and an automatic process for data validations and checking the as built drawing. The use of LiDAR will save time and costs and eliminate human errors. Furthermore, massive data could be collected in a very short time. This process could be done by:

1. MMS surveying that includes mission surveying and data acquisition.
2. Data transfer to the municipality system (both surveyed and trajectory data).
3. This data plus the base station data will be used for MMS data processing software.
4. The resulting processed trajectory will be used subsequently to generate a geo-referenced point cloud (LAS).
5. This file will be used in the feature extraction process to extract roads and features.
6. Then the façades of buildings that are hidden in the survey will be completed with MMS by using the point cloud and one of the orthoimages obtained by satellite.

Phase 4: Approved shop drawings

Shop drawing approval is considered the final planning approval for an intended project. Shop drawing should take into consideration the utilities inside the project area. Shop drawings should follow Spatial Data Division standards.

In the case of existing road maintenance, “Excavate to Locate” permission is needed in this phase to apply a post-construction survey. This (as-built) survey is required to check whether the construction has been carried out according to the approved plans. It also helps to locate the existence of utilities for maintenance purposes. As-built drawings may need modification after this survey, which would result in spatial data updating. Updating the basemap will be completed as explained earlier in phase 3.

Phase 5: Service corridor coordinates

In this phase, contractors can request the coordinates of the intended site, based on the project layout or the reference number. The contractor submits the project layout or reference number to the Urban Planning and Surveying Sector. The output will be a site map with the required coordinates. This phase does not require a site visit: the coordinates will be exported from the Urban Planning and Surveying Sector’s database.

Phase 6: Approved health, safety & environment (HSE) plan

The Health, Safety & Environment (HSE) plan is a systematic, consistent document containing project-related information, HSE management issues, HSE policy, arrangements, control measures and the safe system of work for performing construction activities in a healthy, safe and environmentally friendly manner. The HSE plan is aimed at improving the overall management and coordination of health, safety and the environment throughout various construction phases to eliminate or reduce accidents, ill-health and environmental incidents. The main components of the HSE plan are project details, brief project description and layout and HSE management requirements.

The Environment Agency–Abu Dhabi (EAD) issues no objection certificates (NOCs) or permits for construction and operation to developers or companies involved in development and infrastructure projects. This is done to ensure that they implement the necessary measures to protect the environment during the construction and operation of the project.

There are two types of NOCs or permits for development and infrastructure projects: construction NOCs and operating permits. Any new development, infrastructure project or new addition to an existing project is subject to environmental permit requirements.

Phase 7: Demarcation audit certificate

Before starting any work on the site, the contractor/consultant will need a Demarcation Certificate. This phase starts with a site visit by the survey section to the intended project in which the project boundaries are marked out to start the construction work.

Phase 8: Completion certificate

An inspection must be requested to ensure full completion of road projects and compliance with all required conditions and phases.

Through this service, contractors and business owners can submit a request for the issuance of a project completion certificate from the General Directorate of Civil Defense Abu Dhabi. This is required in order to submit the final as-built drawings, which should include all the final locations of structures, utilities, manholes, valves, storm drains, catch basins, curbs and gutters, pavements, sign structures, light poles, traffic signals, etc. The contractor/consultant should submit a final phase as-built /final spatial conformity certificate. Spatial Data will make the QC/QA process and field visit to obtain as-built site verification, which is submitted after approval. The final as-built drawings should be updated in the central geo-database. The basemap will be updated as explained earlier in Phase 3. The contractor will then obtain permission for closing and releasing the bank guarantee that he presented at the beginning of the project.

Some of these steps may include field visits, while other steps must include field visits. These steps will benefit from integrating MMS into the daily transaction. Examples are given below.

Approving the project plan: in this process, an audit may be completed on the project's construction plan. A field visit (using both GNSS receivers and a total station instrument) may be needed to confirm that the plan will not conflict with the utility services.

Excavate to locate approval: a field visit (using both GNSS receivers and a total station instrument) is needed to confirm that the excavation work will not conflict with the utility services.

Approved shop drawing: in this process, the project's architectural plan may be audited. A field visit (using both GNSS receivers and a total station instrument) may be needed to confirm that the plan will not conflict with the utility services.

Service corridor coordinates: in this process, an audit may be completed to make sure that the service lines and their extensions are arranged and contiguous to achieve the best use of the available land.

Demarcation audit: in this process, border detection is required to mark out and define the corridor borders.

Phased/final spatial conformity certificate: field verification is needed to update the basemap with the new construction (as-built).

4.2.2 "As built" service

Another daily transaction service is frequently requested to serve citizens and contractors in the management of their properties. In this service, the contractor requests the existing drawings for a specific construction area including building, road, curbstones, street lights, street signs, manholes, etc. The workflow is shown below in Figure 4-2 and described in this section.

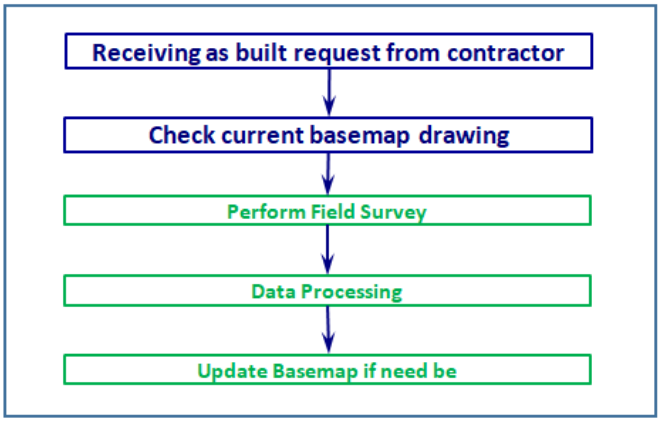

Figure 4-2: Current "as built" workflow. Boxes and text in green could benefit from using and integrating MMS

Phase 1: Receive an as built request from a contractor

Usually, this process starts when contractors request the 'as built' service to start construction projects. The aim of this service is to provide contractors with the current drawings for a specific area.

Phase 2: Check current basemap drawing

In this step, the municipal employee should check the current basemap in order to obtain details about the required area and export the current drawings.

Phase 3: Perform a field survey

In this step, the municipal surveyor visits the field to collect the required data using the traditional method. This methodology could be improved using MMS, as explained below at the end of these phases.

Phase 4: Data processing

In this step, the surveyor transfers the data from the field instrument to the office and processes the data by converting the lines and polygons to points with x,y,z coordinates.

Phase 5: Update basemap (if necessary)

In this step, a comparison is made between the current basemap and the latest 'as built' drawings. If differences are found, the basemap will be updated with the latest 'as built' drawing and the contractor will receive the updated drawings.

After receiving an as built request from a contractor, it is important to check the data to meet the requirements of produce mapping within the specifications of the Abu Dhabi Municipality. The municipal employees randomly perform a GPS observation of the required area and make the required checks to compare it with the as built drawings to reach an accuracy within 15 cm. If the as built drawings are within the standard accuracy required by the municipality, the employees give the contractor approval on the as built drawing mapping.

If this is not the case, the as built drawings will be rejected and the contractor will be asked to draw up a new as built drawing from the field and submit it again to the municipality. This process could be repeated several times if needed until the contractor achieves the municipality's required standard accuracy.

After final approval is given for the as built drawing by the municipality, it can be used to update the existing basemap. The modifications can be added directly to the basemap and used for future applications needed by the municipality. This is one contribution that can be used to update the basemap through daily transactions.

The above services are used by the municipality to serve citizens. Within this study, detailed information and methodologies are provided for updating the basemap with daily transactions. In this scenario, the proposed methodology can be supportive to the traditional methodology to examine the effect of this study on the daily transaction services. 'As built' will be the example we use in this chapter. A comparison will be made between the traditional survey method and the LiDAR MMS system in the 'as built' service. If the area surveyed recently by MMS or traditional survey isn't required to repeat the survey meanwhile there are new development or road construction in the area which require to survey by MMS as explained above for As built comparison and update the basemap.

Integrating the MMS in this daily transaction will save time and provide more accurate data. For each phase that requires or may require surveying, the MMS system can be used as follows:

- Full survey mission planning can be done before each survey in the required area.
- The data collection process will be performed to collect the necessary information.
- Back in the office the data will be downloaded and processed. Trajectory files and point cloud files will be extracted from the data.
- Feature extraction (semi-automated) will be performed to draw the pavement and building corners.
- For the missing details, other methods will be used to extract the data.
- Files from the previous two steps will be used and integrated with the basemap.

5. Updating the basemap in Abu Dhabi Municipalities

The methodology proposed in the previous chapters is applied to the municipalities of Abu Dhabi, where the basemap update service is one of the most important services provided because of the rapid, considerable development of this area. The geoinformation of reference includes all the land development, infrastructure, and any other update that has taken place on the land of Abu Dhabi. The traditional basemap update is carried out by sending surveyors to the area of interest to collect all the new features and updates that have been created by a new development or establishment. Due to the relative high temperature, especially in the summer, and the harsh environment of the desert, a considerable amount of time and effort are required to update the basemap using the traditional method. Basically, points have to be collected for each feature on the land. The extremely long, exhausting process required led Abu Dhabi to consider a supportive method to support the traditional method for basemap updating. That supportive method became the mobile LiDAR system. Abu Dhabi Municipalities started to establish a unified mobile LiDAR unit and build a capacity for human resources and updated mobile LiDAR technologies to support the current activities related to update the basemap and daily transactions as mentioned in chapter 4.

5.1 Abu Dhabi Emirate

5.1.1 Location and characteristics

The United Arab Emirates (UAE) were established on 2nd December 1971. It is a federation of seven emirates (Abu Dhabi, Dubai, Sharjah, Ajman, Ras Al Khaimah, Um Al Qauween and Al Fujairah) comprising an area of 83,600 square kilometers. The UAE are located in Southwest Asia, between 22°50′ and 26° north latitude and between 51° and 56°25′ east longitude, bordering the Gulf of Oman and the Arabian Gulf, between Oman and Kingdom of Saudi Arabia (KSA). It shares a 530-kilometer border with KSA on the west, south and southeast, and a 450-kilometer border with Oman on the southeast and northeast, see Figure 5-1.

The population of the UAE is approximately three million inhabitants with a growth rate of 6.5 percent per year (UAE, 2000). The City of Abu Dhabi is the capital of the Emirate of Abu Dhabi and the federal capital of the United Arab Emirates (UAE). It is the largest emirate and accounts for 87 percent of the UAE's total area (67,340 square kilometers).

Abu Dhabi was first settled in the mid-eighteenth century as a hunting and pearling base. Its significance increased with the mid-twentieth century discovery of oil and the formation of the UAE in 1971. Since then, the city has experienced steady but manageable growth and currently has approximately half a million inhabitants.

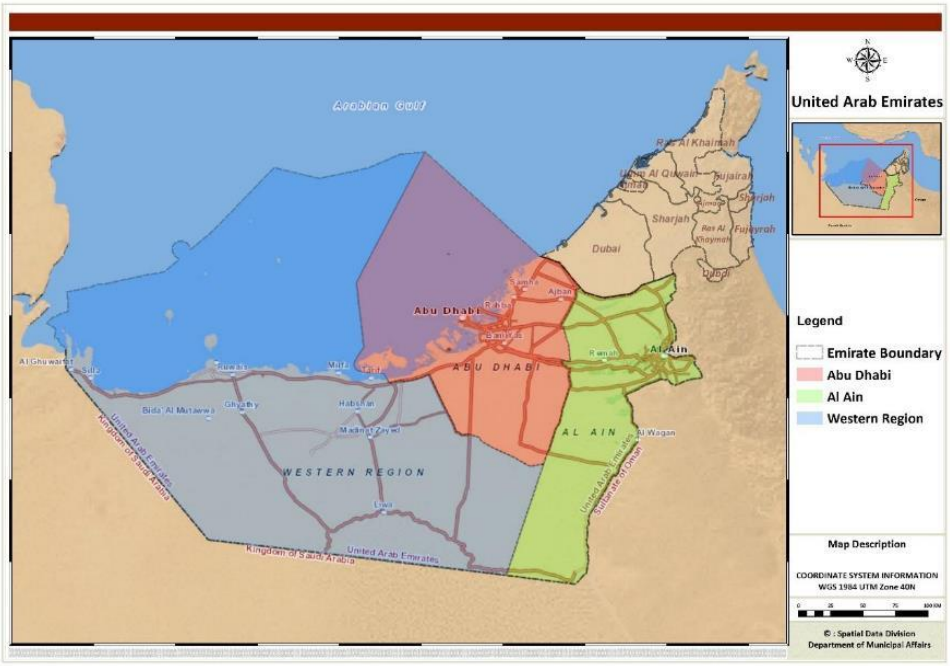

Figure 5-1: Location of the UAE and Admin Boundary of the Abu Dhabi Emirate (Abu Dhabi Municipality, 2012)

5.1.2 Abu Dhabi Spatial Data Infrastructure

The Municipal System in Abu Dhabi plays a central role in the Abu Dhabi Spatial Data Infrastructure (AD-SDI) program, especially as basemap datasets are critical to the work of most, if not all, the AD-SDI community. Municipalities have been leveraging Geospatial Information, Technology and Services (GITS) in their processes and services for some years, with around 15% already geospatially enabled. A further review has established that over 80% would benefit from geospatial enabling.

The business solutions task force includes representatives from each sector to ensure all enterprise applications are fully integrated, interoperable and developed in a full solution framework. The biggest issue in terms of GIS data in Abu Dhabi municipalities is that of keeping the basemap up to date so that it reflects the reality on the field at any time. All the municipalities' business processes leverage up-to-date geospatial information to optimize productivity, efficiency and services to customers.

As mentioned before, this study aims to use and integrate mobile LiDAR technology into the municipalities' daily workflow so that it becomes the new standard cost-efficient operating procedure for updating the basemap in the Abu Dhabi Municipal System, based on the automatic process of element extraction from the point cloud.

This basemap is the origin of several services such as Spatial Data Infrastructure. Abu Dhabi Spatial Data Infrastructure (AD-SDI) is an empowering institution, which is controlled within the Abu Dhabi Systems and Information Centre (ADSIC). AD-SDI is a part of Abu Dhabi's e-

government plan. The Government of Abu Dhabi updates relevant, high-quality geographic data and spatially allowed e-government services.

In an AD-SDI data review, data assessment, data processing, publication of map services, cartography for particular projects and GIS analysis is carried out by deploying a GIS set of software as shown in Figure 5-2.

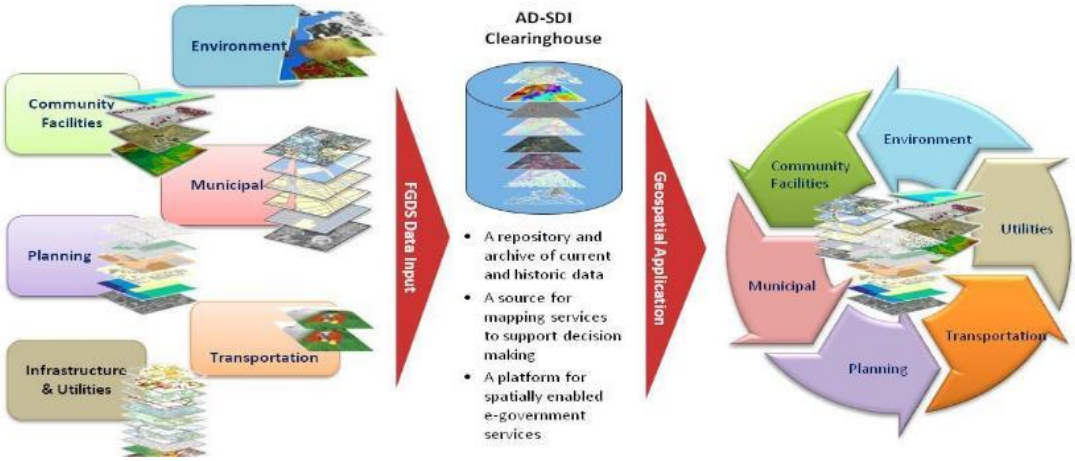

Figure 5-2: Abu Dhabi Spatial Data Infrastructure (Courtesy of ADSIC, 2016)

5.1.3 The LiDAR pilot project areas

The area of interest selected to apply the proposed methodology is Al Hili, located close to the Oman border (Figure 5-3) with a population of 514 and a total of 131 buildings in an area of 1.3 km^2.

Different zoom levels of the selected location are shown in Figure 5-3.

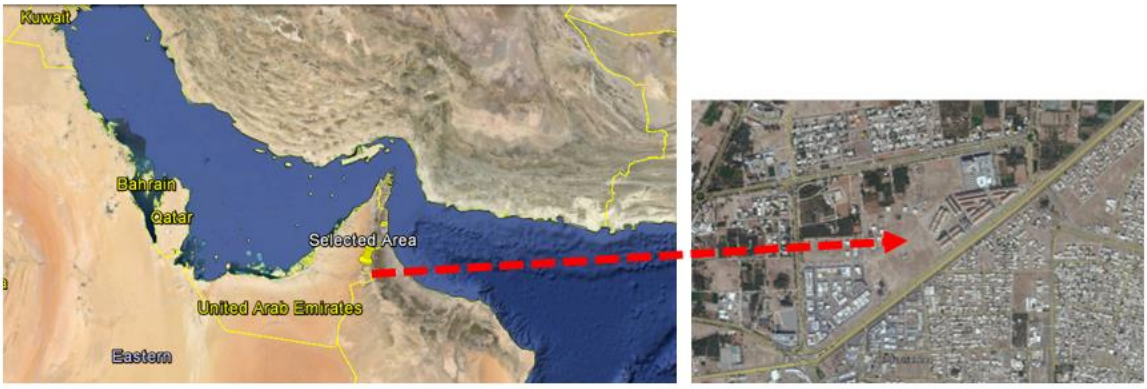

Figure 5-3: Project site location

Al Hili was selected as the study area since it is close to the border, has a range of ground features and has varying visibility from the sky due to obstacles, trees and high buildings, so accuracy fluctuates accordingly (Figure 5-4). This makes the area a good example of application. We can differentiate three zones: the first zone (Area 1) has high-rise buildings and a high level of urbanization; the second zone (Area 2) has a low level of urbanization; and the third zone (Area 3) is peri-urban (Figure 5-4).

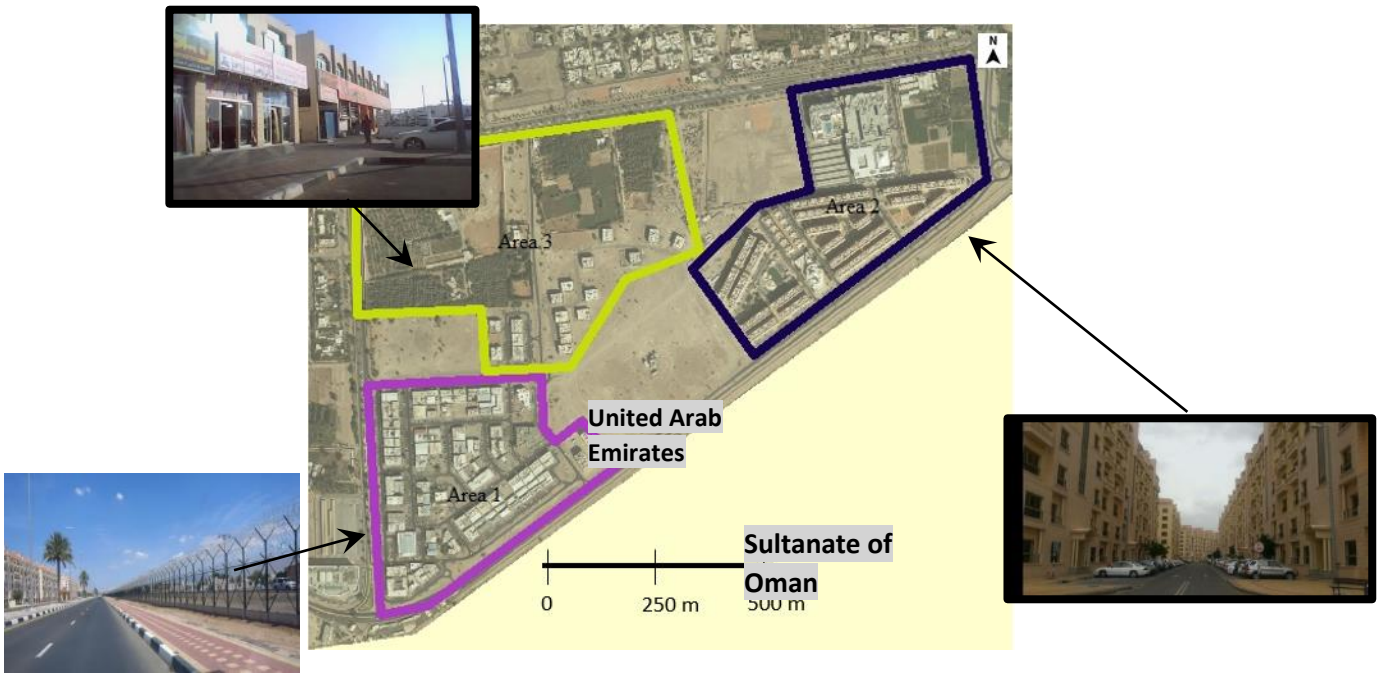

Figure 5-4: Zones with different urban patterns in the study area

5.2 Abu Dhabi mobile mapping system

The solution adopted in Al Ain Municipality to capture 3D information for updating the basemap was a mobile mapping system. Its technical characteristics are described in detail in the next sections.

5.2.1 MMS hardware and functionality

The municipality acquired a mobile mapping system from Optech. It is the Lynx M1 system, with two high-precision LiDAR sensors that can collect highly accurate data at an individual rate of 500 KHz. It allows for high density point clouds to be generated while traveling in a vehicle. The components of this system are:

- Sensor: each sensor can collect hundreds of thousands of shots per second, and each shot has up to four returns.

- The axial fan was designed to prevent sensor overheating caused by the scanning laser, especially in warmer temperatures.
- Camera: there are four locations on the roof rack to attach the camera, two between the sensors and two at the two furthest corners of the roof rack. Each camera connects to the socket on the array box that matches the camera's label (3.5 megapixel). Photographs taken by the camera are used to help in identification of features that may be difficult to delineate from LiDAR.
- The IMU records the roll, pitch and heading of the vehicle in space.
- GPS provides the precise location of the vehicle (X,Y,Z), while secondary GPS provides accurate heading information (up to 0.02°).
- The DMI is attached to the "instrumental wheel" usually on the driver's side. Pulses are converted into incremental distance, the sum of which is the total distance travelled by vehicle.
- The roof rack is designed to be installed onto a standard vehicle roof adapter rack to handle system equipment (64 kg).
- The control rack must be mounted securely inside the vehicle. It is used to run the system and save survey data onto the hard disc.
- A laptop to run system software during the mission.
- A one terabyte hard disk to save survey data (images and position).
- Data extraction (Range, Raw Images, and POS & GPS) from the hard disk using Disk Extract software.
- POS & GPS data processing using GPS base station data in POSPac software to create a smoothed best estimate trajectory (SBET). The format is OUT file.

In addition to the traditional components, the digital camera and scanning laser system and a geo-referencing component, an air conditioning system was custom-designed to allow the Lynx to function within the environmental conditions of the United Arab Emirates. The system installation, mounting and power configurations and the survey were prepared by Optech. The system functionality was checked in the higher temperature environment before the data acquisition process.

The accuracy must meet an absolute value of 10 cm RMSE horizontal and 15 cm RMSE vertical. This means the mobile mapping system must be capable of collecting data at a higher accuracy than these values.

During the test period, several surveys were performed by the Lynx Mobile Mapping system. Two sections of data were collected and compared to ground control points (GCP). Over the four discrete surveys and three sets of ground control points, absolute horizontal accuracies ranged from 1 cm to 5 cm RMS while vertical accuracies spanned 2.5 cm to 12 m. Boresight GCP Set 2 displayed a 10 cm vertical difference from GCP Set 1, which illustrates the importance of having accurate GCPs for proper evaluation.

5.2.2 Georeferencing

The efficiency of the carrier phase differential GNSS positioning is restricted primarily by the effects of the atmosphere, satellite clock and orbital inaccuracies that cause systematic range errors in the observables. The further the rover is from the reference station, the more these errors are decorrelated. In traditional processing approaches, the baseline separation between the rover receiver and the reference station is limited to 20 km to reduce the errors to less than 5 cm. For this reason, the Al Ain base station, which is about 6 km from the study area, was selected to correct POS and GPS data obtained from the Town Planning and Survey Sector (TPSS).

The GNSS-inertial processor performs multiple processing operations to compute intermediate solutions and finally SBET. The number of processing operations depends on the selected processing mode. In all modes, the first operation is a forward-in-time GNSS-inertial integration and the last operation is optimal smoothing to generate the SBET. Intermediate processing operations can include backwards-in-time GNSS-inertial integration using the consolidated ambiguities, to obtain the best achievable navigation accuracy from the input data.

5.3 Application of the proposed methodology

This section includes the work plan for the proposed methodology, the survey results and the quality control process.

The workflow (see Figure 5-5) was comprised of 5 processes: project planning, data acquisition, data processing, quality control and the basemap update. Each process will be explained clearly in this section.

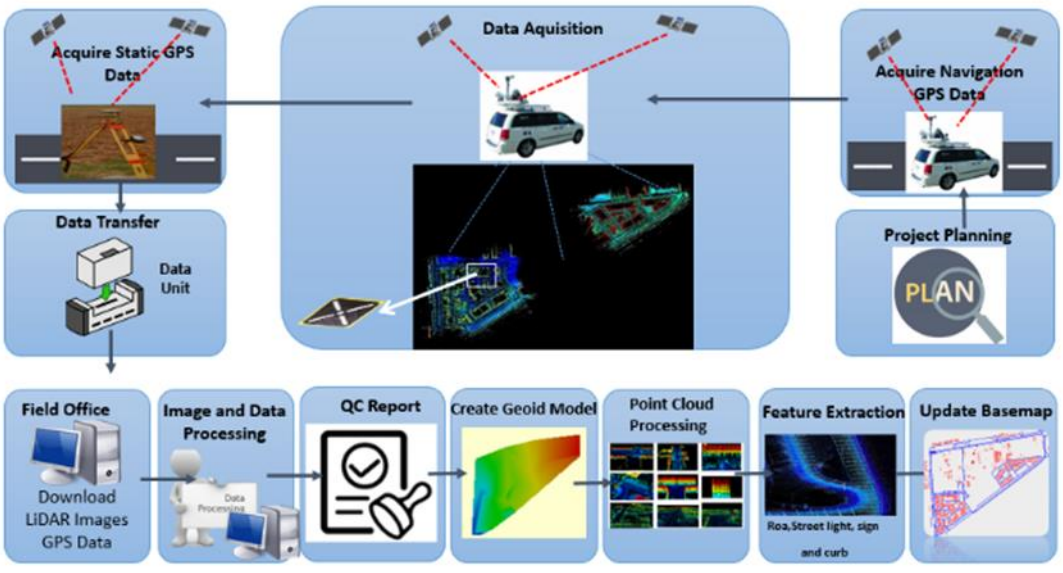

Figure 5-5: Proposed workflow for the basemap update

5.3.1 Mobile LiDAR mission planning

The target area was selected according to the criteria detailed in section 5.1.3. The project area was explored to confirm that it was safe for the project team and the GNSS data collection environment was suitable (and obstructions were identified that could cause GNSS signal loss). The best time for the survey was determined according to traffic volume to minimize obstruction of the LiDAR sensors and digital cameras during the data acquisition process.

It was confirmed that the area of Al Hili met all requirements, such as having enough information about this area to obtain the project deliverables that were needed in this research, the data acquisition process could be completed within the research time frame, and the size of project was suitable.

All information about this area needed to be available before the survey, including the referenced geodetic system, utility line location, as-built drawings of constructions inside the area (to exclude or use less land surveying or avoid repeating the survey on the site).

5.3.1.1 Vehicle trajectory plan

Once the project area had been selected, it was necessary to determine the road drive path and the planned trajectory to help the survey team to identify the start point, the planned trajectory and the end. This can be achieved with Google Earth. This path was exported in KML file format and the route (the planned road drive path) could be used and imported to the Lynx Survey system to guide the team during the data acquisition process.

In order to georeference the point cloud captured by the MMS with enough accuracy during the data acquisition, the baseline between the GNSS base station and the rover receiver was planned to be as short as possible (< 10 km). Short baselines contribute to the best possible positional accuracy outcome.

Before the start of the MMS survey, each step needed to be planned carefully (Figure 5-6). Mission planning is necessary to ensure maximum GNSS signal availability, enough available satellites and that the PDOP meets the requirements during the data collection.

GPS satellite visibility and PDOP forecasts needed to be checked before the mission. During the data collection process there should be at least five satellites in view for the GPS Control Stations in the MMS system. Additionally, the maximum PDOP value during acquisition should be below three to help reach the required accuracy.We reduced the value of the PDOP to three to sure a better quality in urban environments

Trimble’s online software (GPS Planning Online) was used to check satellite sky geometry on the planned date in the project area and to prepare the forecast charts, since the GNSS conditions along the survey route directly contribute to the SBET, that is, the georeferencing accuracy of the survey data.

The best time for data acquisition was between 7 am and 10 am when the number of available satellites was high. Having more available satellites during the data acquisition process improves data quality. A single base station was used in a differential mode later in the data processing phase.

Figure 5-6: MMS mission plan

5.3.1.2 Pre-mission check

The vehicle speed was also determined during the planning phase and the maximum speed was identified for the required density. The plan was to drive 90, 60 and 40 km/h on the highway, city and urban area respectively.

During the survey, data is stored on the hard drive(s). When the Lynx is powered on, the hard drive cannot be changed without corrupting the survey data and possibly damaging the drive. Therefore, before the start of the survey it is vital to ensure that there is enough storage. The manufacturer provided a way to calculate the required storage area on the hard drive according to the required data acquisition.

The weather forecast was checked before survey time, to ensure good driving and atmospheric conditions in the location.

Prior to the data acquisition operation, a procedure should be followed to check the system. The pre-mission procedure includes, but is not limited to:

- Checking cabling to ensure that each cable is in place according to the system's wiring diagram.
- Checking the scanner windows for smudges, cracks or scratches that may interfere with the survey, by removing the protection cabs from the LiDAR sensor and checking all windows.
- Making sure that the scanners and cameras windows are clean to avoid collecting noisy data.
- Choosing the proper scanner data rates based on the required data density. Two parameters should be adjusted at this stage: the pulse repetition rate (PRR) and the mirror rate. The PRR can be configured at 500, 250, and 75 KHz, while the mirror rate can be configured from 80 to 200 Hz. The maximum point density can be taken when the LiDAR PRR and mirror rate are maximum i.e. 500 KHz and 200 Hz respectively. Maximizing both the PRR and mirror rate gives the maximum resolution for the data acquisition.

- Making sure that the hard drive(s) are in the control rack and ensuring that the hard drive contains enough space for the mission data by maintaining 100 GB free space to collect an hour's data at an average speed of 60 Km/h.
- Making sure that the internal flash memory of the system has enough memory to capture the mission POS data. This can be achieved by logging into the POS flash drive and checking the available space. If it is less than 1 GB, the data should be archived somewhere on the acquisition computer and the memory must be cleaned to collect new data and avoid memory overflow.

5.3.2 Data acquisition

5.3.2.1 Installation and previous checking

In this section, we will focus in the MMS installation and checking which it should be completed after every installation (including the first installation) or after modifying the instruments' positions relative to each other.

MMS is a Lynx system that relies on the Applanix POS system to obtain a SBET file to provide accurate geographic coordinates to collect the 3D point cloud. The Applanix POS system relies on three components to calculate its position: IMU, GPS and DMI. Some parameters that need to be measured in the installation process are: the distance between the DMI center with respect to the IMU center (Lever arm measurement 1), the distance between the primary GPS antenna and the IMU center, and the distance between the two GPS antennas and the DMI scale factor.

The MMS vehicle should be checked after installation. In particular, sensors heads were checked to confirm that they are installed correctly.

The parameters presented in section 5.3.2.1 were measure in the MMS vehicle before the survey is started. it was checked that batteries were fully charged, the gas tank is full, all the vehicle lights are functioning properly, the tires are inflated to an acceptable pressure, the fans underneath the LiDAR sensors are clear and can rotate without obstruction and the cables are securely connected.

During the data acquisition process, the procedure detailed below was followed to make data processing easier and to protect the data from error propagation. The procedure mainly includes monitoring GNSS solution, system sensors, system storage and keeping the IMU in adjusted mode. Table 5-1 shows the accepted values that ensure a successful data acquisition process. The in-mission procedure includes but is not limited to:

1. Monitoring the GNSS solution to keep it in the fixed state during the mission, which means that the antenna must see at least four satellites.
2. Collecting static data for five minutes before and after the data acquisition, which helps in post-processing to fix ambiguity and lock the satellite to ensure an accurate smoothed best estimate trajectory (SBET) later in the data post-processing level.
3. Monitoring the system sensors to maintain the temperature within the operating temperature stated in the system manual. The temperature should be kept within 40 to 45ºC. This is a very important parameter, especially in Abu Dhabi in the summer, since

the temperature sometimes exceeds 45ºC, which is risky for the optical and electronic components of the LiDAR and camera sensors.

4. Monitoring the storage of the system to avoid data loss. Storage consumption must be monitored in the Lynx survey window. Once the available hard drive storage falls below 5 GB, the data acquisition should be stopped, the data archived then the hard drive cleaned so that new data can be collected.
5. Ensuring that the planned strips are carried out properly and cover the required area with no data gaps by comparing the mission plan strips with the actual collected strips.
6. Keeping the IMU in adjusted mode i.e. obtaining accurate measurements by doing the "eight- or ∞ figure" calibration whenever possible. This can be achieved by driving around a roundabout about twice each 20 minutes or by making the figure of eight whenever possible. The reason for the "eight- or ∞ figure" practice is that the IMU becomes less accurate if the vehicle moves in a straight line for over 20 minutes. Therefore, the IMU should be readjusted by making an abrupt movement like the "eight- or ∞ figure".
7. Handling GNSS signal absence by collecting static data for five minutes when the GNSS signals go down. Sometimes high-rise buildings or other obstacles can impede the visibility of the sky and the system might lose its lock with the satellites. In this case, the mobile LiDAR system relays the IMU measurements. However, the IMU can maintain its precision for up to a few minutes, which is why it is extremely important after going through any invisible area to stop the car for five minutes in an open area to collect at least five minutes of static data to obtain a fixed solution and then continue the mission.

Program	Location	Item	Acceptable value
LV-POSView	GAMS Solution window	Solution Status	Fixed Integer
Lynx Survey	GPS/INS Data panel	PDOP	Less than 3
		Sat tracked	5 or more
	Logging panel	Rate	Approx. as expected for your survey parameters
	Rack Environment panel	Input Voltage	11.5 to 16 V
		Input Power	360 W
	Cameras view	—	Images have proper exposure, and update at your selected rate

Table 5-1: Steady state values that ensure valid data acquisition

During the data acquisition, two applications are used on the vehicle laptop:

- LV POSView: to monitor, configure and log the POS data for the LiDAR ranges
- Lynx Survey: to configure scanners, collect data strips and monitor the onboard sensors and the real-time point cloud

The data acquisition starts with importing the mission plan to the Lynx survey and configuring the LiDAR and cameras. The LiDAR configuration parameters are basically the PRR and the mirror rate. In terms of the camera configuration, the camera frequency parameter is adjusted so that 1000 ms means one picture in each second. Then the strips are collected. During the

data collection we monitored the system to ensure a fixed solution, acceptable PDOP and continuity in the POS data. In the process to align the survey data after the data acquisition, the exact boresight should be known (that is, the pitch, roll and heading) of the sensors and cameras. Initial values for these parameters are provided by the system manufacturer and these values do not change as long as the system does not move. To calculate the boresight, the best practice is to collect boresight data before every survey, so the default values can be updated.

The calibration site location is selected with an open sky view. The calibration process consists of collecting calibration strips of flat, horizontal and vertical surfaces by making two overlapped passes around a certain building that meets the above criteria. The output strips will then be used to correct the boresight angles and lever arms for each sensor independently. The calibration process takes a very long time since it relies on examination by eye of misalignment and the user's numerical skills to estimate the proper values for boresights and lever arms. When this process has been completed, the data acquisition survey can be started.

5.3.2.2 Acquire static GPS data

Firstly, a Lynx Survey project is created and the sensor configuration parameters are set according to the project requirements i.e. pulse repetition rate and mirror frequency. Then, the LV-POSView is configured to start the GNSS data acquisition internally in the system and/or on the acquisition laptop.

The KML planned route file was imported to the LYNX system. The data capture does not start until the GNSS solution for the position is obtained to fix the ambiguities. In order to guarantee correct georeferencing, five minutes of static GPS data were collected with the vehicle stationary in an area free of obstructions. No LiDAR data should be collected in these five minutes. One to two minutes of dynamic driving should be undertaken to prepare the POS and IMU and check that the logging rate is correct before moving to the survey location.

At the beginning of the mission, the driver and the data acquisition specialist (DAS) perform a test strip to ensure that all sensors are working properly before proceeding with the entire strips. This is important for several reasons. For example, if the DAS forgets to remove the protection caps from the LiDAR sensor, all the collected data will be useless. Alternatively, if POS data are not collected during the LiDAR strip acquisition, the LiDAR data will be useless since there is no direct georeferencing information involved in the process.

Good, dependable GPS information is critical to the georeferencing accuracy of the survey data. The survey area should have adequate GPS coverage during the survey time. It was confirmed that the GPS base stations were set up and provided acceptable GPS position information for post-process purposes. The GPS base station is part of the Alain GSM network and called the Al Ain municipality base station.

According to the manufacturer, the accuracy with the static from a standard antenna is maximum horizontal: 5 mm + 0.5 ppm and vertical: 10 mm + 0.5 ppm. This is the relative accuracy and is sufficient for this kind of work.

As shown in Figure 5-7 , the distance between the base station and the trajectory was a maximum length of 6.4 km and a minimum length of 4.45 km. The left drawing shows the base station and trajectory in POSPac software while the right drawing shows the base station and trajectory on Google Maps. The base station used in the study area is equipped with a GNSS receiver and a dual-frequency geodetic antenna, at an epoch of 1 second.

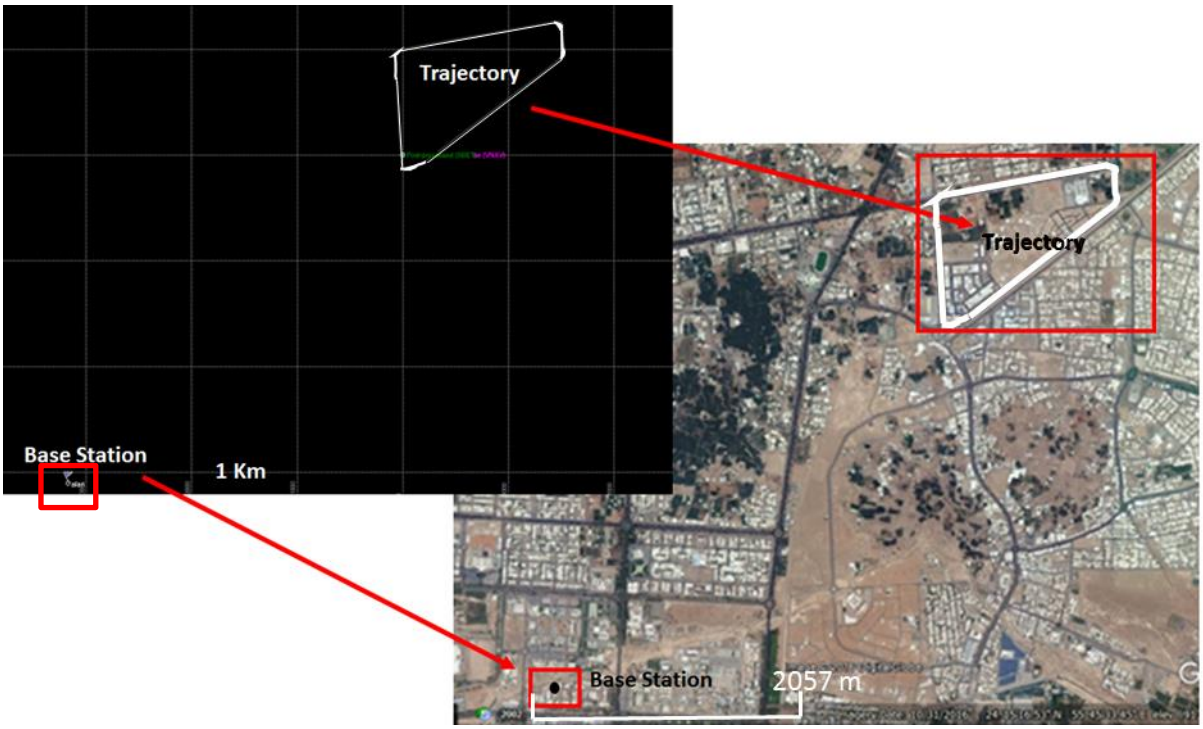

Figure 5-7: Base station and the main trajectory locations: the preview in POSPac software (left) and the preview on Google Earth (right)

From the Municipal GNSS network, our own network was observed and established. All the stations were determined in the ETRS89 system and UTM coordinate system, and only precise dual-frequency GPS receivers were used in the reference stations. The locations of reference station installations were chosen to ensure convenient conditions for GNSS Satellite observation and base line length.

5.3.2.3 Data Acquisition

During the data acquisition process, the following parameters should be monitored to maximize the quality of the RANGE files, SBET files and camera images:

- GAMS solution status in the LV-POSView controller
- Sufficient free space to complete the survey.
- The input voltage and input power regularly during the survey.
- The PDOP value.

- Proper functioning of the laser scanner, camera and sensor and their view.
- Vehicle speed as planned and appropriate for the desired point density.

The data acquisition specialist should also monitor the heath of the entire system in terms of temperature, performance, quality of the real-time data, GPS visibility and quality.

During the data acquisition, the extremely high temperature at noon caused a malfunction in the POS system and it stopped working. This fault was not detected by the data acquisition monitoring software and accordingly a further mission was performed to cover the missing data.

As shown in Figure 5-8, when the driver starts the acquisition at the illustrated position, the resulting data will contain a gap (red circle) because the LiDAR sensor is oriented 45 degrees from the movement direction. Hence, the driver must move the car backwards a little to avoid this gap in the data.

Figure 5-8: Data gaps (line patterned in red) due to sensor orientation

Secondly, the driver was trained on how to perform an IMU excitation every 20 minutes to eliminate noise and biases. This is achieved by going around any roundabout twice as fast as possible and then exiting the roundabout suddenly. This process is equivalent to the ∞-figure calibration in the MMS surveying.

Thirdly, the driver had to handle traffic congestion as well as possible. All the surrounding cars are obstacles for the sensors and will prevent the system from scanning all ground features (shadowing criterion). One more good practice in the data acquisition process is to avoid driving the LiDAR vehicle in line with any other moving cars, since these moving cars will block a portion of the sensors' field of view all the time.

The driver was able to maintain a suitable vehicle speed based on the required point density, the traffic, and the sensor pulse rates to achieve consistent point density that matches the requirements.

The data acquisition specialist (DAS) is responsible for the actual data collection operation and instructs the driver about the start/end time and location for each strip in the data acquisition.

The DAS is also responsible for calibrating the entire system. If any sensor moves relative to another sensor, for example in the maintenance of the system, all sensors should be removed from the vehicle for cleaning and adjustment. Then the sensors should be deployed again on

the vehicle. These procedures will cause a small change in the separation and angles between the sensors that is directly reflected in the resulting accuracy of the system.

Two sets of data were collected: one on 9th April and the other on 10th April. The data collected on 9th April showed high values for north, east and down position errors. After investigation, it was clear that the reason was that the area has high buildings that caused GPS signal loss. Therefore, new data were collected on 10th April to solve this problem by stopping the LiDAR vehicle when the GPS receiver lost the signal to collect static data.

5.3.2.4 Raw data extraction

The survey data includes Lynx LiDAR data, camera data and POS data collected during the survey and stored on a removable solid-state disk (SSD).

There are many types of data to be extracted before data processing:

1. Range data (Range): raw laser range data that comes from the LiDAR sensor. It includes the measured ranges of the targets relative to the LiDAR sensor. The range can be calculated by measuring the time of flight from the LiDAR sensor to the target and using the speed of light in space. The range file format is a special format for each sensor manufacturer, and each manufacturer has its own decoder for the raw range file.
2. Raw Image: the raw image collected by the system cameras compressed in a specific manufacturer format to save the memory of the data acquisition hard drive. These raw image files are then passed to the manufacturer's decoder to extract all the mission images to standard JPEG format to be used as georeferenced images.
3. POS: position and orientation data that comes from the system. This file contains the real time trajectory data for the mission. The format can only be decoded by the system manufacturer.
4. Internal POS: position and orientation data and the DMI data that will be used primarily to generate the SBET which is a post-processed version of the mission trajectory, to obtain the highest accuracy for the point cloud.
5. GPS data (RINEX): this is the reference network data of Abu Dhabi that will be used as base stations for the primary GPS/INS of the system to generate the smoothed best estimate trajectory (SBET).

5.3.3 Data processing

5.3.3.1 Trajectory

Data post-processing is used with differential GPS to obtain precise positions of unknown points by relating them to known points. The scanner data consists of ranges, angles and timestamps collected by the scanner that are referenced from the scanner origin. By combining the laser range, scan angle, scanner position and orientation of the platform from GPS and IMU

data, highly accurate XYZ coordinates of the point scanned by each laser pulse can be calculated. These measurements are then converted to XYZ coordinates as a point cloud.

New POSPac projects were created and named with the mission date. The base station Al-Ain was set to be the project reference. GPS inertial processing was run on each project to obtain the SBET file with the Applanix POSPac software. The Kinematic GPS processing technique was used to enhance the quality of location data gathered using the GPS receivers, to obtain highly accurate measurements and to eliminate errors such as time, wind and velocity. This was accomplished by using two GPS modes. The receiver in the vehicle was used in the kinematic method and one land receiver was used in static mode. The latter was applied to correct the vehicle GPS data by using the same satellite data (that is acquired by keeping the range between the two GPS receivers within 30 km). The processing was performed on data as follows:

1. Vehicle kinematic data that includes:
    - GPS (X ,Y, Z)
    - IMU (omega, phi, kappa)
2. 2. Land static data that includes GPS data (X,Y,Z)

The land static base station was used to resolve vehicle positioning errors. Then, the corrected positioning data was integrated with IMU data to eliminate errors caused by the IMU. POS data processing was carried out to improve the position and orientation data of the system using Applanix POSPac.

The process starts with the importation of real-time data and base station data, setting the base station as a reference. Then, post-processing is performed to obtain the SBET file that contains data about the time, position, velocity, acceleration, angles, angular rates and nadir angle captured every 0.005 sec. When POS data are imported into the project, the IMU, GPS and additional sensor data are automatically extracted and ready for post-processing.

For accurate results, the integer ambiguities must be known for all satellites and maintained or quickly resolved during the mission. A comparison of forward and reverse processing of GPS data can be used to find this problem.

Processing data from 9th April:

The actual number of GPS satellites during the data processing was between 0 to 10 while the PDOP was between 0 to 20. The baseline length was less than 6.4 km and the processing mode was between 0 and 3 (solution status where Mode 0 is equal to a fixed integer narrow lane, for mode 1, 2 and 3 they present forward, backward and combined) that helps to improve the accuracy and consistency of data. More details are given in Appendix A.

After processing the data, it showed high error values in north, east and down positions at a specific time. This was the time when the GPS satellite signal was lost (between UTC time 108,600 sec and 108,800 sec). The reason for this loss was a high building, as the GPS lost the signal from the satellite. The solution was to stop the car until the system obtained at least four signals from different satellites and then proceed. The mean and maximum RMSE values for easting, northing and down for this date were between 1 cm and 4 cm (see all values in Appendix A, Figure A- 5).

Processing data from 10th April:

The actual number of GPS satellites during the data processing was between 0 to 10 while the PDOP was between 0 to 100. The baseline length was less than 6.4 km and the processing mode was between 0 and 3. More details are given in Appendix A (from Figure A- 6 to Figure A- 10).

A static GPS observation was applied when the satellite signal was lost (at the time of high PDOP value) for 40 seconds. High buildings in this area were the reason for this loss.

After processing the data, the errors in north, east and down positions were lower than those for the data collected on 9th April (Figure A- 6 and Figure A- 10 in Appendix A). The mean and maximum RMSE values for easting, northing and down for these dates are shown in Table 5-2.

	9th April	10th April		9th April	10th April
Mean X	0.007	0.0066	**Maximum X**	0.064	0.048
Mean y	0.009	0.0088	**Maximum Y**	0.085	0.062
Mean Z	0.042	0.037	**Maximum Z**	0.13	0.072

Table 5-2: Positioning accuracy (RMSE in meters) for both missions (9th and 10th April)

The main difference between the two datasets can be found in the area of high buildings with a maximum value of 6 cm in the z direction. This area results in high error values in both datasets. A comparison between the datasets in the three study areas are shown below in Table 5-3. The differences increased in the high building zone (Area 2) and decreased in Area 3.

Position Accuracy RMSE in low building area 1			
	Mission day 9-4-2018	**Mission day 10-4-2018**	**Difference**
Max X	0.023 m	0.012 m	**0.011 m**
Max Y	0.054 m	0.036 m	**0.018 m**
Max Z	0.084 m	0.057 m	**0.027 m**
Position Accuracy RMSE in high building area 2			
	Mission day 9-4-2018	**Mission day 10-4-2018**	**Difference**
Max X	0.064 m	0.048 m	**0.016 m**
Max Y	0.085 m	0.062 m	**0.023 m**
Max Z	0.13 m	0.072 m	**0.058 m**
Position Accuracy RMSE in peri-urban area 3			
	Mission day 9-4-2018	**Mission day 10-4-2018**	**Difference**
Max X	0.015 m	0.011 m	**0.004 m**
Max Y	0.023 m	0.026 m	**0.003 m**
Max Z	0.056 m	0.023 m	**0.033 m**

Table 5-3: Difference RMSE (in meters) between 9th and 10th April missions in high buildings area

5.3.3.2 Geoid model generation from highly accurate ground control points (GCPs)

The height measured by the GPS receiver is the ellipsoidal height. To process the LiDAR data, this height must be converted to orthometric height (the height from the geoid surface to the point on the ground surface, as shown in Figure 5-9). Therefore, the main purpose was to determine the height of the geoid surface in the study area. The generation of a geoid model in the study area required knowledge of accurate ellipsoidal (h) and orthometric height (H) for GCPs around this area. The geoid height or undulation (N) is calculated from the difference between the orthometric and ellipsoidal heights (N = h-H) (Eteje et al., 2018).

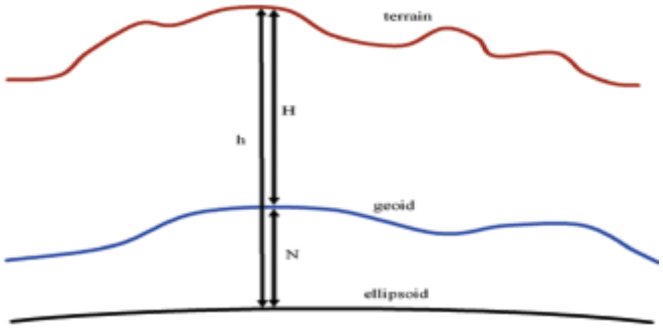

Figure 5-9: Terrain/earth surface, geoid and ellipsoid heights (Eteje et al., 2018)

In this study, the geoid model was created using 31 GCPs coordinates from UTM zone 40 N (WGS84) around the study area. The GCPs distribution in the study area (aerial view) and mission trajectory is shown below in Figure 5-10 .

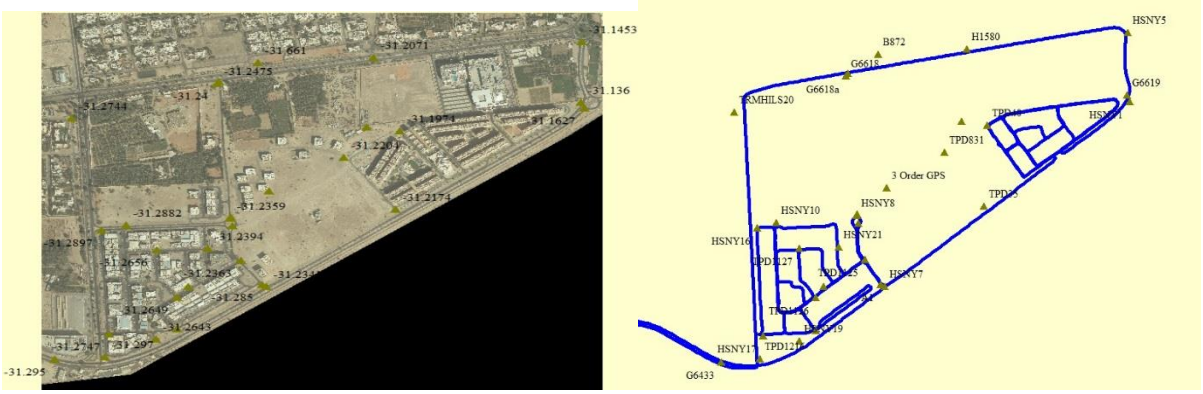

Figure 5-10: GCPs distribution throughout the study area

Seven GCPs (one first order GCP and six third order GCPs) were used as a reference. The orthometric height and ellipsoidal height points were provided by survey section in TPSS for the Al Ain municipality. All 31 points are shown in Table 5-4.

EASTING	NORTHING	Ellipsoidal height (h)	Orthometric height (H)	GEOID_ (N) undulation	POINTNAME
375396.6	2684611	256.145	287.387	-31.242	B8930
375803.5	2684533	257.3213	288.5387	-31.2174	TPD35
375817.5	2684872	257.3795	288.5769	-31.1974	TPD40
375638.2	2684757	256.5586	287.779	-31.2204	TPD831
375229.3	2685077	254.447	285.6945	-31.2475	G6618
376400.9	2684996	260.067	291.203	-31.136	G6619
375272.6	2684495	255.198	286.4339	-31.2359	HSNY8
375198.9	2684364	255.406	286.6454	-31.2394	HSNY21
375308	2684313	256.824	288.0603	-31.2363	TPD1125
375101.9	2684154	255.789	287.0539	-31.2649	TPD1126
375035	2684359	254.675	285.9406	-31.2656	TPD1127
375229.3	2685077	254.447	285.6945	-31.2475	G6618a
375229.3	2685077	254.447	285.687	-31.24	G6618b
375032.9	2683972	256.236	287.5003	-31.2643	HSNY19
375101.9	2684017	256.461	287.7224	-31.2614	HSNY18
375389.7	2684200	257.35	288.5841	-31.2341	HSNY7
375136.5	2684199	255.552	286.816	-31.264	HSNY12
374882.3	2683995	255.949	287.2237	-31.2747	HSNY17
374938.9	2684465	255.961	287.2492	-31.2882	HSNY10
374859.7	2684442	255.589	286.8787	-31.2897	HSNY16
375236.3	2685086	254.406	285.653	-31.247	HSNY9
376403.7	2685256	258.976	290.1213	-31.1453	HSNY5
376411.6	2684970	260.113	291.2757	-31.1627	HSNY1
375710.3	2684888	256.662	287.8764	-31.2144	B8730
375273.5	2684500	255.2059	286.4417	-31.2358	G6621
374763.3	2684925	253.771	285.0454	-31.2744	TRMHILS20
375733.1	2685188	256.418	287.6251	-31.2071	H1580
375374.6	2684207	257.388	288.673	-31.285	A1
375279.6	2684462	255.607	286.871	-31.264	TPD1215
374870.3	2683898	255.838	287.135	-31.297	TPD1216
374707.7	2683884	254.95	286.245	-31.295	G6433

Table 5-4: GCPs ellipsoid and ortometric heights

The previously calculated GCPs coordinates (from Table 5-4) were used to generate a surface model. These points were well-distributed in the study area to guarantee an accurate surface model. These GCPs were used to create a surface model by the ordinary Kriging interpolation method. The geoid height distribution/values were determined by the survey section in TPPS of the Al Ain Municipality. The resulting surface with the geoid height distribution in the study area is shown below in Figure 5-11.

Figure 5-11: Resulting surface with the geoid height distribution

5.3.3.3 Data quality

The final point cloud scanned with LIDAR with a density of 2-3 cm had a total of 1300 million points. To evaluate point cloud accuracy, 12 GCPs were used in the created point cloud and the results were compared with measurements from the current basemap at a scale of 1/1000. Figure 5-12 presents the distribution of the GCPs used for the comparison of both the trajectory and point cloud.

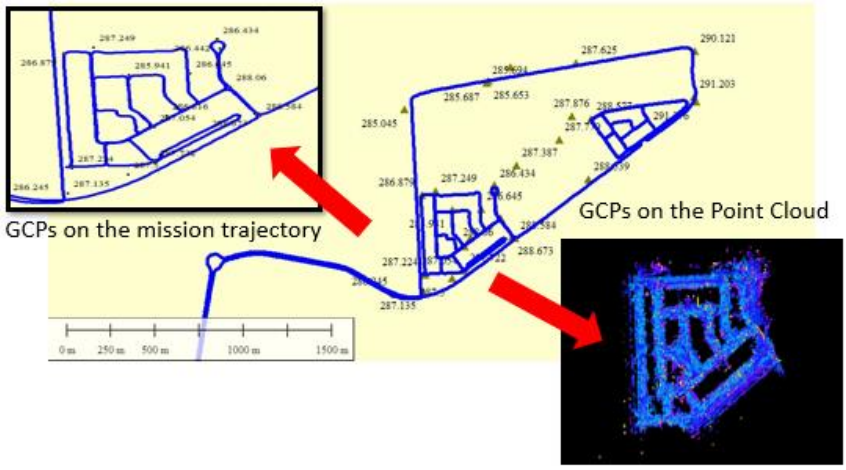

Figure 5-12: Ground control point distribution in the point cloud

The average difference for these points was 0.017 m in planimetry and 0.009 m in Z coordinates respectively. The RMSE for these point differences were 0.005 m, 0.020 m, 0.021 m in planimetry and 0.020 m in altimetry, as shown in Table 5-5. These differences were not significant considering the scale of the basemap. Figure 5-13 shows samples from the created point cloud.

	Difference (Z)	Difference (X)	Difference (Y)
Mean	0.009	0.002	0.017
RMSE	0.020	0.005	0.020
Min	-0.017	0.000	0.002
Max	0.042	0.018	0.043

Table 5-5: Difference between known GCP coordinates and measured coordinates from the point cloud. Units in meters (Alshaiba et al., 2020)

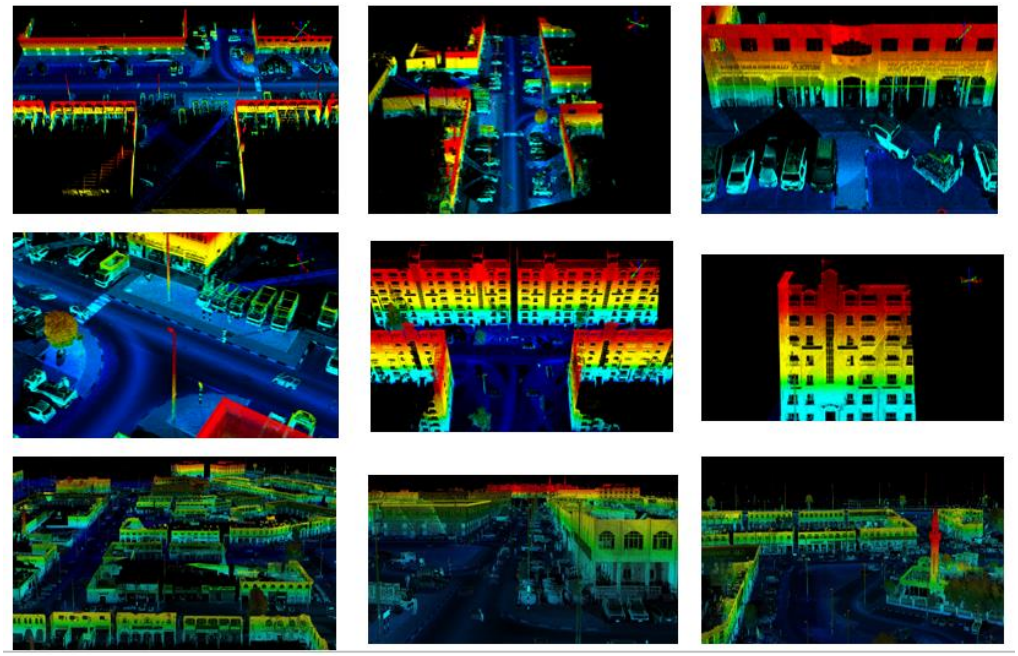

Figure 5-13: Sample of the generated point cloud

Once the point cloud is available, the next step in obtaining the vector basemap is to extract the urban feature, roads and buildings.

5.3.4 Feature extraction

5.3.4.1 Urban furniture feature

In this study, the road features, urban furniture and building corners were extracted using a commercial software program, the Topodot tool. Extracted road features include the road centerline, road edge (curb), streetlights, street signs, and top edges of buildings. A sample of features in the study area is shown below in Figure 5-14 (features include a street sign, curbs and a light pole).

The Topodot tool works within CAD software and detects features by their geometry and intensity. The point cloud was imported to this tool. Each feature (light poles, footpath,

driveway and street signs) was defined as a cell, saved to a library and snapped into the model. The cell enables the software to recognize each feature with its attributers and is saved in CAD format.

To reach the maximum completeness percentage of the feature's extraction, three trials were performed using different parameters, see Table 5-6. The first trial successfully detected up to 84% of each feature. Another run was performed to detect more of the remaining 16%. The second trial adjusted the parameters shown in the table below. The second trial successfully detected up to 92% of each feature. Another run was performed to detect more of the remaining 8%.

The third trial was undertaken by adjusting the parameters shown in the Table 5-6. The third trial successfully detected up to 96% of each feature. The remaining 4% was detected manually. The third trial parameters were used finally as the percentage was satisfactory. Some items had to be extracted manually due to their complexity, including driveways, car parks and footpaths. The automatic detection was performed by cell and based on two parameters: height and intensity values, except for the road centerline and manholes. The values of height and intensity parameters were set for each feature's detection. Samples of the extracted point cloud for the road features are shown in Figure 5-14.

Features	**Parameters**	**Parameters**			
		Height (1st trail)	Height (2nd trail)	Height (3rd trail)	Intensity
Road edges (curb)	Designed by cell	0.25 m	0.20 m	0.18 m	
Road centerline					20 - 55
Building	Designed by cell	3-18 m	5-20 m	6-24 m	
Light poles	Designed by cell	8 m	12 m	10 m	
Street signs	Designed by cell	2.5 m	2 m	1.5 m	
Trees	Designed by cell	1.5-3 m	2-6 m	3-5 m	

Table 5-6: Detection type and parameters for each feature

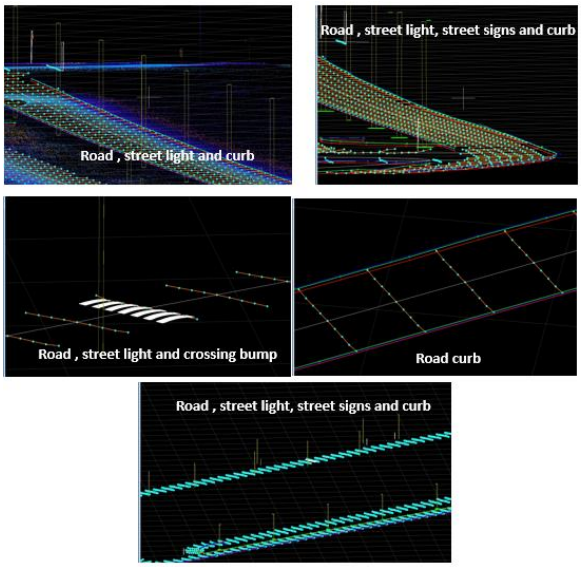

Figure 5-14: Street furniture views in the generated point cloud

The success rate was better in Area 1 than in Areas 2 and 3 (Table 5-7), because in Area 1 there is a proper roadway for LiDAR vehicle movement that is better than in Areas 2 and 3. The roadway allows a clear, full view of the surveyed area and resulted in successful feature detection and extraction at a higher percentage than in Areas 2 and 3. Area 3 is an area of vegetation that is full of trees around the available path of the LiDAR vehicle. This resulted in a higher success rate for trees in Area 3. Figure 5-14 shows samples of the urban features that appear in the point cloud.

	Area 1		**Area 2**		**Area 3***	
Features	Success rate (%)	Quantity	Success rate (%)	Quantity	Success rate (%)	Quantity
Road edges (curb stones)	95	9.6 km	70	12.8 km	60	3.8 km
Road centerline	98	5.2 km	80	7.2 km	90	3.2 km
Buildings	80-90 *	58-65	60-70 *	18-21	40-50	8-10
Light poles	100	122	100	134	40	21
Street signs	100	119	100	225	40	33
Trees	70-80	23-26	70-80	61-70	90	128

* Some places in this area could not be reached by the vehicle. Numbers represent only the reachable places.

Table 5-7: Quantity and successful detection rate for the feature detection process for each area

5.3.4.2 Manholes

Using the methodology proposed in Chapter 3, three factors are used to detect manholes. These factors are intensity, shape and return pulses. Manhole height is almost equal to ground height, which causes difficulties in manhole edge detection. The parts of the manhole that can be seen are affected by the daily passing of cars, which may result in an apparent change in their shape. These difficulties make the automatic detection process for manholes challenging. In this study, a detection method has been developed. It starts by detecting manholes based on their shape (in our case rectangular) and return pulse intensity information from the laser beam. Each road feature has a different intensity value based on its material. The manholes in the study area were detected successfully using intensity values from 2 to 42 strength pulses.

For the use of the collected LiDAR data, the first and second returned pulses for manholes were the strongest returns. These two returns were useful in detecting accurate shapes using a script in MATLAB software. Based on field measurements, three shapes of manhole were found in the study area (Table 5-8).

To extract the manholes, we use the algorithm described above. The first and second returns of the pulses received, analyzed in the time parameter, will correspond mainly to manholes, since the signal returned by metal is more intense. The next parameter to be set is the intensity. In our case, the manholes are made of steel. The wavelength of the laser used and the angles of incidence of the laser beam on the pavement correspond to values of intensity between 2 and

42. In the study area there are three types of manholes according to shape, with the dimensions collected in Table 5-8. The algorithm used is the same for all of them, since only one size has to be entered in each iteration.

Shape	Dimensions (cm)	
	A	B
Type 1	80	80
Type 2	65	65
Type 3	50	50

Table 5-8: Dimensions of the types of manhole covers

To adjust the plane of Equation (1) in Chapter 3, the A and B values in Table 5-8 correspond to the a and b parameters of the plane, while c will be zero if the manhole is at the same height as the road. Then the value of parameter d will correspond to the manhole height. In the case of Abu Dhabi, d is 18 cm, that is the height of the pavement above the road.

The manhole features that matches the known shape and dimensions will then be detected and extracted in the output. These identified cluster objects are irregular, so a last step is required to refine the shape of each identified manhole to a perfect plane with four straight sides and four right angles with equal or unequal adjacent sides, according to the manhole shape. To identify this perfect plane, the minimum bounding rectangle (MBR) or bounding box (BB) is computed to obtain the envelope of each cluster object (Lukić et al., 2018).

The results in Table 5-9 show the completeness (Equation (7), and correctness (8)) for each area with a different urban pattern. The successful detection percentage for each shape was 97%, 97.5% and 87% for Areas 1, 2 and 3 respectively. The percentages of detected manhole correctness were 98%, 98% and 93% for Areas 1, 2 and 3 respectively. The worst rates were obtained for the same features in peri-urban areas (Area 3), due to high vegetation. The reference value for the total number of manholes was calculated from the current accurate basemap (1730 manholes).

$$completeness = \frac{\text{manhole automated detection}}{(\text{manhole ground truth }) \cdot \ 100} \tag{7}$$

$$correcness = \frac{\text{manhole automated detection}}{(\text{manhole} + \text{non} - \text{manhole automated detection}) \cdot 100} \tag{8}$$

The manhole extraction process was applied in Areas 1, 2 and 3 of the study area. A total of 1414 manholes from Area 1 were extracted, while 237 manholes were extracted from Area 2, and 27 from Area 3, as shown in Table 5-9. The completeness percentage for the low-rise

building area was 97.11% while the correctness percentage was 98.33%. In the case of the high-rise building area, the completeness percentage was 97.53% while the correctness percentage was 97.53%. In case of the peri-urban area, the completeness percentage was 87.09% while the correctness percentage was 93.10%.

Area	No. of actual manholes	No. of detected manholes	No. of un-detected manholes	No. of false detected manholes	No. of correctly detected manholes	Accuracy evaluation	
						Completeness	Correctness
1	1456	1438	42	24	1414	97.11 %	98.33%
2	243	242	6	5	237	97.53 %	97.93%
3	31	29	4	2	27	87.09 %	93.10%
Total	1730	1709	52	31	1678	96.99 %	98.18%

Table 5-9: Completeness and correctness of manhole extraction for the three types in Areas 1, 2 and 3 (Alshaiba et al., 2020)

A total of 1678 manholes were detected. When compared to the real number of manholes in the study area (1730), the result was 97% successful detection. Although the script showed a high percentage of successful detection, some manholes may not be detected due to a change in intensity values and may be covered by sand as they are close to ground level. A sample of non-detected manholes is shown in Figure 5-15. Detection of manholes fails when there is any obstacle, such as dust and cars, covering the manhole and LiDAR cannot detect it.

In Area 2 (high building area), the correctness percentage was less than that found in the low building area due to issues in the high building area related to satellite signal loss. Although Area 3 was a difficult survey area, we could survey part of it. The number of detected manholes in this area was 27 with a completeness percentage of 87% and a correctness percentage of 93%. The completeness percentage was the lowest in this area, because it has a lot of objects and sand covering the manholes. This makes the detection survey process very difficult as it depends on intensity, shape and returns of the manhole. These manholes could be detected from a field survey or aerial photogrammetry images. However, this kind of flying is forbidden in the area.

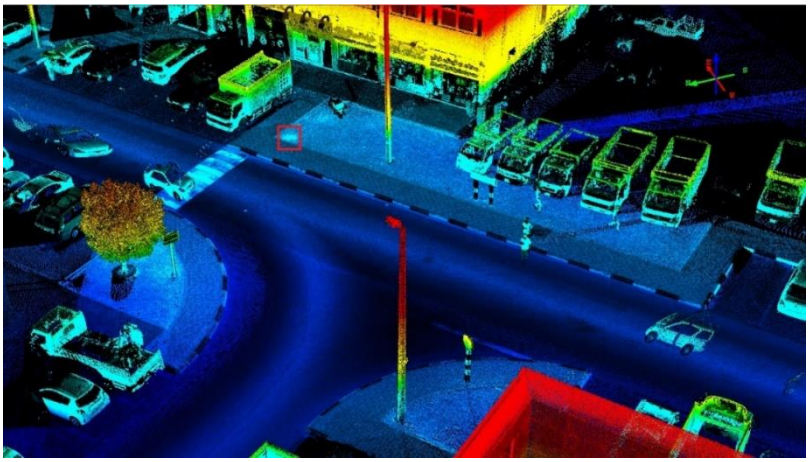

Figure 5-15:Sample of undetected manholes in the survey area

5.3.5 Building layout and filling gaps using satellite images

In the car's trajectory, all the visible features were captured but not all of them were complete. The clearest example are the buildings. In this case, the internal walls were missing, Figure 5-16. Therefore, additional information had to be sought to fill in the gaps. In other countries, the best solution would be a photogrammetric survey with an RPAS platform. However, due to the flight permission problem, the only possibility in the study area was to use satellite images.

The images available for the area are ortoimages from Quickbird with a resolution of 0.61 m. On these images, we digitalized the footprint of each building and then fitted them to the corner points obtained from the point cloud.

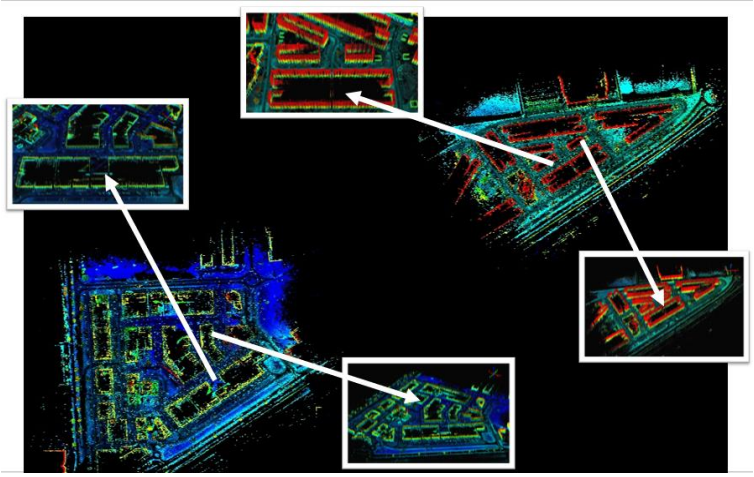

Figure 5-16: Point cloud details in Areas 1 and 2 of the study area

As mentioned above, the digitization process is more accurate when the building area is small and the building height is low. Therefore, buildings are managed in several sets according to their height.

The first step is to digitalize the four corner coordinates of each building in the satellite image (red points in Figure 5-17), then we use the two methods explained in Section 3.3.2: Method 1, average shift; and Method 2, Helmert 2D transformation, to fit these footprints to the LiDAR visible corner coordinates (green points in Figure 5-17). Then, the four corners were adjusted (blue points in Figure 5-17).

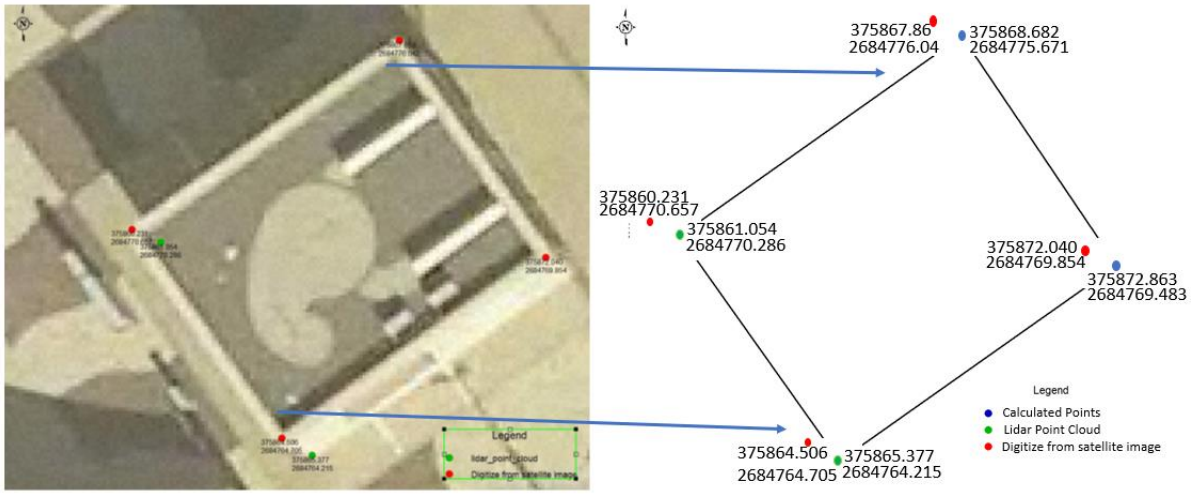

Figure 5-17: Example of building corners fit using the satellite image

A simple approach is used to calculate the difference between the two visible points, in x and y coordinates. The difference is calculated for each point between the measurements in LiDAR and the satellite image. The average for all these differences is calculated for X and Y coordinates and subtracted from the absolute difference (between LiDAR and satellite image) for each point to draw the new enhanced layout (fitting layout). When these shifts (fitting differences) are applied to the entire building, we can successfully extract all missing corners.

In this case, the process analyzed eight buildings in the low building area and four buildings in the high building area. Applying these shifts (fitting differences) to the entire building results in successful extraction of all missing corners. The final accuracy for laying buildings from LiDAR data over the satellite image after the enhanced fitting process was 0.23 m in the X direction and 0.25 m in the Y direction for the low building area and 0.9 m in the X direction and 1.1 m in the Y direction for the high building area, as shown below (Table 5-10). This was achieved by laying the LiDAR data over the satellite image after the enhancement process, and then measuring the difference manually to evaluate accuracy.

The reason for the high differences in the high building area (0.9 m in the X direction and 1.1 m in the Y direction) is because the satellite image that was used was not a true ortoimage. Therefore, the building's façade appears and causes an error in calculating the difference between the roof and bottom coordinates for the building corners and will affect any measurements on the roof corners.

	Low-rise building		High-rise building	
	X	Y	X	Y
Max.	1.174	1.231	3.179	5.254
Min.	0.21	0.027	0.095	0.533
Average difference	0.567	0.527	1.189	2.798
Max.	0.609	0.704	1.99	2.798
Min.	0.006	0.002	0.203	0.078
Average fitting difference	0.226	0.242	0.9	1.095

Table 5-10: Fitting accuracy using the traditional method, values in meters

To obtain the 2D Helmert transformation parameters, a shift to the centroid of each set of buildings was performed on the coordinates, because the transformation is very sensitive to any change in the value of the rotation. A total of six control points have been selected in each area, with low and high buildings, to solve a set of 12 equations with four parameters.

Then, the obtained parameters were applied to other known corners' coordinates extracted from the LIDAR point cloud to establish the goodness-of-fit of the data adjustment. The statistical results for the residual errors are shown in Table 5-11. The low-rise building area shows maximum, minimum and average residual errors of 0.48, 0 and 0.19 meters respectively in the X direction, while maximum, minimum and average residual errors of 0.67, 0.07 and 0.13 meters respectively were found in the Y direction. In the case of the high-rise building area, the maximum, minimum and average residual errors were 0.48, 0.26 and 0.36 meters respectively in the X direction, while the maximum, minimum and average residual errors were 0.78, 0.07 and 0.58 meters respectively in the Y direction. It was clear that the Helmert transformation (Method 2) showed better results than the fitting average method.

	Low-rise buildings		High-rise buildings	
	e_x	e_y	e_x	e_y
Max.	0.480	0.670	0.476	0.782
Min.	0.001	0.070	0.261	0.074
Average	0.196	0.125	0.357	0.578

Table 5-11: Fitting accuracy using the Helmert transformation method. Residual errors (e_x, e_y) in meters (Alshaiba et al., 2020)

As expected, since there are no true ortophotos, the disparity is greater in high-rise areas. Due to the map projection, it is greater in Y coordinates than in X coordinates in this area.

To compare this method with Method 2 (the Helmert transformation), the final accuracy for laying buildings from LiDAR data over the satellite image after the enhanced fitting process

was calculated for all low-rise buildings (102 buildings) and all high-rise buildings (29 buildings) separately (Table 5-12).

The comparison of both methods shows that the application of a Helmert transformation provides the best adjustment. Moreover, this method is faster to apply once we have calculated the parameters for the different areas, since in the first method the shift for each building is computed individually.

5.3.6 Data position accuracy

In this section, we highlight the results generated from the proposed methodology and estimate the cost and time of using mobile Lidar instead of a traditional survey. This estimation provides an indicator of MMS efficiency and accuracy as a support for traditional and daily survey activities.

In previous sections, we mentioned accuracy regarding detection completeness and correctness. In this section, we focus on geometric accuracy taking as a reference the coordinates in the Abu Dhabi official basemap.

Table 5-12 shows the comparison in meters. The difference is presented in planimetry and altimetry.

Survey Features	Road centreline (km)	Curb stone (km)	Buildings	Stree t light	Street Sign	Manhol e
Quantity	18.5	37	102	277	377	1678
AVG (Difference XY)	0.024	0.01	0.12	0.012	0.016	0.009
Max	0.21	0.18	0.8	0.08	0.07	0.05
Min	0.008	0.008	0.06	0.007	0.004	0.004
RMSE (XY)	0.038	0.038	0.015	0.016	0.03	0.028
AVG (Difference Z)	0.009	0.014	0.008	0.008	0.023	0.01
Max	0.15	0.23	0.18	0.011	0.1	0.06
Min	0.002	0.009	0.002	0.005	0.009	0.009
RMSE (Z)	0.019	0.026	0.015	0.019	0.035	0.035

Table 5-12: Comparison (in meters) of accuracy between the extracted features from the LiDAR survey against their coordinates in the Abu Dhabi basemap

An analysis of the extracted features' accuracy compared to the coordinates in the current basemap showed that the differences were within accepted levels. A threshold of 15 cm accuracy was set regarding the basemap. The differences were measured as two values: average

differences and root mean square error (RMSE) values for planimetry and altimetry differences. The aim was to measure the difference between the values from the LiDAR system and the actual values from the current basemap. The maximum difference in road centerline was 21 cm, curb stone was 23 cm, buildings was 80 cm, street light was 8 cm, street signs was 10 and manholes was 6 cm. While the maximum RMSE value in the road centerline was 4 cm, the curb stone was 4 cm, buildings 2 cm, street light 2 cm, street signs 4 cm and manholes 4 cm.

5.4 Comparison between the traditional survey and LiDAR survey in cost and time

In this section, we estimate the cost and time using mobile LiDAR instead of a traditional survey. This estimate gives capability indicators of MMS in terms of efficiency compared with traditional and daily survey activities.

5.4.1 The computational cost

In order to analyze the benefit of the proposed algorithm in terms of computational cost, three linear zones or strips of different lengths were selected. The algorithm was run for each of these strips on a common desktop computer processor i5 and 16 GB DDR4-SDRAM. Table 5-13 shows the number of manholes in each one and the time taken to extract them. The computational time was not related to the number of points in the cloud. However, it was directly proportional to the number of manholes. Based on the results, we can state that the algorithm was fast for point clouds with tens of millions of points.

Sample strip		**Number of manholes**	**Time to extract manhole (second)**
Length (km)	Point cloud size (millions of points)		
0.2	39.8	59	73.75
0.3	37.1	64	80.00
0.5	51.5	73	91.25

Table 5-13: Computation cost in several zones (Alshaiba et al., 2020)

5.4.2 Cost and time saving

The MMS and proposed methodology gave a positive result in saving time, cost and effort. The estimation cost of using a traditional survey method including the system equipment, maintenance and manpower is 609,939 USD in the first year as shown in the details in the following table. In the second year, the total cost will be 201,498 as the cost of the system

equipment is planned for last 10 years. While the cost for the LiDAR system for the same features is 473,000 USD.

		Traditional Survey		LiDAR Survey	
Survey Features	**Quantity**	**Time (hr)**	**Cost (USD)**	**Time (hr)**	**Cost (USD)**
Road centerline (km)	18.5	88	91,491	8	71,069
Curb stone (km)	37	176	182,982	16	142,137
Buildings	102	23	91,491	2	71,069
Street light	277	25	30,497	2.5	23,690
Street sign	377	30	60,994	3	47,379
Manhole	1678	80	152,485	7	118,448
Total		422	**609,939**	38.5	**473,792**

Table 5-14: Comparison between the traditional survey and the LiDAR survey in cost and time (Alshaiba et al., 2020)

The difference between using the LiDAR system to update the current basemap and using the traditional survey was analyzed to calculate the difference in cost and time (Table 5-14). The following comparison shows the difference between the traditional survey and LiDAR in cost and time. Additionally, the MMS survey is safer, especially in harsh and desert environments. The table below shows the cost of using the LiDAR system and the traditional survey system including the manpower needed and all equipment. The time spent in surveying the features under study using the traditional survey methods is 422 hours in the study area (Table 5-15), while the surveying time for the same features in the same area is 38.5 hours (including field work, data transfer, data processing and extraction process).

Comparison	**Traditional survey**	**LiDAR survey**	**Difference**	**Saved percentage**
Total Cost (USD)	**609,939**	**473,792**	**136,147**	22%
Total Time (hr)	422	38.5	383.5	91%

Table 5-15: Difference between the traditional survey and LiDAR survey in total cost and time

After analyzing time and cost differences, it was clear that the LiDAR system saved 22% of the surveying cost (in the first year) and 91% of the time needed to survey the same area.

6. Conclusions and future studies

This study proposes a methodology to update basemaps using the 3D models obtained automatically from an MMS survey in urban areas, with a focus on automatically detecting urban road manhole covers. The methodology was tested in a border area of the Abu Dhabi Emirate, where two datasets were collected using a mobile mapping system (MMS) in an area of 1.3 km2 with a total of 131 buildings. However, this study can be adopted and directly used to extract urban features in other cities when traditional methods are limited. From the safety perspective, LiDAR usage instead of traditional surveying in daily transactions helps to protect land surveyors from hazards, especially since surveyors used to take measurements at the side of the highway.

In order to check the influence of the urban environment on the process, we differentiated three zones: Area 1 with high-rise buildings and a high level of urbanization; Area 2 with high-rise buildings and a low level of urbanization; and finally Area 3, a peri-urban zone.

The next section presents the conclusions obtained about the following key issues that were studied:

1. Planning and collecting data using the Mobile Mapping System (MMS).
2. The data was processed using various software programs and tools and a quality control process was performed to improve the collected data.
3. Several feature extractions were run on the processed LiDAR data to extract 3D features, and satellite image sources were used to obtain the data (building corners) for gap areas.
4. A feasibility study was carried out to compare the suggested methodology with the traditional survey methods in term of cost and time.

The last section discusses some possible future ways of working on the issues discussed here.

6.1 Conclusions

Mission planning is critical to ensure the availability of the GNSS signal during the data collection, to examine the base station for maximum satellite visibility and to ensure the shortest baseline possible. It is important to plan properly to avoid high traffic and obstructions to the vehicle during the survey time. Moreover, the period of observation has to be selected to ensure a high number of satellites, according to the available constellation and the height of buildings in the area.

The minimization of errors during data collection is essential to achieve good accuracy for urban basemaps. Sources of error may be the distance to the base station or the LiDAR sensors, the GNSS and IMU mounted on the vehicle. Errors from the GNSS and base station could be reduced by running a combined solution (forward and backward). Errors that come from sensor alignment could be reduced or removed by calibrating the system.

In order to check the geometry data quality, control points are required with better accuracy. In the case studied in this thesis, the final point cloud scanned with LIDAR with a density of 2-3 cm has 1300 million points. To evaluate the point cloud accuracy, 12 GCPs were used. The average difference for these points was 0.017 m in planimetry and 0.009 m in Z coordinates.

To evaluate the influence of the urban environment, such as high-rise buildings and vegetation, and the economic and time cost of the entire process compared to the traditional method, the extraction of urban elements such as trees, light poles, street signs, roads and curbs was performed with commercial software. The tools of these programs are widely tested for these kinds of applications, except for manholes and hidden corners of buildings, which are not solved correctly.

The parameters for the feature extraction process applied to street furniture in Abu Dhabi had a high success rate, but this rate varied from one zone to another depending on the urban pattern. The existence of high buildings, light poles and street signs had the best success rates (100%) in areas with low buildings (Area 1) and in those with high buildings (Area 2). The worst rate (40%) was obtained for the same features in peri-urban areas (Area 3) due to high vegetation. The road edges were obtained with more success, at around 95% in Area 1 and the worst rate in Area 3. For trees the result was the opposite: 75% in Areas 1 and 2, and 90% in Area 3.

A detection method was developed in this thesis to fill the void that currently exists in the manhole extraction process with commercial software. It starts by detecting manholes based on their shape (usually rectangular or circular) and returned pulse intensity information from the laser beam. The parameters used in this study are easy to adapt to manhole covers made from different material and rectangular or circular geometry for any urban area, using as parameters the intensity range and size. Moreover, the ranges of intensity values adopted for the manholes of Abu Dhabi may be directly used to extract steel manholes in other cities.

Some limitations were found in the automatic detection of manholes using our algorithm. These limitations were due to changes in the perception of manhole shape resulting from car movement and dust, especially in the studied area. Despite these limitations, a good percentage of completeness and correctness was achieved, at around 97% and 98% respectively in the three areas. The algorithm speeds up the data processing and manhole extraction, taking an average of 1.25 seconds per manhole.

The building detection percentage was similar in all areas and was the lowest of all elements. To complete the buildings, additional information must be obtained from a different source. A satellite image provides addition information to mobile LiDAR, since the satellite dataset includes building roofs and the entire canopy. However, satellite images are less accurate than MMS, due to the long distance between the sensor and objects, and the complexity of the sensor calibration parameters. From the two methods used in the adjustment of the buildings, it was shown that the 2D Helmert transformation offers a better, faster outcome than adjusting each building individually. However, it should be considered that this transformation must be computed and applied in different sectors where the buildings have the same height and orientation, since the transformation is sensitive to them.

On average, the positioning accuracy of the navigation data (trajectory) was below 4 cm while the accuracy of the processed point cloud was below 2 cm, which led to an accuracy of 5–10 cm in the feature extraction process. The missing data that are outside the LiDAR camera view (as are some buildings corners) was obtained with an accuracy of 4 cm on average using a satellite image.

Regarding the geometric quality of the new map, it was found that the system produces results that are within the tolerances for the basemap scale (15 cm), i.e. a scale of 1:1000, in all areas regardless of the urban pattern. For all elements, the average discrepancy in position, considering as a ground truth the current map made with more expensive techniques, is less than 2 cm in most elements. Only some maximum values were found as outliers in the area of high buildings, where the GNSS signal was obstructed and therefore the precision of the vehicle's trajectory decreases.

Concerning the cost, the MMS and proposed methodology saved time, cost and effort. Regarding the findings, in this case, where aerial photogrammetry is not an option, the proposed methodology using remote sensing techniques is more effective than conventional methods of surveying, since it allows us to obtain basemaps in less time. The LiDAR system saves around 22% of the cost compared to the traditional survey method and 91% of the time compared to the traditional survey method.

6.2 Recommendation for future work

While the current study provides suggested methodology to update the basemap in a semi-automatic way, several topics were identified during this study that will open up new areas of research. These further areas of research could be:

- There is a need to explore whether there are efficient ways to improve the accuracy of building footprint layout by using advanced satellite imagery accuracy, which is around 30-40 cm. This will help to increase the matchup between the digitized building layout footprint and the point cloud layout. The research should be focused on image management to obtain true orthophotos with a better resolution.
- Research could be done to improve the data accuracy by capturing the data in two directions (north to south then reverse, or east to west then reverse). This way, the data are captured for the same object twice, so these errors could be reduced. In addition, two or more missions could be completed for the same area. Therefore, the collected data could be compared to the same objects to check errors. The cost/benefit of this additional acquisition and processing data should be evaluated.
- The manhole algorithm could be enhanced to increase efficiency by adding intensity parameters for dust to take advantage of the point cloud information that covers not only the ground but also the ground and first floor. An automatized classification of the use of buildings could be carried out: shop, coffee house, religious place, library, etc.

References

Alshaiba, O., Núñez–Andrés, A. M., & Lantada, N. (2020). Automatic manhole extraction from MMS data to update basemaps. *Automation in Construction*, *113*. https://doi.org/10.1016/j.autcon.2020.103110

Alshehhi, R., Marpu, P. R., Woon, W. L., & Mura, M. D. (2017). Simultaneous extraction of roads and buildings in remote sensing imagery with convolutional neural networks. *ISPRS Journal of Photogrammetry and Remote Sensing*, *130*, 139–149. https://doi.org/10.1016/j.isprsjprs.2017.05.002

American Society for Photogrammetry and Remote Sensing (ASPRS). (2004). *Manual of Photogrammetry* (5th ed.). Bethesda, MD: ASPRS.

Balaguer–Puig, M., Marqués–Mateu, Á., Lerma, J. L., & Ibáñez–Asensio, S. (2017). Estimation of small–scale soil erosion in laboratory experiments with Structure from Motion photogrammetry. *Geomorphology*, *295*, 285–296.

Barazzetti, L., Scaioni, M., Feng, T., Qiao, G., Lu, P., Tong, X., & Li, R. (2013). Photogrammetry in Experiments for Hydrogeological Risk Assessment. In Proceedings of *International Archives of the Photogrammetry, Remote Sensing and Spatial Information Sciences – ISPRS Archives* (pp. 145–152). Padua, Italy: International Society for Photogrammetry and Remote Sensing.

Barber, D., Mills, J., & Smith–Voysey, S. (2008). Geometric validation of a ground–based mobile laser scanning system. *ISPRS Journal of Photogrammetry and Remote Sensing*, *63*(1), 128–141. https://doi.org/10.1016/j.isprsjprs.2007.07.005.

Becker, S., & Haala, N. (2007). Refinement of building fassades by integrated processing of LIDAR and image data. *International Archives of Photogrammetry, Remote Sensing and Spatial Information Science*, *36*(2007), 7–12.

Bitenc, M., Lindenbergh, R., Khoshelham, K., & Van Waarden, A. P. (2011). Evaluation of a LiDAR land-based mobile mapping system for monitoring sandy coasts. *Remote Sensing*, *3*(7), 1472–1491. https://doi.org/10.3390/rs3071472

Brenner, C., Dold, C., & Ripperda, N. (2008). Coarse orientation of terrestrial laser scans in urban environments. *ISPRS Journal of Photogrammetry and Remote Sensing*, 63(1), 4–18. https://doi.org/10.1016/j.isprsjprs.2007.05.002

Campbell, J. B. (2002). *Introduction to remote sensing* (3rd ed.). New York, NY: The Guilford Press.

Che, E., Jung, J., & Olsen, M. J. (2019). Object recognition, segmentation, and classification of mobile laser scanning point clouds: A state of the art review. *Sensors*, 19(4), 1–42. https://doi.org/10.3390/s19040810

Chen, Q. (2007). Airborne lidar data processing and information extraction. *Photogrammetric Engineering and Remote Sensing*, *73*(2), 109–112.

Commandre, B., En–Nejjary, D., Pibre, L., Chaumont, M., Delenne, C., & Chahinian, N. (2017). Manhole cover localization in aerial images with a deep learning approach. In Proceedings of *International Archives of the Photogrammetry, Remote Sensing and Spatial Information Sciences – ISPRS Archives* (pp. 333–338). Padua, Italy: International Society for Photogrammetry and Remote Sensing. https://doi.org/10.5194/isprs–archives–XLII–1–W1–333–2017

Conforti, D., & Zampa, F. (2011). Lynx mobile mapper for surveying city centers and highways. In Proceedings of *International Archives of the Photogrammetry, Remote Sensing and Spatial Information Sciences – ISPRS Archives* (pp. 219–222). Padua, Italy: International Society for Photogrammetry and Remote Sensing.

Cracknell, A. P., & Hayes, L. (2007). *Introduction to remote sensing* (2nd ed.). Boca Raton, FL: CRC Press.

Craig, N. (2000). Real–Time GIS construction and digital data recording of the Jiskairumoko excavation. Peru. *The Society for American Archaeology Bulletin*, *18*(1), 24–28.

Cramer, M., & Stallmann, D. (2001). On the use of GPS/inertial exterior orientation parameters in airborne photogrammetry. In Proceedings of *OEEPE Workshop on Integrated Sensor Orientation* (pp. 32–44) Hannover, Germany: OEEPE.

Dolan, A. M., & Li, R. M. T. (2013). Integration of drones into domestic airspace: Selected legal issues. *Current Politics and Economics of the United States, Canada and Mexico*, *15*(1), 107–137.

Duffell, C. G., & Rudrum, D. M. (2005). Remote sensing techniques for highway earthworks assessment. In Proceedings of *GeoFrontiers* (pp. 1–13). Austin, TX: American Society of Civil Engineers (ASCE). https://doi.org/10.1061/40785(164)3

Ellum, C., & El–Sheimy, N. (2002). Land–based mobile mapping systems. *Photogrammetric Engineering and Remote Sensing*, *68*(1), 13–28.

El–Sheimy, N. (1996). A mobile multi–sensor system for GIS applications in urban centers. In Proceedings of *International Archives of the Photogrammetry, Remote Sensing and Spatial Information Sciences* (Vol. xxxi, part. B2, pp. 95–100). Vienna, Austria: Springer.

El–Sheimy, N. (2005). An overview of mobile mapping systems. In Proceedings of *FIG Working Week* (pp. 16–21). Cairo, Egypt: FIG

Eteje, S. O., Oluyori, P. D., & Ono, M. N. (2018). Computations of Geoid Undulation from Comparison of GNSS/Levelling with EGM 2008 for Geodetic Applications. *International Journal of Scientific and Research Publications*, *8*(10), 235–241.

Fan, Y., & Sisson, S. A. (2011). Reversible jump Markov chain Monte Carlo. In B. S. Carlo, A. Gelman, G. Jones. X. L. Meng. (Eds.), *Handbook of Markov Chain Monte* (pp. 67–92). Boca Raton, FL: CRC Press

Fernandez, J. C., Singhania, A., Caceres, J., Slatton, K. C., Starek, M., Kumar, R. (2007). *An overview of lidar point cloud processing software* (GEM Center Report No. Rep_2007–12–001). Gainesville, FL: Geosensing Engineering and Mapping (GEM), Civil and Coastal Engineering Department, University of Florida.

Gao, J. (2008). *Digital analysis of remotely sensed imagery*. Auckland, New Zealand: McGraw Hill Professional.

Gilvear, D., & Bryant, R. (2005). Analysis of aerial photography and other remotely sensed data. *Tools in Fluvial Geomorphology*, 135–170. https://doi.org/10.1002/0470868333.ch6

Glennie, C. (2007). Rigorous 3D error analysis of kinematic scanning LIDAR systems. *Journal of Applied Geodesy*, *1*(3), 147–157. https://doi.org/10.1515/jag.2007.017

Glennie, C. (2009). Kinematic terrestrial light–detection and ranging system for scanning. *Transportation Research Record, 2105*(1), 135–141. https://doi.org/10.3141/2105–17

Golovinskiy, A., Kim, V. G., & Funkhouser, T. (2009, September). Shape–based recognition of 3D point clouds in urban environments. In Proceeding of *2009 IEEE 12th International Conference on Computer Vision* (pp. 2154–2161). New York, NY: IEEE. https://doi.org/10.1109/ICCV.2009.5459471

Graham, L. (2010). Mobile mapping systems overview. *Photogrammetric Engineering and Remote Sensing, 76*(3), 222–228.

Grant, W. B. (1995). Lidar for atmospheric and hydrospheric studies. In F. J. Duarte (ed.), *Tunable Laser Applications* (pp. 213–305). New York, NY: Marcel Dekker.

Green, P. J., & Hastie, D. I. (2009). Reversible jump MCMC. *Genetics, 155*(3), 1391–1403.

Guan, H., Li, J., Yu, Y., Wang, C., Chapman, M., & Yang, B. (2014). Using mobile laser scanning data for automated extraction of road markings. *ISPRS Journal of Photogrammetry and Remote Sensing, 87*, 93–107. https://doi.org/10.1016/j.isprsjprs.2013.11.005

Guan, H., Yu, Y., Ji, Z., Li, J., & Zhang, Q. (2015). Deep learning–based tree classification using mobile LiDAR data. *Remote Sensing Letters*, *6*(11), 864–873. https://doi.org/10.1080/2150704X.2015.1088668

Haala, N., Peter, M., Kremer, J., & Hunter, G. (2008). Mobile LiDAR mapping for 3D point cloud collection in urban areas—A performance test. *The International Archives of the Photogrammetry, Remote Sensing and Spatial Information Sciences*, *37*, 1119–1127.

Heipke, C. (2004). Some Requirements for Geographic Information Systems. *Photogrammetric Engineering & Remote Sensing, 70*(2), 185–195. https://doi.org/10.14358/PERS.70.2.185

Hu, M., Yang, W., Ren, M., & Yang, J. (2004). A vision based road detection algorithm. In Proceedings of *IEEE Conference on Robotics, Automation and Mechatronics* (vol. 2, pp. 846–850). New York, NY: IEEE. https://doi.org/10.1109/ramech.2004.1438028

Hu, Y., Li, X., Xie, J., & Guo, L. (2011). A novel approach to extracting street lamps from vehicle–borne laser data. In Proceedings of *2011 19th International Conference on Geoinformatics* (pp. 1–6). New York, NY: IEEE. https://doi.org/10.1109/GeoInformatics.2011.5981183

Hwang, J., Yun, H., Jeong, T., Suh, Y., & Huang, H. (2013). Frequent unscheduled updates of the national base map using the land–based mobile mapping system. *Remote Sensing*, *5*(5), 2513–2533. https://doi.org/10.3390/rs5052513

Ishikawa, K., Takiguchi, J. I., Amano, Y., & Hashizume, T. (2006). A mobile mapping system for road data capture based on 3D road model. In Proceedings of *2006 IEEE Conference on Computer Aided Control System Design, 2006 IEEE International Conference on Control Applications, and 2006 IEEE International Symposium on Intelligent Control* (pp. 638–643). New York, NY: IEEE. https://doi.org/10.1109/CACSD–CCA–ISIC.2006.4776720

Jaakkola, A., Hyyppä, J., Kukko, A., Yu, X., Kaartinen, H., Lehtomäki, M., & Lin, Y. (2010). A low–cost multi–sensoral mobile mapping system and its feasibility for tree measurements. *ISPRS Journal of Photogrammetry and Remote Sensing, 65*(6), 514–522. https://doi.org/10.1016/j.isprsjprs.2010.08.002

Jacobs, G. (2005). High definition surveying & 3D laser scanning uses in transportation. *Professional Surveyor Magazine*, *25*(4), 1–1.

Jensen, J. R. (2005). *Introductory digital image processing: A remote sensing perspective* (2nd ed.). Upper Saddle River, NJ: Prentice–Hall.

Jochem, A., Höfle, B., & Rutzinger, M. (2011). Extraction of vertical walls from mobile laser scanning data for solar potential assessment. *Remote Sensing*, *3*(4), 650–667. https://doi.org/10.3390/rs3030650

Kaartinen, H., Hyyppä, J., Kukko, A., Jaakkola, A., & Hyyppä, H. (2012a). Benchmarking the performance of mobile laser scanning systems using a permanent test field. In Proceedings of *International Archives of the Photogrammetry, Remote Sensing and Spatial Information Sciences* (pp. 471–476). Padua, Italy: International Society for Photogrammetry and Remote Sensing. https://doi.org/10.5194/isprsarchives–XXXIX–B5–471–2012.

Kaartinen, H., Hyyppä, J., Kukko, A., Jaakkola, A., & Hyyppä, H. (2012b). Benchmarking the performance of mobile laser scanning systems using a permanent test field. *Sensors*, *12*(9), 12814–12835. https://doi.org/10.3390/s120912814

Kalantari, M., Lester, C., Boyle, D. R., & Coupar, N. (2009). Towards e–Land administration: electronic plans of subdivisions in Victoria. In B. Ostendorf, P. Baldock, D. Bruce, M. Burdett, & P. Corcoran (eds.), In Proceedings of *SSC2009 Surveying and Spatial Sciences Institute Biennial International Conference* (pp. 155–162) Adelaide, South Australia: Surveying & Spatial Sciences Institute.

Kang, J. M., Park, J. K., & Kim, M. G. (2008). Digital mapping using aerial digital camera imagery. *The International Archives of the Photogrammetry, Remote Sensing and Spatial Information Sciences (ISPRS), XXXVII*, 4521-4524.

Kim, S. (2007). *Individual tree species identification using lidar– Derived crown structures and intensity data* (PhD Thesis). University of Washington, USA.

Kingston, T., Gikas, V., Laflamme, C., & Larouche, C. (2007). An integrated mobile mapping system for data acquisition and automated asset extraction. In Proceedings of *International Archives of the Photogrammetry, Remote Sensing and Spatial Information Sciences* (pp. 185–190). Padua, Italy: International Society for Photogrammetry and Remote Sensing.

Kwak, E., Al–Durgham, M., & Habib, A. (2012). Automatic 3D building model generation from lidar and image data using sequential minimum bounding rectangle. *International Archives of the Photogrammetry, Remote Sensing and Spatial Information Sciences*, *39*(B3), 285–290. https://doi.org/10.1.1.837.4779

Lato, M. J., & Diederichs, M. S. (2014). Mapping shotcrete thickness using LiDAR and photogrammetry data: Correcting for over–calculation due to rockmass convergence. *Tunnelling and Underground Space Technology*, *41*(1), 234–240. https://doi.org/10.1016/j.tust.2013.12.013

Lehtomäki, M., Jaakkola, A., Hyyppä, J., Kukko, A., & Kaartinen, H. (2010). Detection of vertical pole–like objects in a road environment using vehicle–based laser scanning data. *Remote Sensing*, 2(3), 641–664. https://doi.org/10.3390/rs2030641

Leslar, M., Perry, G., & McNease, K. (2010). Using mobile lidar to survey a railway line for asset inventory. In Proceedings of *ASPRS 2010 Annual Conference* (pp. 526–533). San Diego, CA: ASPRS.

Li, R., Schwarz, K. P., Chapman, M. A., & Garcel, M. (1994). Integarate GPS and related technologies for rapid data aquisition. *GIS World*, *7*(4), 41–43.

Lin, Y., Jaakkola, A., Hyyppä, J., & Kaartinen, H. (2010). From TLS to VLS: Biomass estimation at individual tree level. *Remote Sensing*, *2*(8), 1864–1879. Retrieved April 06, 2018, from http://www.mdpi.com/2072–4292/2/8/1864/

Lin, Y., & Hyyppa, J. (2011). *k*–segments–based geometric modeling of VLS scan lines. *IEEE Geoscience and Remote Sensing Letters*, *8*(1), 93–97. https://doi.org/10.1109/LGRS.2010.2051940

Lowe, D. G. (2004). Distinctive image features from scale–invariant keypoints. *International Journal of Computer Vision*, *60*(2), 91–110.

Lukić, I., Hocenski, Ž., Köhler, M., & Galba, T. (2018). Parallel mining of uncertain data using segmentation of data set area and Voronoi diagrams. *Automatika*, *59*(3–4), 349–356. https://doi.org/10.1080/00051144.2018.1541645

Maltezos, E., Doulamis, A., Doulamis, N., & Ioannidis, C. (2018). Building extraction from LiDAR data applying deep convolutional neural networks. *IEEE Geoscience and Remote Sensing Letters*, *16*(1), 155–159. https://doi.org/10.1109/LGRS.2018.2867736

McQuat, G. J. (2011). *Feature extraction workflows for urban mobile–Terrestrial lidar* data (M.Sc. Thesis). Queen's University, Kingston, ON, Canada. Retrieved June 21, 2018, from http://qspace.library.queensu.ca/bitstream/1974/6530/1/Mcquat_Gregory_J_201105_MSc.pdf

Morel, J. M., & Yu, G. (2009). ASIFT: A new framework for fully affine invariant image comparison. *SIAM Journal on Imaging Sciences*, *2*(2), 438–469.

Nex, F., & Remondino, F. (2014). UAV for 3D mapping applications: a review. *Applied Geomatics*, *6*(1), 1–15. https://doi.org/10.1007/s12518–013–0120–x

Novak, K. (1991). The Ohio State University highway mapping system: The stereo vision system component. In Proceedings of *47th Annual Meeting of the Institute of Navigation* (pp. 121–124). Williamsburg, VA: The Institute of Navigation.

Núñez, M. A., Buill, F., Regot, J., & De Mesa, A. (2008). 3D Digital documentation for the restoration of cultural heritage. The experience of the old city of Aleppo rehabilitation Project. In Proceedings of *Digital International Conference on Virtual Systems and MultiMedia* (pp. 74–78). Limassol, Cyprus: VSMM.

Okeke, F., & Karnieli, A. (2006). Methods for fuzzy classification and accuracy assessment of historical aerial photographs for vegetation change analyses. Part I: Algorithm development. *International Journal of Remote Sensing*, *27*(1), 153–176. https://doi.org/10.01431160500166540

Olsen, M. J., Roe, G. V., Glennie, C., Persi, F., Reedy, M., Hurwitz, D. & Knodler, M. (2013) Guidelines for the Use of Mobile LIDAR in Transportation Applications. *TRB NCHRP Final Report*. Washington, DC: Transportation Research Board.

Ostrowski, W. (2016). Accuracy of measurements in oblique aerial images for urban environment. In Proceedings of *International Archives of the Photogrammetry, Remote Sensing & Spatial Information Sciences* (vol. xlii–2/w2, pp. 79–85). Athens, Greece: 3D Geoinfo.

Petrie, G. (2010). An introduction to the technology: mobile mapping systems. *Geoinformatics*, 13(1), 32–43.

Pu, S., Rutzinger, M., Vosselman, G., & Elberink, S. O. (2011). Recognizing basic structures from mobile laser scanning data for road inventory studies. *ISPRS Journal of Photogrammetry and Remote Sensing*, *66*(6), S28–S39. https://doi.org/10.1016/j.isprsjprs.2011.08.006

Qiu, K., Sun, K., Ding, K., & Shu, Z. (2016). A fast and robust algorithm for road edges extraction from lidar data. In Proceeding of *International Archives of the Photogrammetry, Remote Sensing and Spatial Information Sciences, ISPRS Archives* (vol. 41, pp. 693–698). Padua, Italy: International Society for Photogrammetry and Remote Sensing. https://doi.org/10.5194/isprsarchives–XLI–B5–693–2016

Rabbani, T., Van Den Heuvel, F., & Vosselmann, G. (2006). Segmentation of point clouds using smoothness constraint. *International Archives of Photogrammetry, Remote Sensing and Spatial Information Sciences,* 36(5), 248–253.

Rau, J. Y., Habib, A. F., Kersting, A. P., Chiang, K. W., Bang, K. I., Tseng, Y. H., & Li, Y. H. (2011). Direct sensor orientation of a land–based mobile mapping system. *Sensors*, *11*(7), 7243–7261. https://doi.org/10.3390/s110707243

San, D. K., & Turker, M. (2010). Building extraction from high resolution satellite images using Hough transform. In Proceedings of *International Archives of the Photogrammetry, Remote Sensing and Spatial Information Sciences, ISPRS Archives* (vol. xxxviii, pp. 1063–1068). Padua, Italy: International Society for Photogrammetry and Remote Sensing.

Schloderer, G., Bingham, M., Awange, J. L., & Fleming, K. M. (2011). Application of GNSS-RTK derived topographical maps for rapid environmental monitoring: a case study of Jack Finnery Lake (Perth, Australia). *Environmental monitoring and assessment*, 180(1-4), 147-161. https://doi.org/10.1007/s10661-010-1778-8

Schofield, W., & Breach, M. (2007). *Engineering surveying* (6th ed.). Oxford, UK: Elsevier.

Schwarz, K. P., Chapman, M. A., Cannon, M. W., & Gong, P. (1993). An integrated INS/GPS approach to the georeferencing of remotely sensed data. *Photogrammetric Engineering and Remote Sensing*, *59*(11), 1667–1674.

Shan, J., & Toth, C. K. (2009). *Topographic laser ranging and scanning: Principles and processing*. Boca Raton, FL: CRC Press.

Singh, R. (2008). *Engineering automation: Key concepts for a 25 year time horizon* (2nd ed.). Oregon, US: Oregon Department of Transportation, Highway Division.

Sonnen, D. (2007). Emerging issue: Spatial data quality. *Directions Magazine January 2007*. Retrieved August 12, 2016, from https://www.directionsmag.com/article/2755

Sonnentag, O., Hufkens, K., Teshera–Sterne, C., Young, A. M., Friedl, M., Braswell, B. H., & Richardson, A. D. (2012). Digital repeat photography for phenological research in forest ecosystems. *Agricultural and Forest Meteorology*, *152*(1), 159–177. https://doi.org/10.1016/j.agrformet.2011.09.009

Stöcker, C., Bennett, R., Nex, F., Gerke, M., & Zevenbergen, J. (2017). Review of the current state of UAV regulations. *Remote Sensing*, *9*(5), 1–26.

Tao, C. V. (1999). Error analysis and modelling of terrestrial stereo imaging systems. *Journal of Surveying and Land Information Systems*, *59*(3), 187–196.

Tao, C. V., Chapman, M. A., & Chaplin, B. A. (2001). Automated processing of mobile mapping image sequences. *ISPRS Journal of Photogrammetry and Remote Sensing*, *55*(5–6), 330–346. https://doi.org/10.1016/S0924–2716(01)00026–0

Tao, C. V., & Li, J. (2007). *Advances in mobile mapping technology*. London, UK: Taylor and Francis.

Tatoglu, A., & Pochiraju, K. (2012). Point cloud segmentation with LIDAR reflection intensity behavior. In Proceedings of *2012 IEEE International Conference on Robotics and Automation* (pp. 786–790). New York, NY: IEEE.

Timofte, R., & Van Gool, L. (2011). Multi–view manhole detection, recognition, and 3D localisation. In Proceedings of *2011 IEEE International Conference on Computer Vision Workshops (ICCV Workshops)* (pp. 188–195). New York, NY: IEEE.

Ussyshkin, R. V., & Boba, M. (2008). Performance characterization of a mobile lidar system: Expected and unexpected variables. In Proceedings of *ASPRS Conference Proceedings* (pp. 177–182). Ontario, Canada: Optech.

Vallet, J., Panissod, F., Strecha, C., & Tracol, M. (2011). Photogrammetric performance of an ultra–light weight swinglet "UAV". In Proceedings of *International Archives of the Photogrammetry, Remote Sensing and Spatial Information Sciences* (vol. xxxviii–1/c22, pp. 253–258). Zurich, Switzerland: ISPRS. https://doi.org/10.5194/isprsarchives–XXXVIII–1–C22–253–2011

Wang, C., Hsieh, C., & Tseng, Y. (2011). Determination of object point coordinates by MMS image sequences using multiple image matching. In Proceedings of *International Symposium on Remote Sensing International Conference on Space, Aeronautical and Navigational Electronics* (pp. 1–4). Taiwan: National Cheng–Kung University.

Wendel, J., Meister, O., Schlaile, C., & Trommer, G. F. (2006). An integrated GPS/MEMS–IMU navigation system for an autonomous helicopter. *Aerospace Science and Technology*, *10*(6), 527–533.

Wei, Z., Yang, M., Wang, L., Ma, H., Chen, X., & Zhong, R. (2019). Customized Mobile LiDAR System for Manhole Cover Detection and Identification. *Sensors*, *19*(10), 2–18.

Xu, Z. H., Wu, L. X., Gerke, M., Wang, R., & Yang, H. (2016). Skeletal camera network embedded structure–from–motion for 3D scene reconstruction from UAV images. *ISPRS Journal of Photogrammetry and Remote Sensing*, *121*, 113–127. https://doi.org/10.1016/j.isprsjprs.2016.08.013

Yang, B., Fang, L., Li, Q., & Li, J. (2012). Automated extraction of road markings from mobile LiDAR point clouds. *Photogrammetric Engineering & Remote Sensing*, *78*(4), 331–338. https://doi.org/10.14358/PERS.78.4.331.

Yokoyama, H., Date, H., Kanai, S., & Takeda, H. (2013). Detection and classification of pole–like objects from mobile laser scanning data of urban environments. *International Journal of CAD/CAM*, *13*(2), 31–40. Retrieved September 24, 2019, from http://147.47.106.98/ojs/index.php/ijcc/article/view/247

Yoo, H. J., Goulette, F., Senpauroca, J., & Lepère, G. (2010). Analysis and improvement of laser terrestrial mobile mapping systems configurations. *International Archives of Photogrammetry, Remote Sensing and Spatial Information Sciences*, *38*(5), 633–638.

Yousif, H., Li, J., Chapman, M., & Shu, Y. (2010). Accuracy enhancement of terrestrial mobile lidar data using theory of assimilation. In Proceedings of *International Archives of Photogrammetry, Remote Sensing and Spatial Information Sciences – ISPRS Archives* (pp. 639–645). Padua, Italy: International Society for Photogrammetry and Remote Sensing.

Yu, Y., Li, J., Guan, H., Wang, C., & Yu, J. (2014a). Automated detection of road manhole and sewer well covers from mobile LiDAR point clouds. *IEEE Geoscience and Remote Sensing Letters*, *11*(9), 1549–1553. https://doi.org/10.1109/LGRS.2014.2301195.

Yu, Y., Li, J., Guan, H., Wang, C., & Yu, J. (2014b). Semiautomated extraction of street light poles from mobile LiDAR point–clouds. *IEEE Transactions on Geoscience and Remote Sensing*, *53*(3), 1374–1386. https://doi.org/10.1109/TGRS.2014.2338915

Yu, Y., Guan, H., & Ji, Z. (2015). Automated detection of urban road manhole covers using mobile laser scanning data. *IEEE Transactions on Intelligent Transportation Systems*, *16*(6), 3258–3269. https://doi.org/10.1109/TITS.2015.241381

Zhang, W. (2010). Lidar–based road and road–edge detection. In Proceedings of *2010 IEEE Intelligent Vehicles Symposium* (pp. 845–848). New York, NY: IEEE.

Zhu, L., Yang, X., & Liu, Y. (2013). Role of basic surveying and mapping production in urban management. In Proceedings of *International Conference on Education Technology and Information System* (ICETIS 2013) (pp. 1089–1092). Paris, France: Atlantis Press.

Appendix A

Two datasets were used in this thesis from two different days: 9th and 10th of April. Charts are presented in this section including: PDOP, the number of satellites, the processing mode and the baseline.

Processing data from 9th April:

The Actual number of GPS satellites during the data processing was between 0 to 10 while the PDOP was between 0 to 20. The baseline length was less than 6.4 km and the processing mode was between 0 and 3 as shown below in the figures (from A1 to A5). Regarding the north, east and down position error RMS Figure A- 5 is the reference for the data presented in Table 5-2 for 9th April data.

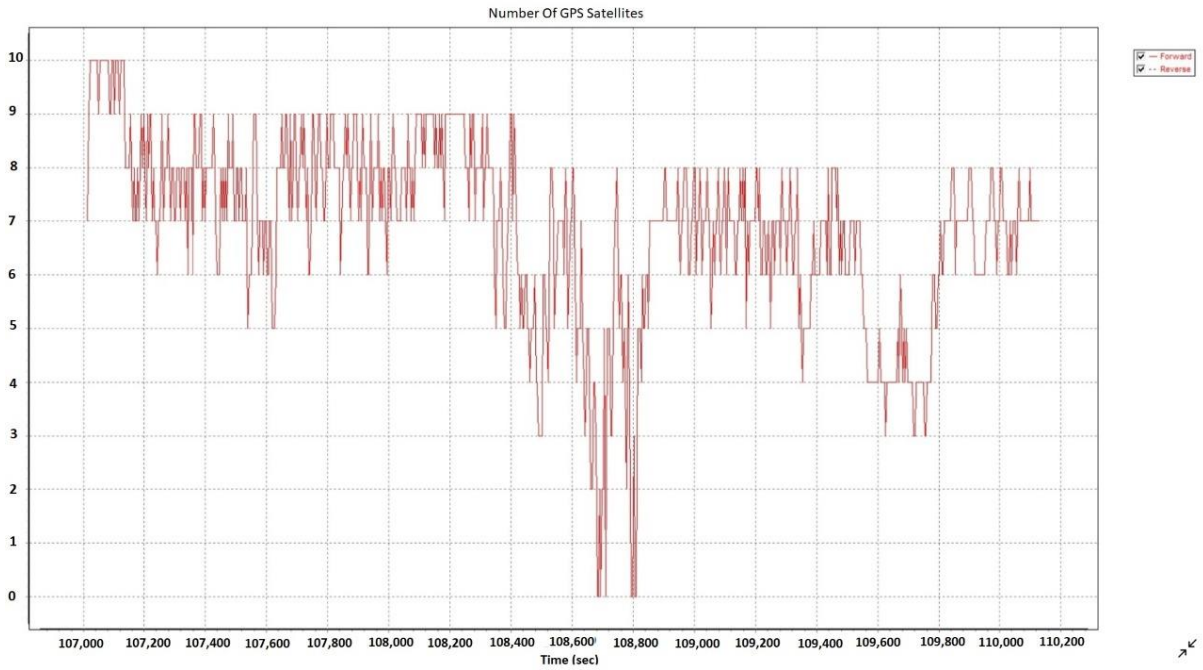

Figure A- 1:Number of GPS satellites, 9th April

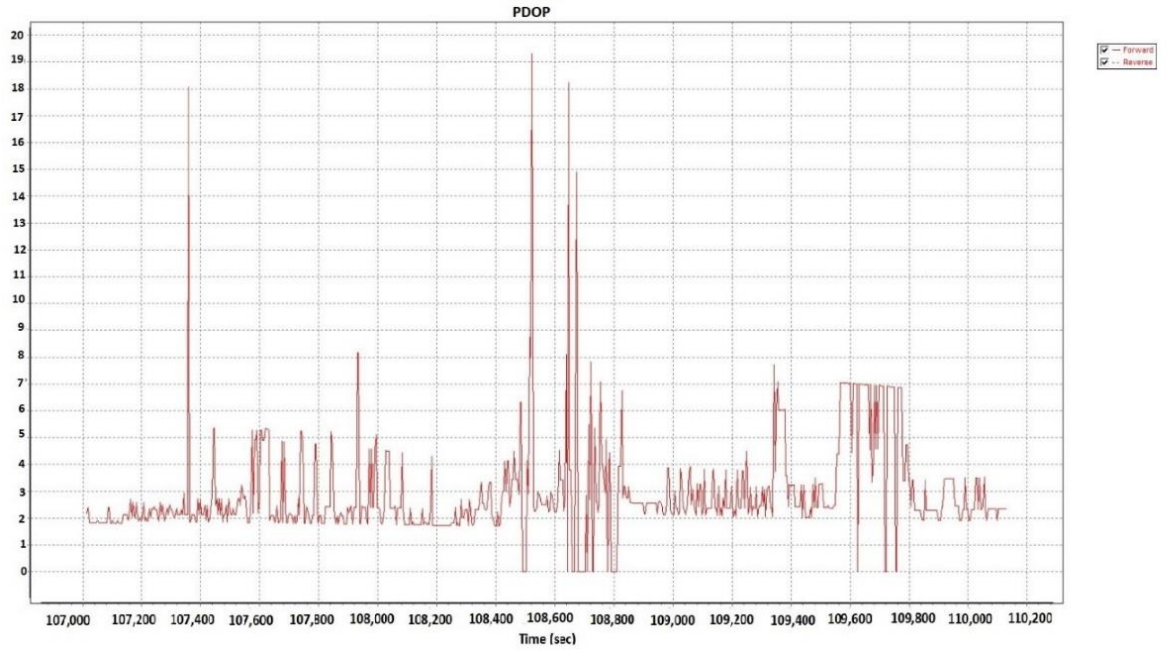

Figure A- 2: PDOP chart for 9th April

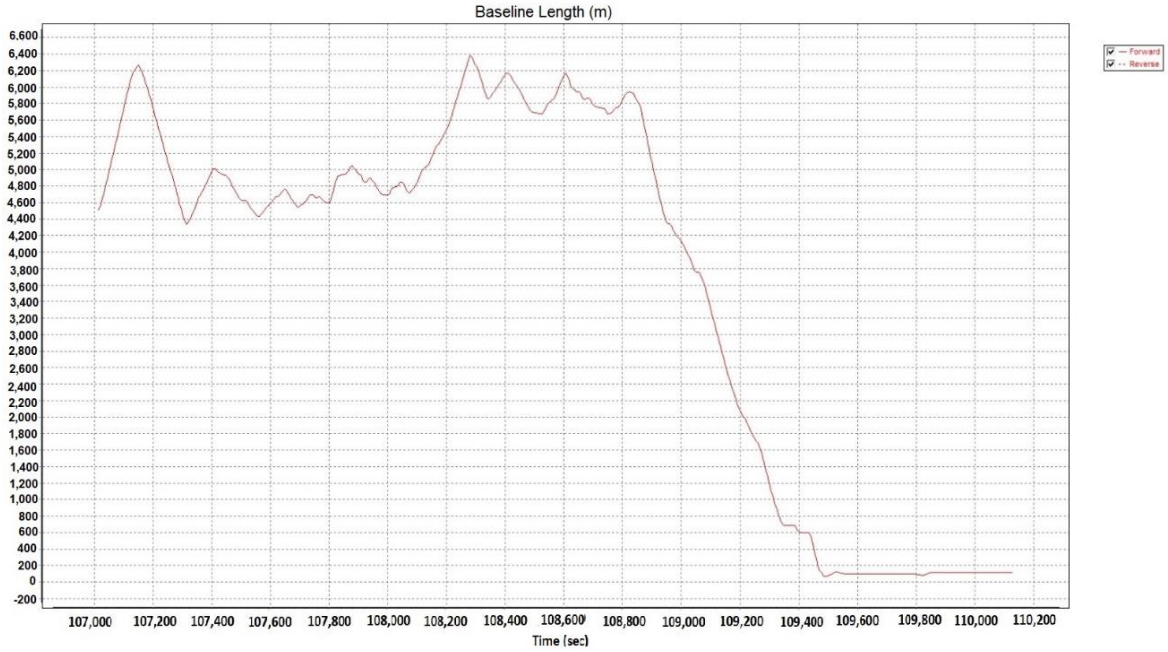

Figure A- 3: Baseline length, 9th April (m)

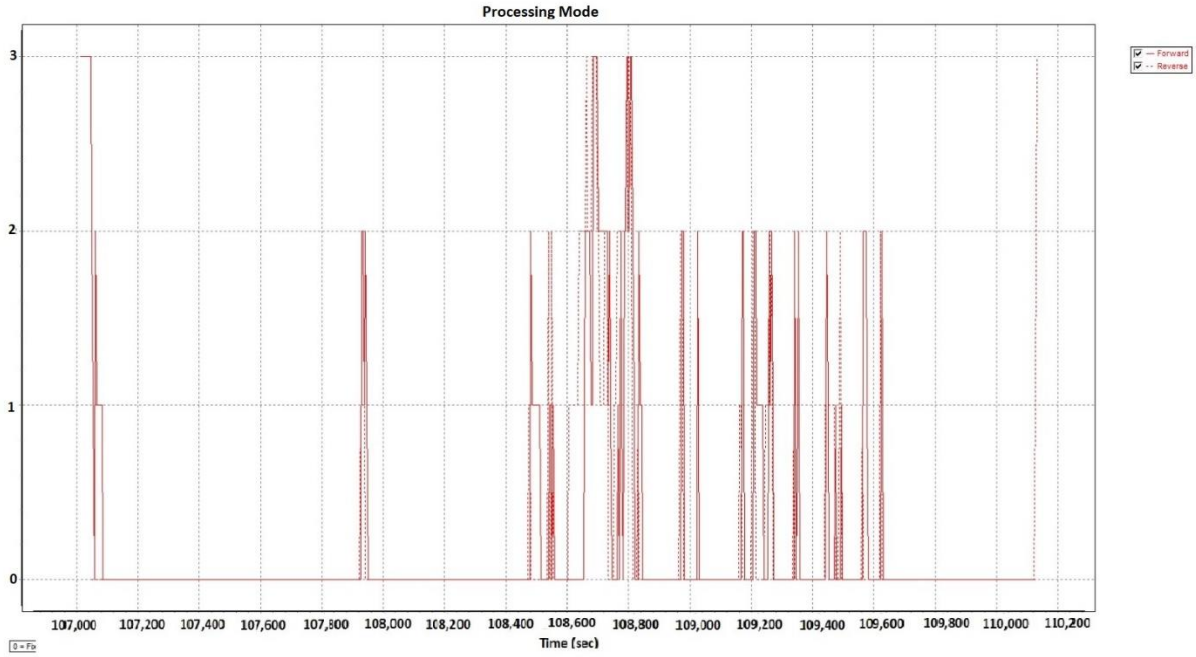

Figure A- 4: Processing mode, 9th April

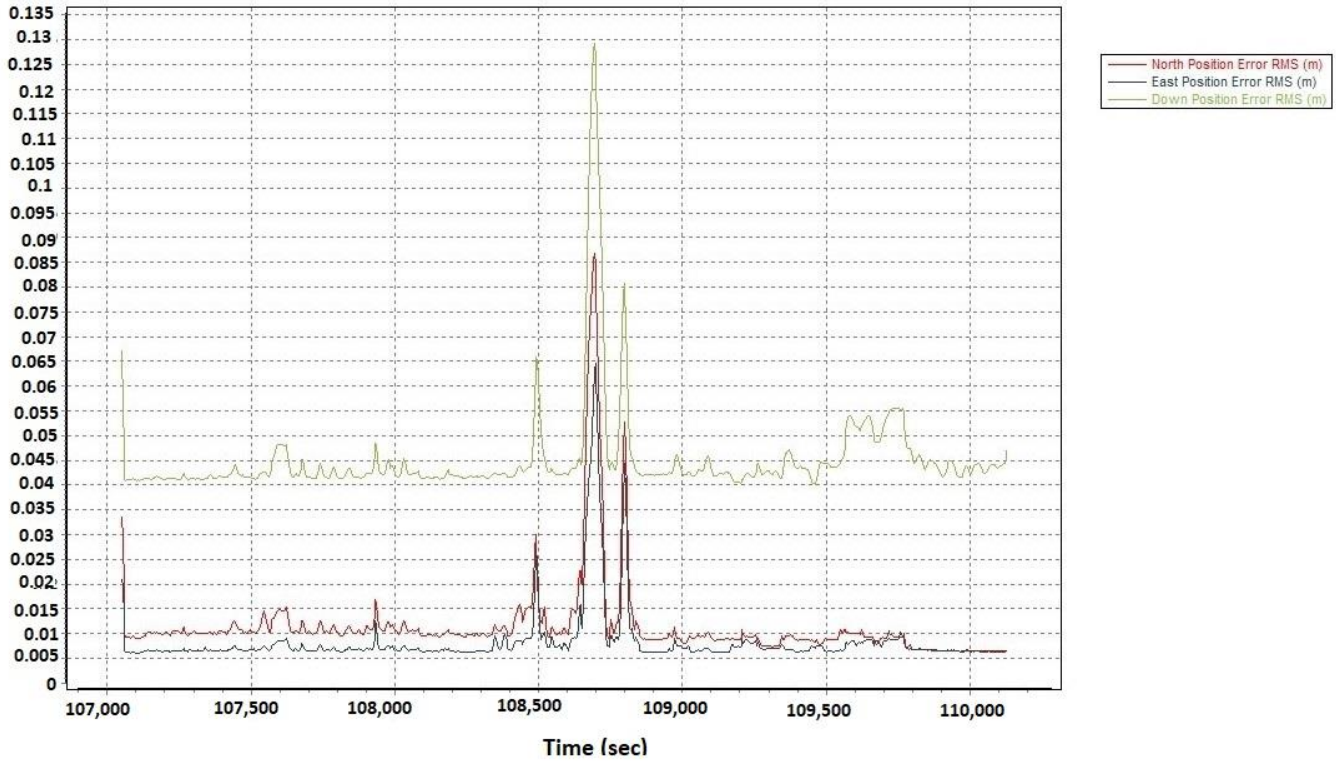

Figure A- 5: North, east and down position error, RMS (m)

Processing data for 10th April:

The Actual number of GPS satellites during the data processing was between 0 to 10 while the PDOP was between 0 to 100. The baseline length was less than 6.4 km and the processing mode was between 0 and 3 as shown below in the figure (from 6 to 10). Regarding the north, east and down position error RMS Figure A- 10 is the reference for the data presented in Table 5-2 for 9th April data.

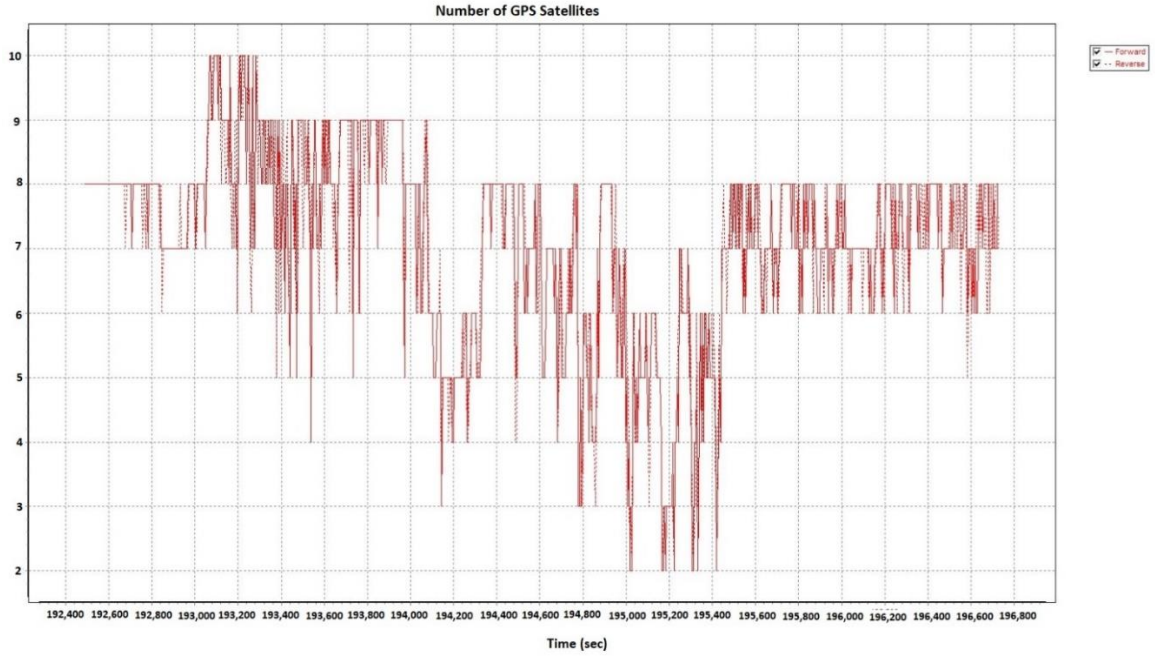

Figure A- 6: Number of GPS satellites, 10th April

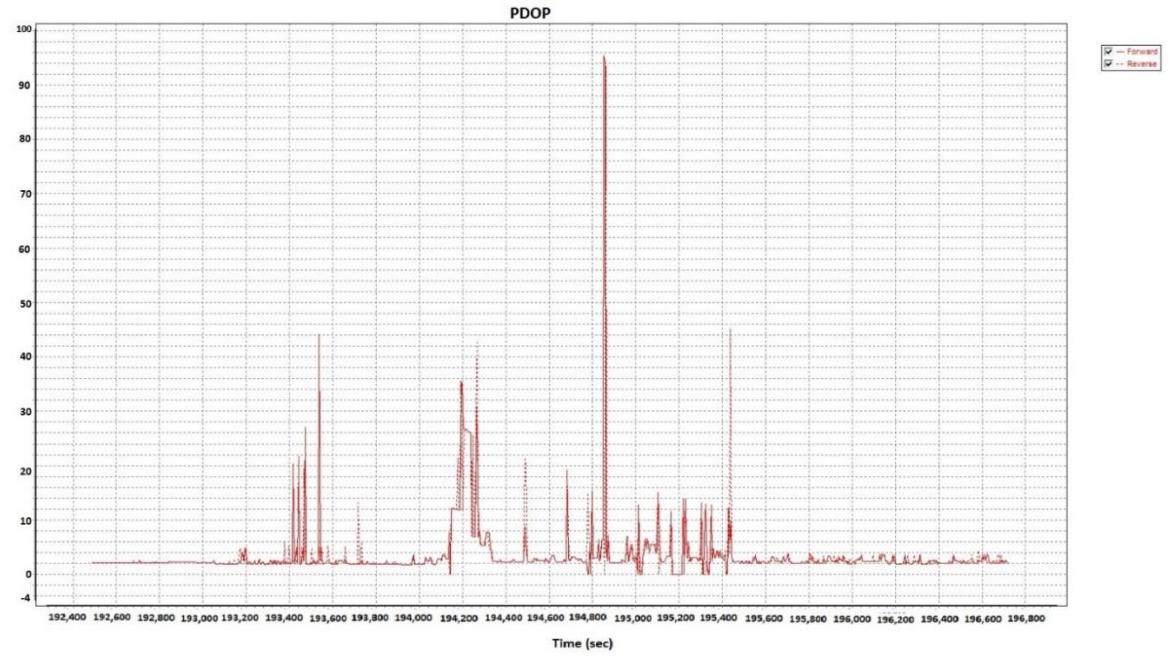

Figure A- 7: PDOP chart for 10th April

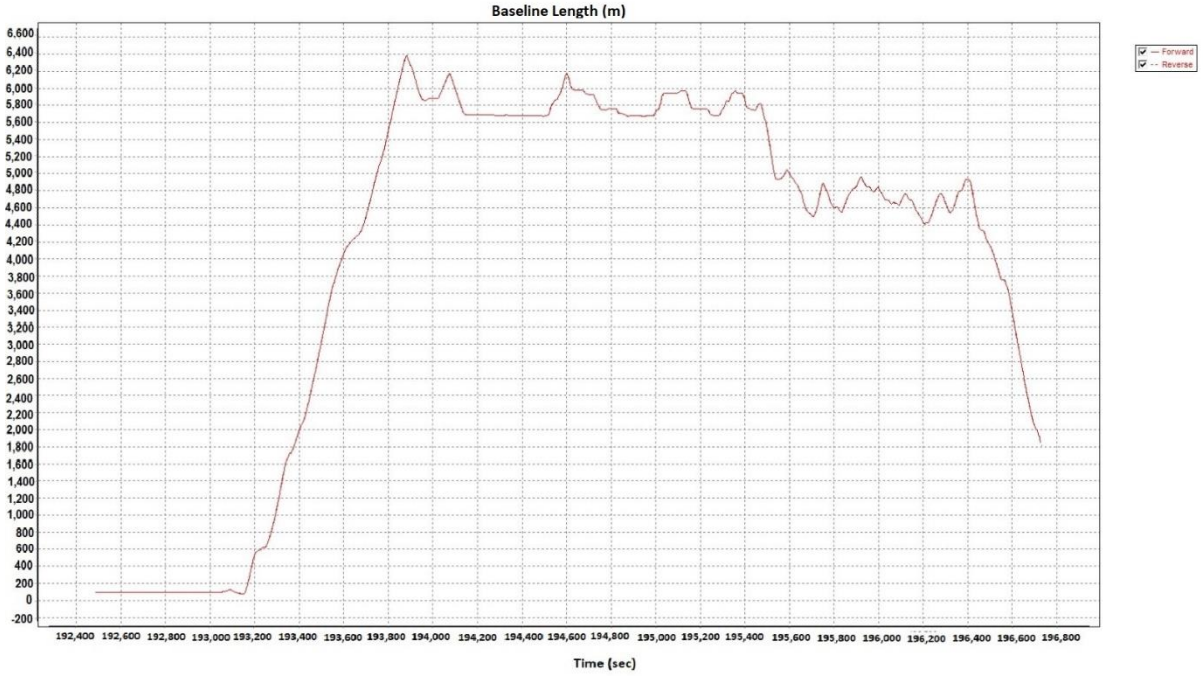

Figure A- 8: Baseline length, 10th April (m)

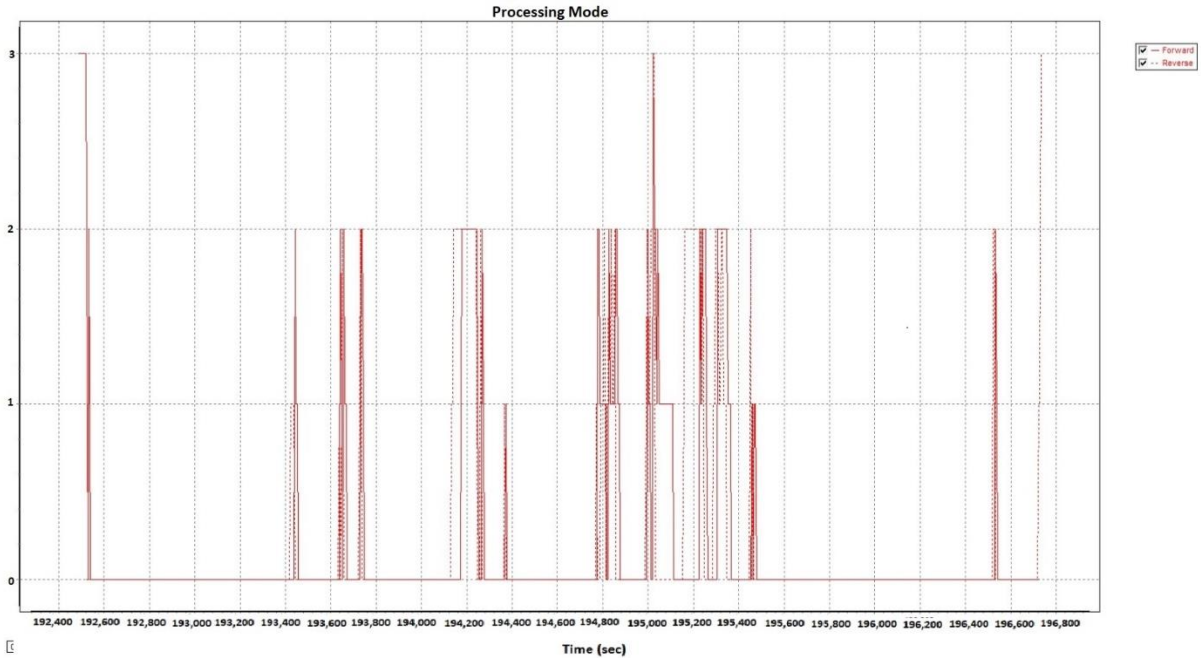

Figure A- 9: Processing mode, 10th April

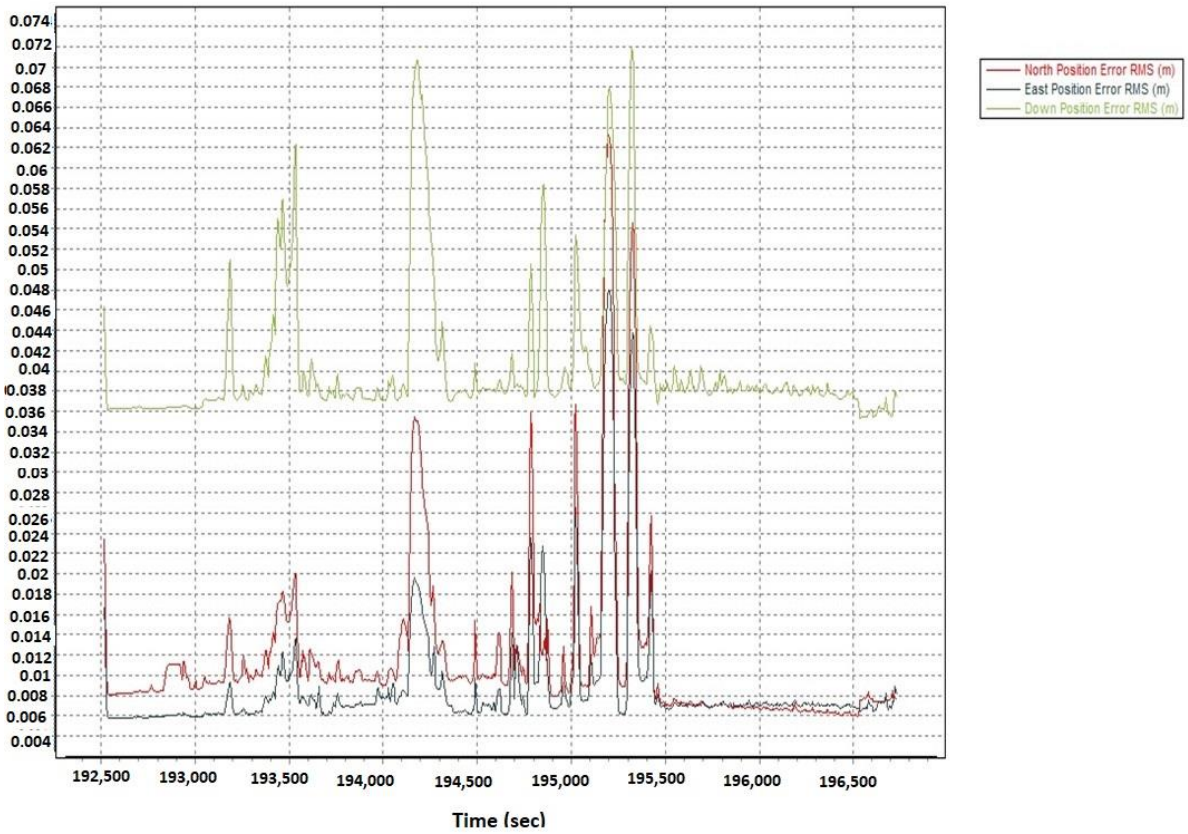

Figure A- 10: North, east and down position error RMS (m)